# Basic Studies of UCST Polymers in Water and their Processing as Films and Fibers

## DISSERTATION

zur Erlangung des akademischen Grades einer Doktorin der
Naturwissenschaften (Dr. rer. nat.)
an der Bayreuther Graduiertenschule für Mathematik und
Naturwissenschaften (BayNAT) der Universität Bayreuth

vorgelegt von

## Beatriz Amanda Pineda Contreras

aus *Mérida-Venezuela*

Bayreuth, 2016

Die vorliegende Arbeit wurde in der Zeit von April 2013 bis April 2016 in Bayreuth am Lehrstuhl Makromolekulare Chemie II unter der Betreuung von Frau Prof. Dr. Seema Agarwal angefertigt.

Vollständiger Abdruck der von der Bayreuther Graduiertenschule für Mathematik und Naturwissenschaften (BayNAT) der Universität Bayreuth genehmigten Dissertation zur Erlangung des akademischen Grades eines Doktors der Naturwissenschaften (Dr. rer. nat.).

Dissertation eingereicht am: 14.12.2016

Zulassung durch das Leitungsgremium: 09.01.2017

Wissenschaftliches Kolloquium: 24.05.2017

Amtierender Direktor: Prof. Dr. Stephan Kümmel

Prüfungsausschuss:

Prof. Dr. Seema Agarwal          (Erstgutachter)

Prof. Dr. Matthias Breuning      (Zweitgutachter)

Prof. Dr. Birgit Weber           (Vorsitz)

Prof. Dr. Georg Papastavrou

"Success is a science; if you have the conditions, you get the result".

by Oscar Wilde

# Table of Contents

# List of symbols and abbreviations

| | |
|---|---|
| AAc | acrylic acid |
| AAm | acrylamide |
| AIBN | 2,2´-azobisisobutyronitrile |
| AN | acrylonitrile |
| BCP | block copolymer |
| CMDT | cyanomethyl dodecyl trithiocarbonate |
| CTA | chain transfer agent |
| $C_{tr}$ | chain transfer constant |
| Cryo-TEM | cryogenic-transmission electron microscopy |
| Đ | molar mass dispersity |
| Da | Dalton |
| DMF | *N,N′*-dimethylformamide |
| DMSO | dimethyl sulfoxide |
| DSC | differential scanning calorimetry |
| *e.g.* | exempli gratia (for example) |
| equiv | equivalents |
| *et. al.* | et alii (and others) |
| FRP | free radical polymerization |
| GPC | gel permeation chromatography |
| HCl | hydrochloric acid |
| I$^{\bullet}$ | initiator radical |
| IPNs | interpenetrating polymer networks |
| IR | infrared spectroscopy |

| | |
|---|---|
| LAMs | less-activated monomers |
| LCST | lower critical solution temperature |
| λ | wavelength |
| MAMs | more-activated monomers |
| MHz | megahertz |
| $M_n$ | number average molar mass |
| $M_w$ | weight average molar mass |
| NAGA | *N*-acryloylglycinamide |
| NaOH | sodium hydroxide |
| NIPAM | *N*-isopropylacrylamide |
| NIPS | non-solvent induced phase separation |
| NMR | nuclear magnetic resonance |
| p.a. | pro analysis |
| PAAc | poly(acrylic acid) |
| PAAm | polyacrylamide |
| PAN | polyacrylonitrile |
| PBS | phosphate buffered saline |
| PMMA | poly(methyl methacrylate) |
| $P_n^{\bullet}$ | polymeric radical |
| PNAGA | poly(*N*-acryloylglycinamide) |
| PNIPAM | poly(*N*-isopropylacrylamide) |
| PS | polystyrene |
| P4VP | poly(4-vinylpyridine) |
| R | rest (chemical structure) |

| | |
|---|---|
| R$^\bullet$ | radical |
| RAFT | reversible addition fragmentation chain transfer |
| RDRP | reversible deactivation radical polymerization |
| rpm | revolutions per minute |
| RT | room temperature |
| SAXS | small-angle x-ray scattering |
| SEM | scanning electron microscopy |
| St | styrene |
| TEM | transmission electron microscopy |
| $T_g$ | glass transition temperature |
| THF | tetrahydrofuran |
| UCST | upper critical solution temperature |
| UV | ultraviolet light |
| VP | vinylpyridine |
| $\nu$ | wavenumbers |
| wt% | weight% |

# 1 Introduction and aim of the work

Responsive polymers represent an important research field, since they allow the understanding and the possible imitation of nature. For instance, plants and animals can change their form and color in dependence of the environmental conditions. The introduction of functional groups in polymer chains can induce this type of "responsive" behavior towards external stimuli. Biopolymers such as polysaccharides and proteins are often used as reference systems to design and develop responsive synthetic polymers.[1] The macroscopical changes of responsive polymers are based on the formation or break of hydrogen bonds, electrostatic interactions, hydrophobic effects, acid-base reactions, among others.[1] A remarkable property of this type of materials is their reversible response.

Responsive polymers are often synthesized as homopolymers, copolymers and block copolymers. Different architectures can be obtained depending on the synthetic method and the required application field. Water-soluble responsive polymers are, for instance, of high relevance, since the development of responsive materials in water increases the application range. Especially in the field of biomedicine for drug delivery systems.[2,3] However, the use of synthetic responsive polymers in the human body is a challenge, which is approached by science over the last years.[4] Therefore, the interest in the development of new water-soluble responsive materials and the study of their properties in water increased. Hence, thermoresponsive polymers have found a remarkable progress for different applications. Poly(*N*-isopropyl acrylamide) (PNIPAM) is a thermoresponsive polymer with lower critical solution temperature (LCST) behavior and therefore belongs to the class of the most studied responsive polymers. Due to its LCST (~32 °C) near body temperature, low dependency on the molecular weight and concentration in solution, it is especially interesting for biomedical applications.[5] Thermoresponsive materials showing a reversible upper critical solution temperature (UCST) behavior in water are other type of thermoresponsive polymers, which are gaining in relevance over the last years, in particular the non-ionic UCST polymers. Poly(*N*-acryloyl glycinamide) (PNAGA), has been used as reference system for the first fundamental studies on non-ionic UCST polymers.[6] Agarwal and coworkers showed the synthesis of non-ionic UCST polymers using cost-effective monomers of acrylamide (AAm) and acrylonitrile (AN).[7] Since the manipulation of the thermoresponsivity of this system was very effective, different synthetic approaches have been developed to increase the understanding and applications of UCST polymers.[8–10] However, the water-soluble properties of UCST polymers

limits utility in solid state, which is important for promising applications, since these polymers disintegrate after water contact.

Non-ionic UCST-type polymers represent a class of thermoresponsive system that have not been extensively studied. Some progress made in the last years, established the influence of different parameters on the UCST behavior *e.g.* molar mass, chain end groups, polydispersity, etc.[11,12] However, there are still remaining issues to be solve, that are highly interesting to improve the understanding of this type of thermoresponsive polymers, such as the effect of compositional homogeneity and the influence of the polymerization method on the phase transition temperature. Moreover, since the known examples of non-ionic UCST polymers are based on amide monomers such as NAGA or AAm, which are prone to hydrolysis, it is important to study the chemical stability in aqueous media as well as the effect of parameters influencing the hydrolysis such as pH variation and temperature.

Therefore, the aim of this thesis is to provide fundamental studies of the UCST behavior with main focus on the effect of compositional chain homogeneity as well as the chemical and thermoresponsive stability under different pH conditions. A further aim was set on the processing of water-stable non-ionic UCST polymers as film and fiber material, to increase the possible application fields of this type of thermoresponsive system, in particular with porous morphologies, which enhance the active surface and create interpenetration properties.

In order to obtain water-stable responsive materials with responsive behavior, there are different alternatives to follow *e.g.* crosslinking as post-modification step; however, this method can be very laborious and not suitable for sensitive systems or industrial applications. Consequently, the synthesis of new polymer structures such as block copolymers represent a suitable type of material to avoid post modifications steps and to allow processing as well as maintenance of responsive properties in aqueous solution. In block copolymers, the use of a hydrophobic matrix can provide materials that can be processed by industrial methods such as electrospinning and non-solvent induced phase separation (NIPS). These methods are used to form materials with "on-off" switchability, using external stimuli like temperature or pH.[13–16]

Electrospinning is a known versatile method, that can be used for the formation of complex structures and hybrid materials, by encapsulation of inorganic and organic compounds.[17] The design of porous electrospun fibers *via* phase separation methods for example, has not been extensively studied as in the case of polymeric films.[18] The vast potential of porous electrospun fibers with thermoresponsive properties opens new possibilities, particularly in the fields of scaffolds materials and immobilized biological systems, were an interpenetration with the application media is required.

The results of this thesis are presented in three parts, in each part the systems are investigated in order to extent the understanding and possible application of these materials.

The first part implicates the design of a new UCST polymer system, based on commercially and cost effective monomers such as acrylamide (AAm) and St.

Due to the considerable difference in reactivity ratios of these monomers, systematical studies using conventional and controlled radical polymerization methods were carried out to investigate the influence of a homogeneous/heterogeneous chain growth for copolymers of UCST type.

Part two deals with studies based on the hydrolytic stability and retention of thermoresponsive behavior of UCST copolymers in aqueous media. Intentional hydrolysis under acidic and alkaline conditions were carried out to analyze chemical and thermoresponsive stability of the system. The loss and recovery of the thermoresponsive behavior, based on the protonation/deprotonation of the formed carboxylic groups in the polymer structure, gave a new approach to UCST systems, since a pH- dependent responsive behavior was obtained.

The third part reveals a new approach for UCST polymers, since block copolymers were synthesized to achieve water-insoluble polymers with responsive properties, even after processing, based on a model LCST block copolymer system of NIPAM and St. Thereby, different processing methods were used, such as NIPS and electrospinning. By changing the hydrophobic content in the block copolymers, different structures were obtained going from thermoresponsive micelles to stable films and fibers in aqueous media. Furthermore, non-ionic UCST block copolymers were synthesized using two different synthetic routes. The manipulation of the sequence of monomer addition, allowed the investigation of a new thermoresponsive system and demonstrated the influence of the changed synthetic route on the phase transition temperature. Further, both the obtained film and fiber morphology were analyzed in detail as well as the thermoresponsive behavior of the processed materials.

# 2 Theoretical background

## 2.1 Responsive polymeric systems

Stimuli responsive polymers undergo physical and chemical changes in their environment upon the minimal application of an external stimulus. Responsivity in aqueous media is of particular interest, due to the versatility and wide application fields of this natural solvent. Currently there is a vast diversity of synthetic polymers able to react to external stimuli such as temperature, pH and light. The present work is focused on thermoresponsive polymers; therefore, the following part will describe the fundamental theory and state of the art for this type of material. Figure 1 illustrates the behavior of the polymer chain and its interaction with the surrounding water molecules upon temperature change.
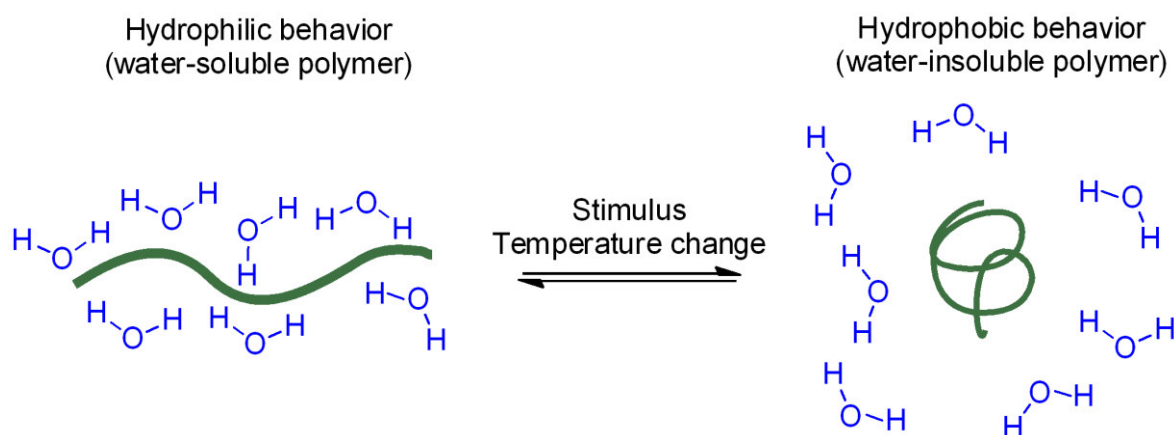


Figure 1: Reversible responsive behavior of polymer chains after the application of temperature as external stimulus.

### 2.1.1 Thermoresponsive polymers

Thermoresponsive polymeric systems have been intensively investigated, since temperature is an easily controlled external stimulus. Hydrogen bonding interactions allow changes between hydrophilic and hydrophobic properties of the polymer chains in aqueous media at different temperatures. Thermoresponsive behavior can be divided in two types: upper critical solution temperature (UCST) and lower critical solution temperature (LCST). Polymers with UCST show a miscibility gap at low temperatures, which induces phase separation due to strong polymer-polymer interactions. The responsivity of the LCST type present a phase separation,

upon heating due to the disruption of polymer-water interactions above the LCST. These materials are of significant interest for a wide range of applications such as drug delivery systems,[19,20] sensors,[21] bioseparation,[22] chromatographic columns,[22,23] hydrogels,[24,25] etc.

The phase transition temperature is one of the most important characteristics of thermoresponsive materials, since it defines the possible application conditions. Thermodynamics provide the basis of the phase separation of thermoresponsive polymers. The solubility of a polymer in water is dependent on the Gibbs energy (ΔG), which is negative upon dissolution. In the case of a water-soluble UCST polymer, the enthalpy (ΔH) and entropy (ΔS) of dissolution are positive parameters. By increasing the temperature the term T·ΔS exceed ΔH, inducing the solubility of the polymer (equation 1). On the contrary, LCST polymers show negative values of ΔH and ΔS.[7,11] The negative ΔS is based on the well-known hydrophobic effect.

$$\Delta G = \Delta H - T \cdot \Delta S \tag{1}$$

Moreover, the phase behavior of thermoresponsive polymers is commonly displayed using phase diagrams (Figure 2). These show that the polymer sample not only precipitates from the solution at a specific temperature but that is also an equilibrium, forming a polymer rich phase and a second polymer poor phase.[26]

### 2.1.1.1 Thermoresponsive behavior of UCST-type

UCST behavior can be obtained *via* hydrogen bonding (non-ionic) or Coulomb (ionic) interactions.[27] One remarkable characteristic of non-ionic UCST polymers is the low sensitivity against the addition of salts or pH changes. Allowing a stable response upon temperature changes based only on reversible hydrogen bonding.[11] Phase transitions in water under relevant conditions (0–100 °C) are unusual for non-ionic UCST polymers.[11] However, due to the mentioned advantages, there is an increasing interest in this type of thermoresponsive system.
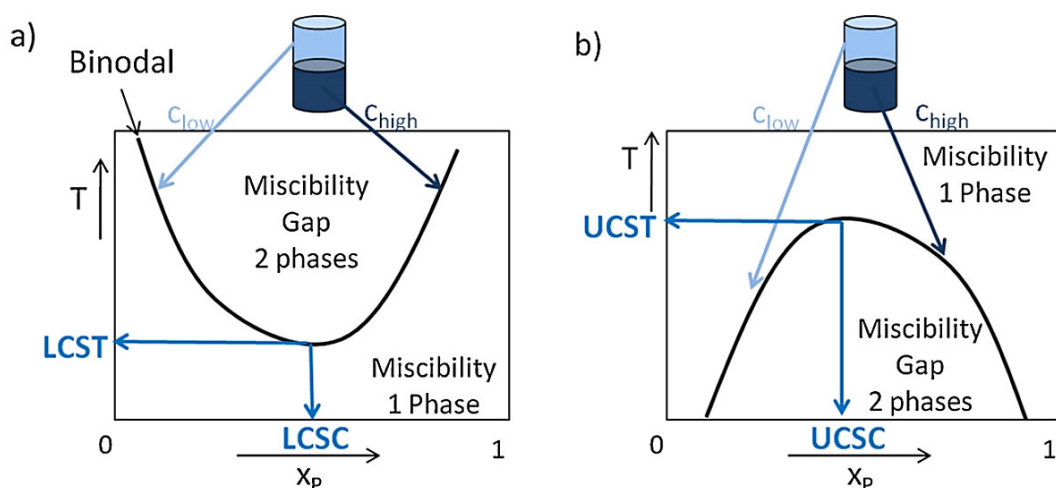
Figure 2: Typical phase diagram for water-soluble systems displaying (a) LCST and (b) UCST behavior. Reproduced Figure from Ref.[26] with permission. Copyright from Elsevier.

Fundamental research on non-ionic UCST polymers has been carried out using the monomer *N*-acryloyl glycinamide (NAGA). Agarwal and coworkers showed for the first time the UCST-type thermoresponsive behavior of the homopolymer PNAGA.[6] The authors remarked the importance of an ion-free polymerization system to prepare UCST samples. Since even low concentration of ionic groups as impurity in the polymer chain originated from the initiator or the monomer itself, could decrease or hinder the thermoresponsive behavior in water.[28] Further exploration of this system showed as well the importance of the sample preparation conditions, to avoid the hydrolysis of the amide functionalities into ionized carboxylic groups.[28] These elemental research on PNAGA allowed the rapid increased of further non-ionic UCST systems based on PNAGA copolymers.[7] The phase transition behavior of UCST polymers can be manipulated using mostly hydrophobic comonomers. This is a useful tool to extend the application rage of this type of polymers, since the phase transition could be modified in a controllable manner to temperatures similar to the human body. However, it should be notice that the copolymerization process involves new parameters such as monomer reactivity, hydrolysis stability, and polymerization time as well as polymerization methods. Therefore, copolymer systems could enable or interfere with the observation of a thermoresponsive behavior. For example, the copolymerization of NAGA and St allowed the formation of a new UCST system that was, however, highly dependent on the polymer conversion.[7] In this case, it was evident that the difference in reactivity between the two monomers (NAGA and St) hindered the formation of a homogeneous chain composition, which is highly important to induce a sharp phase transition temperature.[11,29]

Improvements in the field of UCST polymers were obtained with low cost and commercially available monomers, such as AAm for hydrogen bonding formation and hydrophobic comonomers like AN and St.[7,29] Particularly, copolymers of AAm and AN have been establish as successful UCST system, due to the easy manipulation of the phase transition temperature by changing the AN content in polymer.

The scientific interest in UCST polymers is evident, which increases the fields of possible applications. In particular, the use of RAFT polymerization has become a valuable tool for the preparation of new UCST polymers as well as for the synthesis of complex BCP micelles structures.[8,29] Figure 3, shows the development of UCST polymers, from thermoresponsive properties in solution until formation of self-assembly structures and future materials, processed as film and fibers.
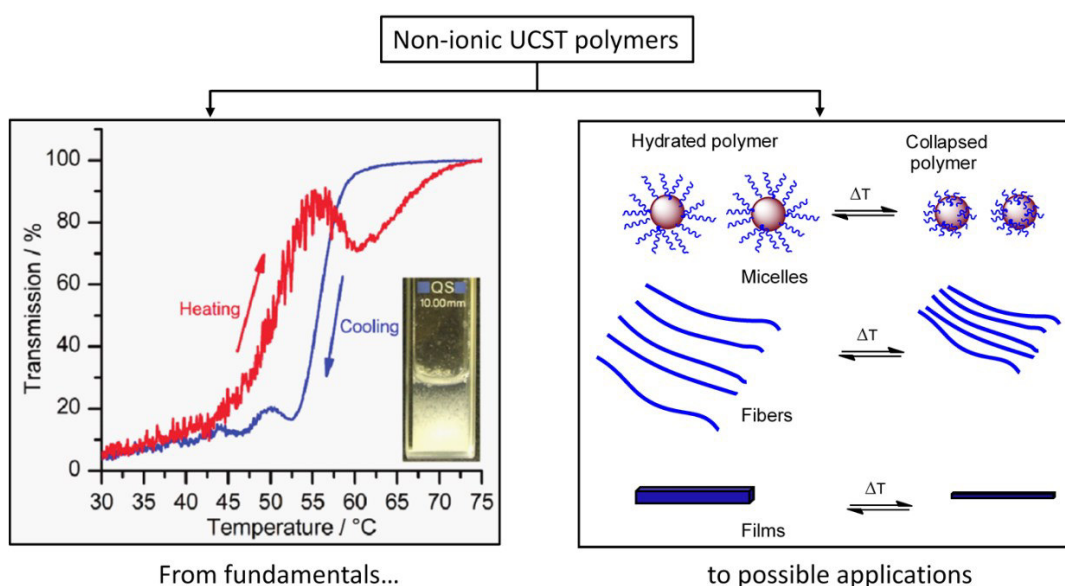


Figure 3: Development of non-ionic UCST polymers from fundamental studies (left-side Figure reproduced from Ref.[7] Copyright from American Chemical Society) to complex polymeric structures (right-side Figure).

Further, the use of UCST polymers with ionic groups could be useful for the preparation of dual or even multi-responsive polymers. For instance, thermo-pH-responsive polymers can be synthesized using proline-based monomers with ionic polyelectrolyte comonomers.[30] Particularly important are the possible applications of these type of system as biocompatible material for medical applications.[30] Therefore, the increased interest of research in this filed over the last years.

Copolymers of AAm and AN could be also the base for the preparation of dual responsive polymers (Figure 4). One method to manipulate the responsivity of the AAm-AN system is the introduction of ionic functionalities through copolymerization with ionizable monomers such as acrylic acid (AAc) or 4-vinylpyridine. The presence of ionizable moieties confer pH responsive characteristics. Which depend on the content of the ionic groups in the polymer. Zhang and coworkers investigated this type of system. They showed the influence of pH on the thermoresponsive behavior of the polymers, proving a high sensibility of the polymers towards very small pH changes.[9] Further thermo- and pH-responsive systems based on AAm-AN, can be obtained by intentional hydrolysis of the UCST functional groups, especially from the AAm units. In dependence of the hydrolysis conditions, different content of ionic groups are achieved.[10] A more detailed discussion on this system is presented on Section 3.2.
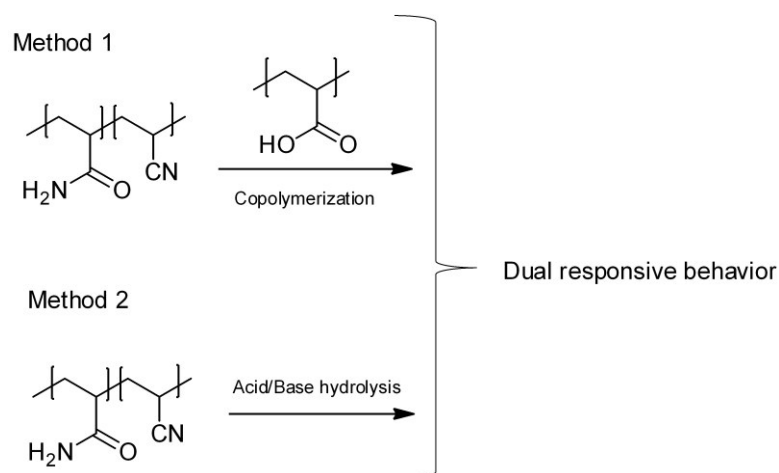


Figure 4: Possible methods for modification of the UCST AAm-AN system to prepare dual responsive polymers in aqueous media.

The incorporation of different interactions such as hydrogen bonding and interelectrolyte interactions provides highly complex polymeric systems using different types of stimuli.

## 2.1.1.2   Thermoresponsive behavior of LCST-type

Despite the continuous development of UCST materials over the past years, polymers of LCST-type still remain as established thermoresponsive system for most applications. PNIPAM has become the best studied thermoresponsive polymer after the first report of its phase transition in 1967.[31] Since this polymer phase separates in aqueous media close to physiological conditions around 32 °C.[31] Phase transition temperatures between room and body temperature is an important requirement for applications in the medical field.[32] As previously mention, the

8

phase transition of thermoresponsive polymers can be manipulated by copolymerization with hydrophobic or hydrophilic comonomers. In the case of LCST polymers, the copolymerization with hydrophilic monomers induce the increase of hydrogen bonding formation, which consequently increase the phase transition temperature of the polymer. The inverse effect is obtained by copolymerization with hydrophobic monomers.[32] There are different parameters affecting the phase transition temperature of the polymers such as concentration, molecular weight, salts, cosolvents, etc.[32–34] For instance, the addition of salt influences the phase transition in dependence of the Hofmeister series. Anions induce polarization of neighboring water molecules, increase surface tension and can bind the polyamide functionality directly. These effects can lead to salting-out or salting-in of the polymer chains, which influences directly the phase transition (Figure 5).[33]
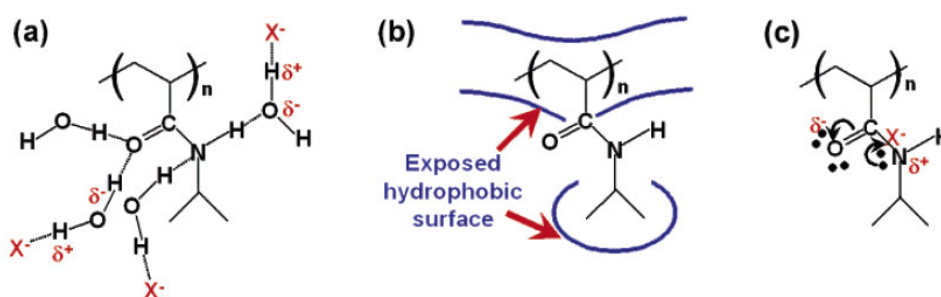


Figure 5: Different type of interactions of anions on the structure of PNIPAM in aqueous media. (a) Polarization of the water molecules by the anion $X^-$ and consequent destabilization of the polymer chains. (b) Hydrophobic hydration of the polymer chains. (c) Direct binding of the anion $X^-$ to the amide functionality. Figure reproduced from Ref [33]. Copyright from American Chemical Society.

The isopropyl groups of PNIPAM induce a strong hydrophobic effect, which enables the ease detection of the phase transition in solution as well as in the solid state. However, it is important to remark that PNIPAM preserves a hydrophilic behavior above and below the LCST. Since above the LCST the isopropyl groups are in contact with water as well as with the polymer chains. Therefore, PNIPAM can be define as "amphiphilic" polymer, which has hydrophilic and hydrophobic groups interacting with water molecules below and above the LCST.[35]

The synthesis of PNIPAM based copolymers and BCPs allows not only the manipulation of the phase transition temperature but also the preparation of different types of new processable polymeric materials.

Copolymerization of NIPAM with acidic or basic comonomers are often used to induce dual responsivity in the obtained polymers. For example copolymers of PNIPAM and AAc showed

a decreased phase transition temperature at pH values below 5.5, since in this case the amide functionalities interacted *via* hydrogen bonding with the protonated carboxylic (RCOOH) groups.[36] PNIPAM based copolymers are in general less sensitive to ionic groups than UCST systems. Based on the thermodynamics (equation 1) and under the assumption of a phase transition in a pure solvent and a pure polymer phase, $\Delta G = 0$. In this case, equation 1 is simplified to $T = \Delta H / \Delta S$; the presence of ionic groups (RCOO⁻) increase the entropic contribution $\Delta S$, however, a strong compensation is achieved by the enthalpic component ($\Delta H$) of PNIPAM. In the case of UCST polymers $\Delta H$ is significantly lower (two magnitudes) than the $\Delta H$ of PNIPAM, therefore, the compensation of the $\Delta S$ contribution (ionic groups) is not successful.[11]

## 2.2  Self-assembly behavior of block copolymers

Self-assembly of molecules is a widespread process not only in chemistry but also in nature.[37,38] Therefore, an increased interest in the understanding and preparation of self-assembled structures has been developed. Block copolymers (BCPs) are synthetic covalently bonded macromolecules, built from two or more mostly chemically divergent polymers.[37–39] The variety and complexity of self-assembly morphologies obtained with BCPs confer these types of materials valuable properties.[40,41] There are different types of BCPs such as di-block, tri-block and multi-block copolymers. However, this work focuses on linear A-B di-block copolymers, which are the most investigated type. These BCPs consist of a sequence of monomers A covalently bonded to a second monomer sequence of type B. Thereby, self-assembly of BCPs produces specific composition patterns, which are commonly known as microphases. Depending on the scale, mesophases or nanophases can also be obtained.[41] In general, the microphase separation of A-B BCP macromolecules is based on the chemical incompatibility of the interacting block segments, inducing the formation of spontaneous patterns on the scale of 10-100 nm.[42–44] Based on the developed phase diagrams of Matsen and Bates, following morphologies are obtained in bulk for A-B diblock copolymers: body-centered spheres, hexagonal closed packed cylinders, cubic gyroids and alternating lamellae (Figure 6).[45]
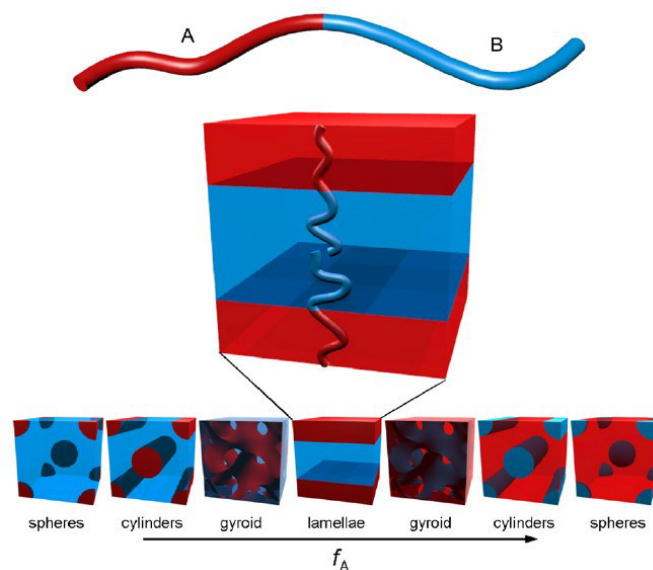
Figure 6: Typical A-B block copolymer morphologies in dependence of the volume fraction of a specific segment. Reproduced figure excerpt from Ref.[38] with permission. Copyright from Elsevier.

Further, BCPs can be used for the preparation of thin films. Kumar and coworkers have shown the importance of self-assembly for the successful immobilization of protein molecules on BCPs substrates.[46] Other important applications have been found in nanoscale templates,[47,48] coatings,[49] and nanoporous membranes.[50,51] There are different parameters affecting the morphology of the systems, such as the copolymer volume fractions, segregation strengths as well as the degree of confinement, which is dependent on the film thickness. Moreover, controlled interactions of the polymer chains with the substrate surface- and free surface-energy during film formation are highly important to prepare defined BCP structures, in particular, when specific functional groups should be oriented along the surface to allow further chemical modification.[43,52]

The self-assembly of BCPs in solution is a complex process that can be influenced by alteration of the interfaces between the block segments or by changing the polymer environmental conditions.[43] For a possible processing of thermoresponsive BCP materials, it is necessary to understand and characterize the self-assembly morphologies that can be obtained under different applied conditions. For instance, in solution the self-assembly of BCPs is highly influenced by the interactions with the solvent/non-solvent.

Amphiphilic BCPs, which are formed from hydrophilic and hydrophobic segments can acquire diverse microphase configurations in aqueous media, to build micelles of different types as well as vesicles.[37,53] These self-assemblies in water as solvent, could be used as effective

encapsulation/delivery systems in the fields of medicine and biology.[54–57] Different parameters, affect the morphology of the BCPs, such as chemical composition, functional groups, molecular weight and the used solvent. The influence of these parameters on the stability of the formed micelles is the base of innovative research and for the development of future applications.[43,58–60]

In the case of thermoresponsive BCPs, copolymers of UCST type of AAm and AN have been established as suitable system for the preparation of novel BCPs. Hence, there are different modifications of poly(AAm-*co*-AN) copolymers that allowed the exploration of new possible applications. For example, di-block copolymers have been developed for the preparation of UCST micelles in aqueous media. Zhang et al. showed the successful chain extension of copolymers of AAm and AN with hydrophobic and hydrophilic block segments *via* RAFT.[8] Furthermore, the same UCST copolymer system was used for the preparation of amphiphilic BPCs with poly(ethylene glycol) as hydrophilic segment. This type of BCPs allowed the encapsulation of doxorubicin as reference drug in UCST-core micelles.[61] Moreover, in a recent work of our group, double thermoresponsive behavior (LCST and UCST type) was observed in BCPs based on AAm and AN polymerized *via* free radical polymerization with an poly(ethylene glycol) macro-azoinitiator. This dual responsive system presented low cytotoxicity, which in the future could make it suitable for biomedical applications.[62] Moreover, a significant progress has been also observed in LCST di-block copolymers with stepwise phase separation transitions. For instance, BCPs of A-B type based on a PNIPAM and a poly(NIPAM-*co*-(*N*-hydroxymethyl) acrylamide) segment, represent a convenient system for the modification of the phase transition temperature in two different cloud points.[63]

Further improvements can be achieve with thermoresponsive BCPs based on PNIPAM, which are often prepared *via* RAFT. In dependence of the block lengths different type of polymer structures are prepared in solution such as micelles or vesicles.[34] Interesting are thermoresponsive BCPs with biodegradable properties, prepared by introducing block segments of PLA.[34] The possible formation of dual responsive systems as well as the preparation of biodegradable polymers makes PNIPAM a candidate for drug delivery applications.[32]

## 2.3 RAFT polymerization

RAFT (Reversible Addition/Fragmentation Chain Transfer) polymerization is a well-known reversible deactivation radical polymerization (RDRP) method, reported for the first time by CSIRO scientists in 1998.[64] The base of this type of polymerization is the fractioning of propagating radicals into active and dormant species by a reversible activation and deactivation process. The RAFT polymerization method has been widely studied due to its vast advantages, since it allows the polymerization of large types of monomers, to produce numerous of functional polymeric materials with defined composition and narrow molar mass distributions.[65,66] Thiocarbonylthio groups (ZC(=S)S-) are commonly used within the RAFT process as chain transfer agents (CTAs).[67] The activity of these unsaturated compounds is based on their reactivity towards radical addition.[68] Figure 7 illustrates typical structures of frequently used CTAs for RAFT polymerization.



Trithiocarbonates    Dithiobenzoates    Dithiocarbamates
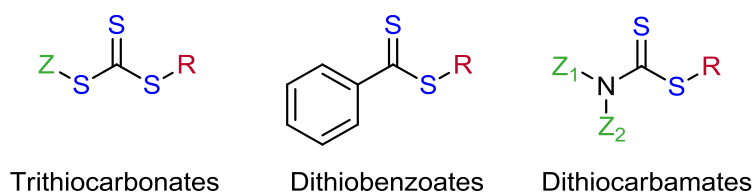
Figure 7: Chemical structures of different types of CTAs used for RAFT polymerization.

The success of the controlled polymerization is dependent on the ability of the chemical rest (R) as leaving radical group, as well as on the chosen substituent Z, which enables the control of the addition-fragmentation rates.[66] The influence of the R and Z groups on the polymerization behavior have been, therefore, extensively studied.[66,68,69] In general, the addition of radicals to the reactive double bond (C=S) is high for Z = aryl, trithiocarbonates, dithioesters and low for Z = dithiocarbamates and xanthates.[67] The chain transfer constant ($C_{tr}$) represents the reactivity of a specific RAFT agent. The relation between the relative rates of chain transfer ($k_{tr}$) with the propagation ($k_p$) are given in equations 2 and 3.[66]

$$k_{tr} = \phi k_{add} \tag{2}$$

$$C_{tr} = \frac{k_{tr}}{kp} \tag{3}$$

Since the RAFT polymerization process is based on the conventional free radical polymerization of monomers, using a convenient CTA, the concentration of radicals is not influenced. Therefore, the polymerization rates should not differ considerably from the free radical polymerization. However, even small incompatibilities between monomer and CTA can lead to retardation reactions.[66,70] The mechanism that allows the controlled polymerization *via* RAFT is shown in Figure 8. The initiation stage is started with the formation of an initiator radical ($I^\bullet$), which propagates to the monomer (M) forming a polymer radical ($P_n^\bullet$). The further propagation allows the addition to the thiocarbonylthio compound (ZC(=S)S-). The following fragmentation of the intermediate radical species provides a polymeric thiocarbonylthio group as well as a new radical ($R^\bullet$). The obtained radical ($R^\bullet$) reacts with further monomer molecules to form ($P_m^\bullet$) as new propagating radical species. The fast equilibration between the polymeric propagating radicals ($P_n^\bullet$) and ($P_m^\bullet$) as well as the dormant polymeric chains induces an equal growth opportunity for the polymer chains and low molar mass distributions.[68,71,70]

1. Initiation

$$\text{Initiator} \longrightarrow I^{\bullet} \xrightarrow{\ \ M\ \ } P_n^{\bullet}$$
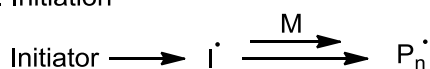
2. Reversible chain transfer

$$P_n^{\bullet} + M \xrightarrow{k_p} \quad S\!\!=\!\!C(Z)\!\!-\!\!S\!\!-\!\!R \underset{k_{-add}}{\overset{k_{add}}{\rightleftharpoons}} P_n\!\!-\!\!S\!\!-\!\!C^{\bullet}(Z)\!\!-\!\!S\!\!-\!\!R \underset{k_{-\beta}}{\overset{k_{\beta}}{\rightleftharpoons}} P_n\!\!-\!\!S\!\!-\!\!C(Z)\!\!=\!\!S + R^{\bullet}$$

3. Reinitiation

$$R^{\bullet} \xrightarrow[k_i]{\ \ M\ \ } R\!\!-\!\!M^{\bullet} \xrightarrow{\ \ M\ \ } P_m^{\bullet}$$

4. Chain equilibration

$$P_m^{\bullet} + M \xrightarrow{k_p} \quad S\!\!=\!\!C(Z)\!\!-\!\!S\!\!-\!\!P_n \underset{k_{-add}}{\overset{k_{add}}{\rightleftharpoons}} P_m\!\!-\!\!S\!\!-\!\!C^{\bullet}(Z)\!\!-\!\!S\!\!-\!\!P_n \underset{k_{-\beta}}{\overset{k_{\beta}}{\rightleftharpoons}} P_m\!\!-\!\!S\!\!-\!\!C(Z)\!\!=\!\!S + P_n^{\bullet} + M \xrightarrow{k_p}$$

5. Termination

$$P_n^{\bullet} + P_m^{\bullet} \xrightarrow{k_t} \text{Dead polymer}$$
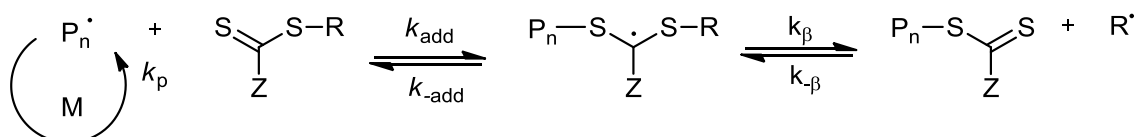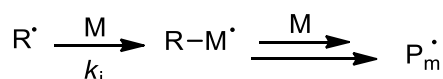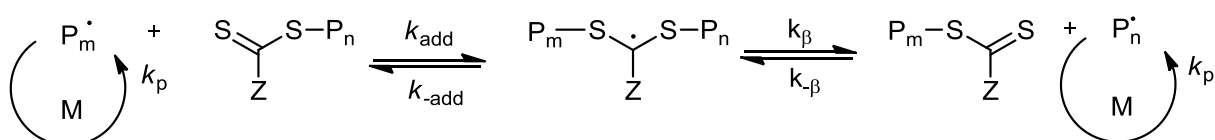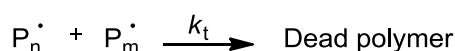
Figure 8: Generally accepted RAFT polymerization mechanism (based on Ref.[69]).

RAFT polymerizable monomers are generally divided in two different groups: the "more-activated monomers" (MAMs) and "less-activated monomers" (LAMs). The MAMs present conjugated vinylic groups with following functionalities: (meth)-acrylates, (meth)-acrylamides and styrenics, whereas the vinylic group of LAMs are characterized by the neighboring to electron rich atoms such as oxygen or nitrogen. The varied reactivity of monomers requires, therefore, a meticulous selection of the CTA. Thus, RAFT polymerization of LAMs for example requires low active CTAs, due to the high reactivity of the propagating radical. In the case of MAMs, these are often polymerized with trithiocarbonates, which present high transfer constants ($C_{tr}$) and are hydrolytically stable.[66,70] However, there are other high reactive CTAs for the polymerization of MAMs, some of them are illustrated in Figure 9.

Figure 9: Diverse RAFT agents for the controlled polymerization of MAMs.

Since throughout the RAFT polymerization process all polymer chains grow with a similar composition, copolymers synthesized *via* RAFT show a homogeneous microstructure in comparison to conventional copolymers.[72] The controlled polymerization of AAm as MAM, has proven to be challenging not only with living but also with controlled polymerization techniques.[73] Therefore, it is important an accurate choice of the CTA and polymerization conditions for AAm monomers. McCormick and coworkers studied intensively the kinetics of the controlled polymerization of AAm *via* RAFT. They observed that high polymerization rates and high polymer conversions were obtained with trithiocarbonate based CTAs in DMSO as solvent.[74] Moreover, fundamental stud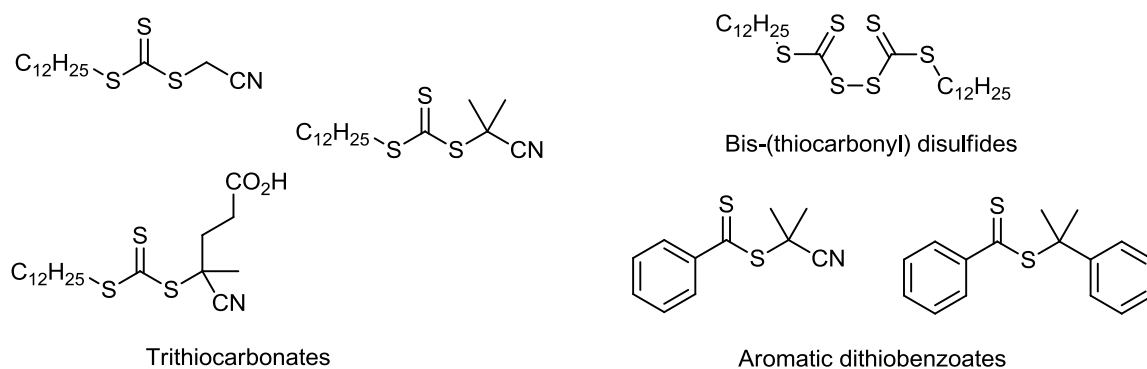ies for the controlled polymerization of UCST polymers carried out by Agarwal et. al., confirmed the work of McCormick. The authors showed the synthesis of well-defined UCST polymers based on PNAGA, using cyanomethyl dodecyl trithiocarbonate (CMDT) as CTA. Kinetic experiments demonstrated a precise molar mass control and successful chain extension experiments.[12]

The importance of a controlled polymerization to form homogeneous chain compositions was observed in thermoresponsive copolymers of LCST-type.[75,76] Mori and coworkers synthesized LCST copolymers of *N*-acryloyl-L-proline methyl ester and *N,N*-dimethylacrylamide *via* RAFT showing sharp phase transition temperatures. However, the same copolymers prepared by conventional free radical polymerization showed extremely broad phase transition curves (~20 °C).[76]

The homogeneous polymer composition is of relevance for the synthesis of UCST copolymers with very different monomer reactivity, such as observed in the systems of poly(NAGA-*co*-St) and poly(AAm-*co*-St). In both copolymers, the use of free radical polymerization induced polymer conversion dependent phase transitions or even hindered the observation of a

thermoresponsive behavior. The study of the poly(AAm-*co*-St) system will be discussed in the Section 3.1 of this work.

In the previous Section (2.2) were described the diversity and the possible application fields of thermoresponsive BCPs. Sequential polymerization process *via* RAFT allows the preparation of well-defined BCPs, based on the monomer and CTA reactivity. For instance, the synthesis of A-B di-block copolymers starts with the preparation of a macro-RAFT agent, end functionalized with the thiocarbonylthio group. Which is used after purification for a further polymerization step. However, the preparation sequence of BCPs is restricted to poly(MAMs)-*b*-poly(LAMs), due to the poor leaving ability of LAMs during polymerization.[70] The synthesis of BCPs, using methyl methacrylate (MMA), represents an example that highlights the importance of the sequence of monomer addition also for MAMs, since MMA forms better stabilized propagating radical species in comparison to styrene or acrylate radicals.[71] Therefore, highly reactive MAMs, such as methacrylate or acrylonitrile should be polymerized at first to form chain extendable macro-RAFT agents.[39,66,77] Figure 10 illustrates a general mechanism for the synthesis of di-block copolymers by sequential RAFT polymerization.
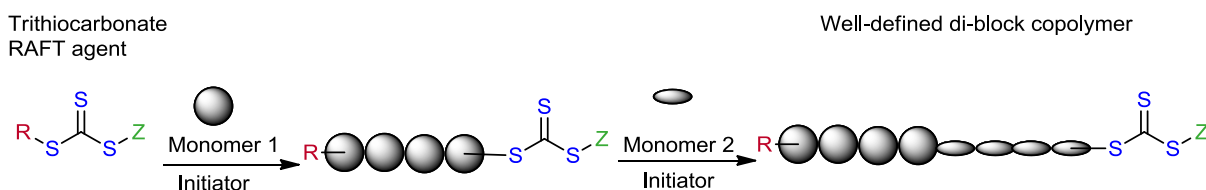


Figure 10: Sequential RAFT polymerization scheme for the synthesis of A-B di-block copolymers.

The diverse advantages of RAFT polymerization are unarguable. Nevertheless, there are different limiting factors that affect the use of this method, such as the difficult preparation of high molecular weights and long polymerization time.[70]

## 2.4 Processing of responsive polymeric materials

There are different types of methods for the processing of polymers, the most important are extrusion and injection molding.[78] The use of these methods allow the production of variable materials, which are of high significance in actual technology. However, there are other processing methods of polymers, which allow the fabrication of complex structures. Film formation and electrospinning represent a part of valuable methods for the preparation of

polymeric filtration membranes, scaffolds, as well as carrier materials.[17,79–81] In the present work, film preparation and electrospinning were the main processing methods of the synthesized responsive BCPs. The formation of different surface area structures, for example porous morphologies were of especial interest.

Polymer films prepared by a dry-casting process require the total evaporation of the used solvent. In this case, the polymer chains entangle to form a solid material. Different film fabrication techniques are based on this type of method, *e.g.* solvent- and spin-casting, freeze-drying and electrospinning.[82] The evaporation of the solvent of a polymer solution over time mostly leads to dense polymer films without porous structures. The film thickness of this type of materials dependent on the type of polymer and the concentration of the solution. In order to obtain porous structures, porogen additives can be used in the polymer solution. These additives can be particles or ice crystals, which can be washed or leached out from the formed polymer film. Another method to induce porosity is based on a wet phase inversion process. Immersion precipitation is one of the most investigated and used membrane formation method.[79] The preparation process and application fields will be describe in detailed in the following part. Important film preparation methods are summarized schematically in Figure 11.
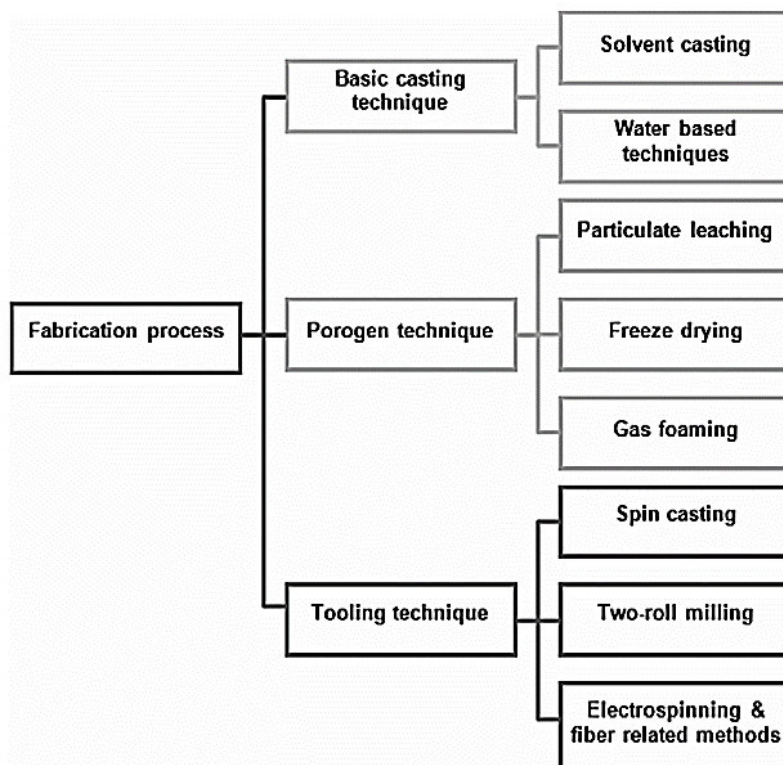


Figure 11: Scheme of typical methods used for the processing of polymers as film material. Figure reproduced from Ref.[82] Copyright from John Wiley and Sons.

## 2.4.1 Non-solvent induced phase separation (NIPS) as processing method for polymers

Membrane formation *via* a phase separation process is based on the separation of a solid from the polymer solution. NIPS is a very versatile processing method due to the possible formation of different porous morphologies. In the NIPS process, a polymer solution of a specific concentration (mostly between 12-25 wt%) is immersed in a coagulation or non-solvent bath, that can contain different types of additives to influence the phase separation behavior. The interactions between the solvent and non-solvent, after immersion of the polymer solution, induces the phase separation.[79] In order to obtain specific membrane structures, different factors should be taken into consideration such as miscibility of the solvent and non-solvent system, coagulation bath (with or without additives), polymer properties and composition of the polymer solution, concentration and environmental casting conditions.[79]

The use of BCPs as polymeric material influences directly the development of a porous structure, due to the self-assembly of the block segments. Moreover, porous morphologies are highly dependent on the amount of a volatile solvent in the polymer solution as well as on the evaporation time before the immersion in the coagulation bath. The phase separation of amphiphilic BCPs after the immersion process is due to the different affinities of the block segments to a specific solvent. For example, the hydrophilic segment will interact with water molecules and the hydrophobic segment will collapse in order to avoid water contact. Mixtures of high and low volatile solvents are frequently used for BCPs, such as a THF/DMF solvent system. The use of THF as highly volatile solvent allows the formation of a dense, pore-free skin or tight pore structures in dependence of the evaporation time.[50] The phase inversion process for the formation of porous membranes based on a BCP is schematically explained in Figure 12.
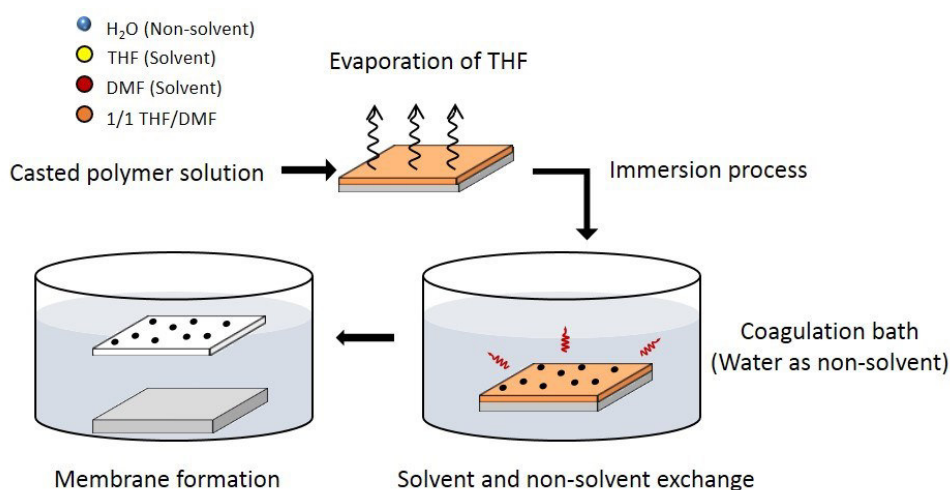
Figure 12: Schema of the NIPS method for the formation of porous structures using amphiphilic BCPs dissolved in organic mixtures of THF/DMF. Immersion of the casted solution in an aqueous coagulation bath allows the formation of porous morphologies.

Based on thermodynamic aspects, an instantaneous or a delayed demixing process can lead to different types of membrane morphology. Moreover, the precipitation rate of the polymer solution in the coagulation bath also influence the obtained structures. Based on the precipitation rate, which is the time between the immersion and the phase separation of the polymer in the non-solvent, two different types of structures are formed. For a slow precipitation process, membranes with a "sponge-like" morphology are obtained, and "finger-like" macrovoids structures are produced in the case of a fast precipitation.[79]

In general, asymmetric membranes prepared *via* NIPS present a thin top layer or "skin" with a porous sublayer structure, which frequently contain different type of void structures. The formation of void or macrovoids diversify the use of membranes from reverse osmosis to ultrafiltration applications.[79]

The formation of porous membranes with responsive polymers is an attractive approach, due to the possible control of water flux using external stimuli such as temperature or pH. The responsive behavior of membranes can be achieved by grafting functional responsive groups to a support membrane,[83,84] or by using responsive BCPs.[16,50] The use of BCP materials are an interesting alternative for the direct formation of responsive membranes. Schacher and coworkers showed the preparation of dual responsive membranes *via* NIPS. The prepared material was able to react independently to temperature and pH stimuli. Moreover, separation properties were observed at different pH for the filtration of silica particles of different sizes (12-100 nm).[85] More recently, pH responsive membranes based on tri-block copolymers

showed a possible molecule attachment by providing thiol functional groups. The authors proved that click chemistry reactions *via* thiol-ene groups, allow the study of a new application field for the covalent bonding of biomolecules.[86] Responsive membranes enable a higher selectivity and permeability in filtration processes. It is important to remark, that the most synthesized BCPs for membrane preparation *via* NIPS are pH responsive polymers with vinylpyridine (VP) moieties. Therefore, further investigations in this field using for example thermoresponsive polymers are require to improve not only the selectivity properties but also to extend the possible applications.

## 2.4.2 Electrospinning as processing method

The processing of polymers as fiber material show a significant amount of applications going from clothing to bio-hybrid materials.[87] Electrospinning have become a versatile method for the processing of a wide range of polymer solutions, which allow the formation of fibers in different diameter ranges. This method was first patented in 1934 by Formhals.[88] However, Reneker presented main scientific contributions in the early 1990s.[89] In general, the electrospinning process uses high voltage to form charged jets of polymer solutions or melts. At a specific voltage, the droplet coming out of the nozzle change its form to what is commonly known has the Taylor cone. The formed jet stretches and loops from the nozzle to the collecting counter electrode. The obtained fibers are the result of a drying process by evaporation of the solvent and instability of the charges in the polymer that repelled each other. Therefore the decrease of the fiber diameter and the length increment.[87]

The simple electrospinning set up consists in the pumping of a polymer solution through a syringe with a cannula (or nozzle), which is used as electrode, placed at a specific distance from the counter electrode (opposite charge) or metal collector. A voltage generator is connected to the electrodes. A schematic example of the used electrospinning set-up for this work is shown in Figure 13.
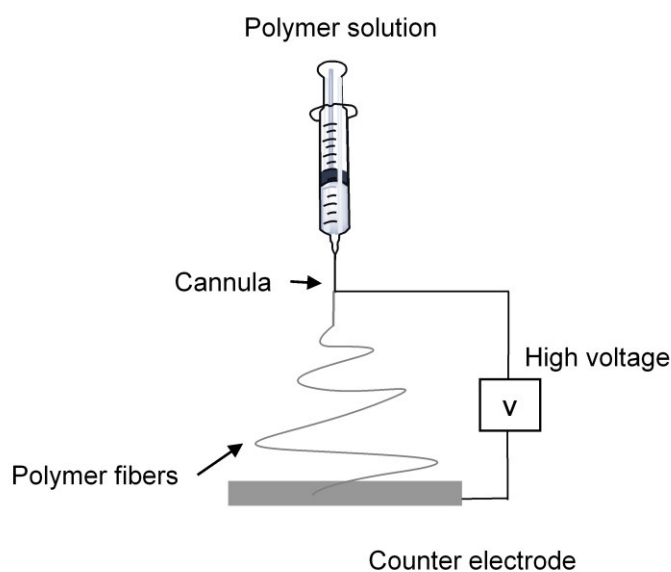
Figure 13: Schematic illustration of the used electrospinning setup to process responsive BCPs.

The electrospinning process is influenced by different working parameters, which are divided in three groups: solution parameters, ambient parameters and process parameters. The successful electrospinning process as well as the possible formation of complex structures is dependent on the control of different processes. In this work, the main studied conditions were based on the solution and ambient parameters.

Solution parameters affecting the electrospinning process are concentration, molecular weight, viscosity, surface tension and conductivity.[90]

The concentration of the polymer solution is important, since for low or very low polymer concentrations only particles are obtained.[91] This process is also known as electrospraying, which is based on the low viscosity of the solution and the high surface tension. By increasing the concentration of the polymer solution, a mixture of beaded fibers or particles with fibers is commonly achieved. A further increase of the concentration allows the formation of well defined fiber morphologies. In general, the increase of the concentration is directly proportional to the increase of the obtained fiber diameter.[90,91]

Further, the molecular weight of the used polymer influences the structure of the formed fibers, since the viscosity of the polymer solution will dependent on the entanglement of the polymer chains. Therefore, if the concentration is maintain constant and the molecular weight is continuously decreasing, bead formation is observed.[90] However, for polymers of low molecular weight different strategies can be applied, such as blending with high molecular

weight polymers or the used of complex electrospinning methods such as coaxial electrospinning.

Solution viscosity represent also a key parameter for the formation of defined and continuous fibers. Viscosity can be manipulated by the variation of the polymer concentration. However, it is also intrinsically related to the molecular weight of the polymer.

Moreover, surface tension and conductivity are other important solution parameters influencing the electrospinning process, since they depend on the type of used solvent composition and on the addition of salts. In electrospinning, the conductivity of the polymer solution is often changed with the addition of salts to obtain thin fiber diameters and to avoid the formation of beads.[90,91]

The environment of the electrospinning process influences as well the morphology and diameter of the fiber material. Humidity is a controllable parameter, which supports the formation of thin and thick fibers in dependence of the humidity condition. Under high humidity conditions, an increase of the fiber diameter is expected, due to lowering of the stretching forces by neutralization of charges at the formed jet. Further, it is also known that high humidity during electrospinning induces surface changes, such as porous structures on the electrospun fibers.[90]

The use of electrospinning to form hybrid materials is of special interest in biology and medical fields, due to the possible encapsulation of active biomolecules or cells into the electrospun fibers, maintaining their activity and viability.[92,93] In this type of materials, the polymer structure serves as matrix that protects and supports the properties of the encapsulated components. For instance, tissue-engineering applications are considerably improved by the incorporation of polymer-protein hybrid materials, since it favors the mechanical properties and the cell proliferation in electrospun scaffolds,[94] since porous fibrous structures are comparable to a natural extracellular matrix.[95]

Considering that electrospinning is a method employed for encapsulation of sensitive compounds and living cells, the use of functional polymers to prepare porous fibers increase the advantages and applicability of these electrospun materials. For instance, fibers based on responsive polymers are advantageous due to the reversible switching of their properties upon external stimuli. Thermoresponsive fibers are commonly investigated in drug delivery systems, especially polymers with a response at temperatures similar to physiological conditions. For example PNIPAM as thermoresponsive polymer is often used in copolymers, BCPs or cross-linked systems to induce responsivity in fibers.[96–100] Tran and coworkers showed recently the fabrication of thermoresponsive composite fibers of PNIPAM and poly(ε-caprolactone) (PCL) for the controlled release of ibuprofen as possible switchable delivery system.[101] Significant

interest has been addressed to the versatility of thermoresponsive BCPs based on PNIPAM, which allow the preparation of polymers with reduced solubility in water, however preserving the responsive behavior. This type of materials are important for the preparation of thermally switchable polymer surfaces,[102,103] actuators,[98] filtration membranes,[104] fibers,[96] etc. To achieve a stable non-soluble thermoresponsive system in water, different strategies can be followed. The first one is the synthesis of BCPs of PNIPAM with a hydrophobic block segment, which induce the desired insolubility in water in dependence of the block length. Typical examples of this system are di- and tri-block copolymers of PNIPAM and PS, prepared *via* RAFT polymerization. Nykänen and coworkers showed an important contribution in the field of filtration of aqueous systems, using thermoresponsive composite membranes, in which the water flux was regulated by an on/off switch behavior in dependence of the temperature.[104] The same NIPAM-PS system was used as well for the preparation of thermoresponsive electrospun fibers. Which were characterized by *cryo*-TEM and sessile drop method. The stability of the obtained fibers in contact with water was highly dependent on the PS block length.[96]

The second strategy to obtain thermoresponsive insoluble polymers is achieved by a crosslinking process. NIPAM can be easily copolymerized with a hydrophobic photo crosslinkable comonomer, which allows for instance the preparation of water stable thermoresponsive films and fibers after the crosslinking under UV-light.[98,105,106] In dependence of the amount of the photo crosslinking comonomer and the crosslinking time, different degrees of swellability are obtained in water.

Stable thermoresponsive fibers of UCST type have been prepared as well by crosslinking copolymers of AAm and AN with *N*-(4-benzoylphenyl) acrylamide as photo crosslinkable comonomer. The crosslinking of the electrospun fibers provided water stability without sacrificing the UCST responsive behavior, which can be manipulated in dependence of the amount of AN. This material with tunable phase transition behavior could be utilized as microactuator in aqueous media.[107]

However, it is important to notice that polymers processed with this type of crosslinking cannot be further modified, since it is an irreversible crosslinking. Moreover, the use of extended exposure to UV-light can induce depolymerization of the prepared materials.[108]

A further strategy for the formation of water resistant thermoresponsive fibers is based on click chemistry. In this type of chemical modification, different steps under heterogeneous conditions are required. Based on this method, Agarwal et. al., showed an easy concept for a quick grafting *via* atom transfer radical polymerization (ATRP) of NIPAM onto copolymer fibers of methyl

methacrylate and 2-hydroxyethyl methacrylate. The grafting procedure is not only of relevance for industrial application but is also transferable to further polymeric fiber systems.[109]

In addition, other responsive fibers have been developed using pH sensitive polymers. This type of materials have found application in the wastewater treatment for the selective separation of organic compounds and oil from water, which represents a cost-effective alternative for water purification processes.[14] Furthermore, biomedical applications are also of relevance, Yuan and coworkers showed the inhibition of inflammation effect using acid responsive fibers loaded with ibuprofen. This material allows the regeneration of damaged cells and hinders the formation of scar defects.[110]

Further, responsive BCPs systems offer an extensive potential to be used as polymeric material for the fabrication of fibers, since different important properties such as self-assembly and responsivity are combined in one polymer. In the case of encapsulation of sensitive compounds, amphiphilic BCPs can offer a controlled diffusion (hydrophilic segment) and stability in an aqueous media (hydrophobic segment). The self-assembly in different morphologies in addition to the responsivity of the material towards temperature or pH enhances the complexity of the system and opens new possible applications.

# 3 Results and Discussion

## 3.1 Effect of compositional homogeneity on the UCST behavior

(This work has been published in *J. Polym. Sci. Part A Polym. Chem.*, 2014, **52**, 1878–1884, with the title: "Importance of Compositional Homogeneity of Macromolecular Chains for UCST-Type Transitions in Water: Controlled Versus Conventional Radical Polymerization" by Beatriz A. Pineda-Contreras, Fangyao Liu and Seema Agarwal.)

Several non-ionic thermoresponsive copolymers of UCST-type can be synthesized with commercially available monomers. Their phase transition temperatures are based on reversible hydrogen bonding, dependent on the variation and content of hydrophobic units in the polymer.[7,28] UCST copolymer synthesis of amide based monomers such as AAm and NAGA with hydrophobic comonomers of AN or St, have shown the adjustment of transition temperatures in a wide and useful range.[7]

In the case of thermoresponsive copolymers, the homogeneity of the copolymer composition becomes important, in particular for the polymerization of monomers with extremely different reactivites.[11,29,76] For instance, copolymers of NAGA and St show broad phase transition temperature curves with high dependence on the polymer conversion.[7] The synthesis *via* free radical polymerization of these copolymers, which exhibit extreme difference in monomer reactivity, induced the formation of inhomogeneous macromolecular chains with different St content. This effect could be the reason for the conversion dependent UCST transition.

Therefore, in this part of the work, detailed studies were carried out to understand the function of copolymer composition on the UCST behavior. The investigated system is based on AAm as model monomer, bearing H-donor and H-acceptor sites. Its copolymers with St should allow the modification of the phase transition temperature, in dependence of the St content in the polymer. Due to the different monomer reactivity ratios between AAm and St, it was considered that the method of polymerization should influence the phase transition of the new UCST copolymer system, according the different polymer chain-homogeneities. Consequently, it was hypothesized that only homogeneous chain compositions should provide defined and reversible UCST behavior of the copolymers. Since copolymerizations *via* free radical polymerization includes typical termination reactions and very different monomer consumption rates, synthesis *via* RAFT as controlled polymerization method, should provide a proper tool for a homogeneous chain growth throughout the entire polymerization process.

The present investigation is highly important for the development of new thermoresponsive polymers systems with sharp and reversible UCST type phase transition temperatures.

### 3.1.1  Synthesis of poly(AAm-*co*-St) *via* free radical polymerization

Copolymers of AAm with different St compositions were synthesized *via* free radical polymerization based on the reference system of NAGA and St.[7] The synthesized copolymers are summarized in Table 1. $^1$H NMR spectroscopy shows the incorporation of AAm and St in the synthesized copolymers. Figure 14 A, shows the characteristic peaks of the comonomer units, which were calibrated to the $D_2O$ solvent signal at 4.79 ppm; $\delta$/ppm = 1.7−2.5 (backbone, -$CH_2$-), 2.5−2.9 (backbone, -CH-), 7.3-8.0 (phenylic protons, -$C_6H_5$). The content of St in the copolymer was calculated based on the integral ratio between the aromatic protons of St and the backbone signals of AAm and St. Moreover, as expected for a free radical polymerization, a high molar mass dispersity (Đ ~ 1.7-2.0) was obtained. Figure 14 B, shows a representative monomodal GPC curve without shoulders of the sample with 10 mol% St in polymer.



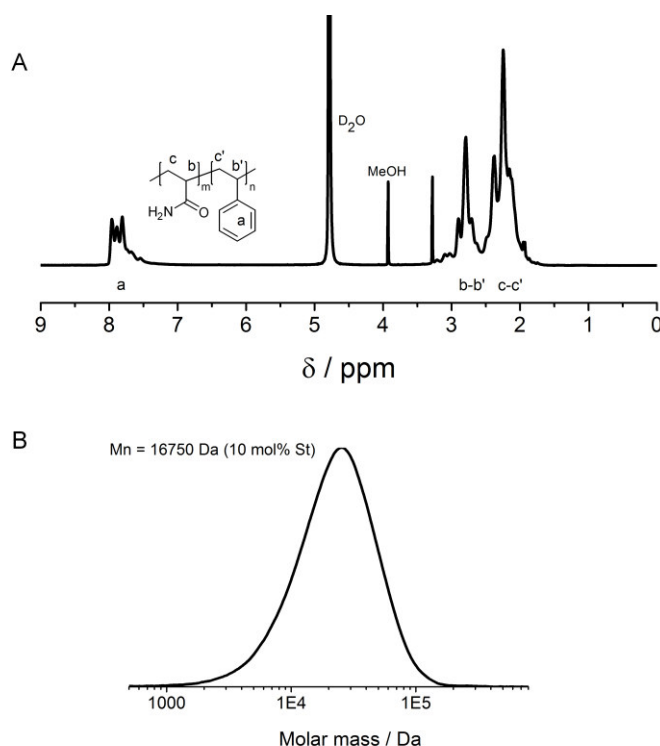Figure 14: (A) $^1$H NMR spectrum of poly(AAm-*co*-St) with 10 mol % St in polymer ($D_2O$ was used as solvent at 80 °C). (B) DMSO-GPC curve of the same copolymer sample synthesized by conventional free radical polymerization in DMSO.

To analyze the solubility and responsivity of copolymers, the prepared samples were tested in water (1.0 wt %) at various temperatures. Polymers with < 10 mol % of St content, were completely soluble, whereas samples with > 10 mol % of St content were water-insoluble at all tested temperatures (20-75 °C). A single sample with 10 mol % (Table 1, entry 3) showed a slight turbid solution, which remained turbid independently of the applied temperature.

The synthesis of copolymers *via* free radical polymerization does not allow the formation of a uniform composition on molecular level, due to inherent termination and transfer reactions. The heterogeneous composition is more pronounced for monomers with very different reactivity ratios, as used in this case (St ($r_{st} = 2$) and AAm ($r_{AAm} = 0.2$)[111]).

Table 1: Free radical polymerization of AAm and St with AIBN as initiator (70 °C). The monomer concentration was set to 3.1 M. Table based on own publication ref. [29], permission not required. Copyright from John Wiley and Sons.

| Entry | St in feed / mol % | St in polymer / mol % | Polymerization time / h | Yield [a] / % | $M_n$ [b] / Da | Đ | Solubility in water (1 wt%) |
|---|---|---|---|---|---|---|---|
| 1 | 4 | 2 | 20 | 64 | 42350 | 2.0 | Soluble |
| 2 | 11 | 8 | 6.5 | 80 | 16400 | 1.8 | Soluble |
| 3 | 12 | 10 | 6.5 | 67 | 16750 | 1.7 | Stable suspension |
| 4 | 13 | 14 | 20 | 60 | 22300 | 1.7 | Insoluble |
| 5 | 14 | 16 | 20 | 62 | 23250 | 1.7 | Insoluble |

[a] Obtained gravimetrically, [b] DMSO GPC

The absence of UCST thermoresponsive behavior in the synthesized copolymers *via* free radical polymerization, irrespective of the St content in the polymer, evidences the requirement of defined polymer microstructures to achieve sharp phase transition temperatures. For this reason, the following studies focus on the synthesis *via* RAFT polymerization to design copolymers of homogenous chain composition.

## 3.1.2 Synthesis of poly(AAm-*co*-St) with variable St content *via* RAFT

Copolymers of AAm and St in different compositions were synthesized *via* RAFT polymerization using cyanomethyl dodecyl trithiocarbonate (CMDT) as RAFT agent (Figure 15). This method allows the preparation of thermoresponsive polymers with sharp and tunable phase transition temperatures. Cloud point (CP) will be in the following defined as the

inflection point obtained from the transmittance curve of the turbidity measurements, which is determined from the first derivative of the cooling or heating curves. Table 2 summarizes the details of the investigated samples.
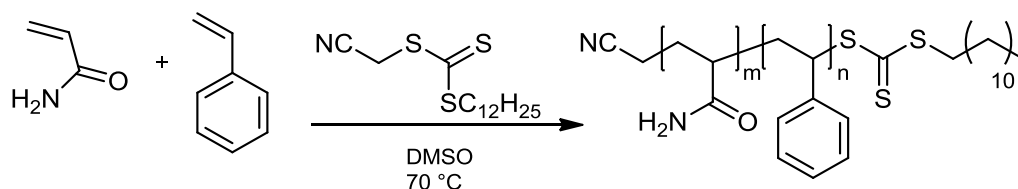


Figure 15: Reaction scheme of the synthesis of AAm and St at 70 °C in DMSO *via* RAFT, using CMDT as RAFT agent.

Table 2: RAFT polymerization of AAm and St with AIBN as initiator and CMDT as CTA at 70 °C. The monomer: CTA ratio was 200:1, the monomer concentration 8.0 M. Table based on own publication ref. [29], permission not required. Copyright from John Wiley and Sons.

| St in feed / % | St in polymer [a] / % | Yield [b] / % | $M_n$ [c] / Da | Đ | CP in water [d] / °C (cooling) |
|---|---|---|---|---|---|
| 11.0 | 10.0 | 99 | 13400 | 1.2 | soluble |
| 12.0 | 12.0 | 99 | 11700 | 1.2 | soluble |
| 13.0 | 14.0 | 99 | 12900 | 1.1 | 49.8 |
| 14.0 | 15.0 | 90 | 13000 | 1.2 | 55.0 |
| 15.0 | 16.0 | 88 | 13300 | 1.1 | 62.0 |
| 16.0 | 22.0 | 70 | 10300 | 1.2 | insoluble |
| 17.0 | 27.3 | 42 | 14700 | 1.2 | insoluble |
| 20.0 | 28.0 | 40 | 10900 | 1.2 | insoluble |

[a] Values obtained from $^1H$ NMR, [b] values obtained gravimetrically, [c] DMSO GPC, [d] polymer concentration 0.5 wt% in water

The $^1H$ NMR characterization of the synthesized copolymer (16% St in polymer) is shown in Figure 16. The spectrum of the purified sample was measured in $D_2O$ at 80°C. The characteristic peaks of the comonomer units were calibrated to the $D_2O$ solvent signal at 4.79 ppm; δ/ppm = 1.8−2.6 (backbone, -$CH_2$-), 2.6−3.0 (backbone, -CH-), 7.2-8.0 (phenylic protons, -$C_6H_5$). The content of St in the synthesized copolymers was calculated by comparing the integral of the phenylic protons to the integral of the backbone protons of AAm and St.

A remarkable decrease of the reaction yields was obtained with increasing St ratio in feed. Further, a higher deviation between the St content in feed and in the copolymer was observed. This could be attributed to the slower incorporation of AAm units under the reaction conditions (Figure 17).
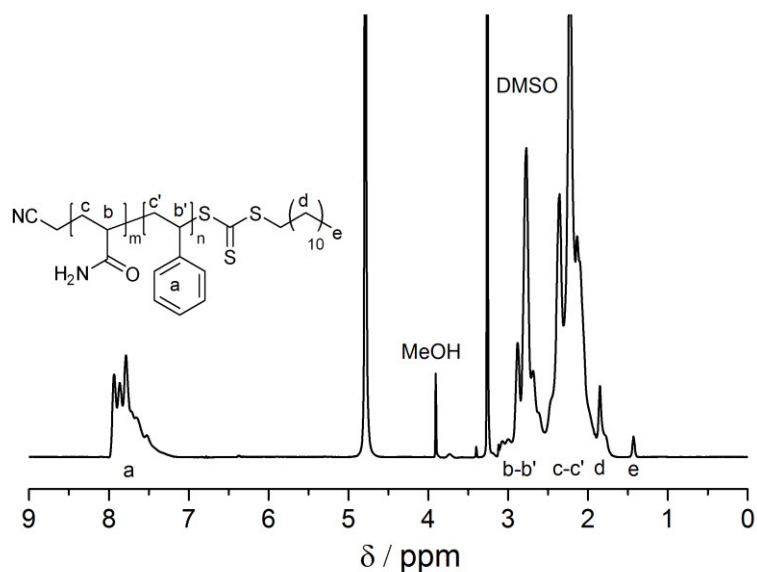
Figure 16: ^{1}H NMR spectrum of poly(AAm-*co*-St) with 16 mol % styrene, synthesized by RAFT. The NMR spectrum was recorded in $D_2O$ at 80 °C (500 MHz). Figure based on own publication ref.[29], permission not required. Copyright from John Wiley and Sons.
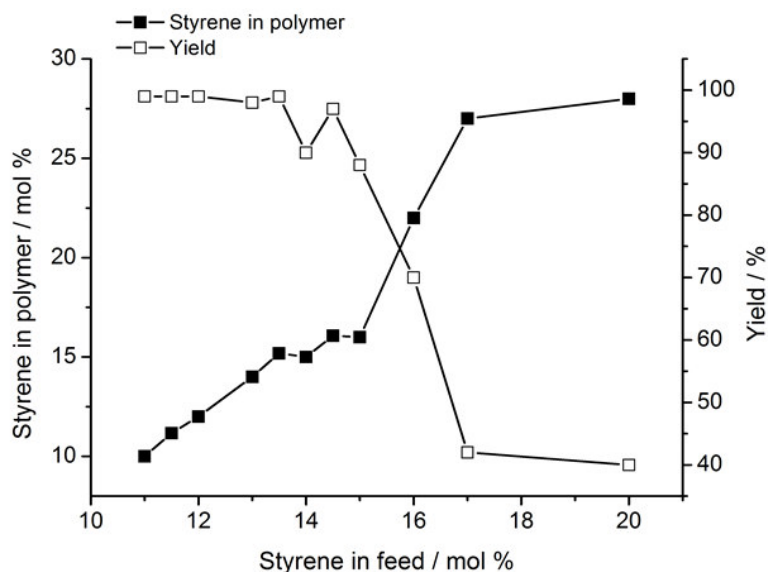


Figure 17: Correlation between St content and the effects on the copolymerization yields.

## 3.1.3 Thermoresponsive behavior in aqueous media and influencing factors

The use of St as hydrophobic moiety allows the variation of the phase transition temperatures of the obtained copolymers. Figure 18 shows sharp and low hysteresis turbidity curves of poly(AAm-*co*-St) samples. The continuous increase of St content in the copolymers induces

the increment of the phase transition temperature in a specific range, from 50 °C (14 mol% St) to 62 °C (16 mol% St). Copolymer samples below 14 mol% St or above 16 mol% St were completely soluble or insoluble in water, respectively (Figure 19).



Figure 18: Turbidity curves of poly(AAm-*co*-St) samples in water (0.5 wt%), synthesized by RAFT with different content of St. Samples were prepared at 70 °C over 1.5 h. Figure based on own publication ref.[29], permission not required. Copyright from John Wiley and Sons.

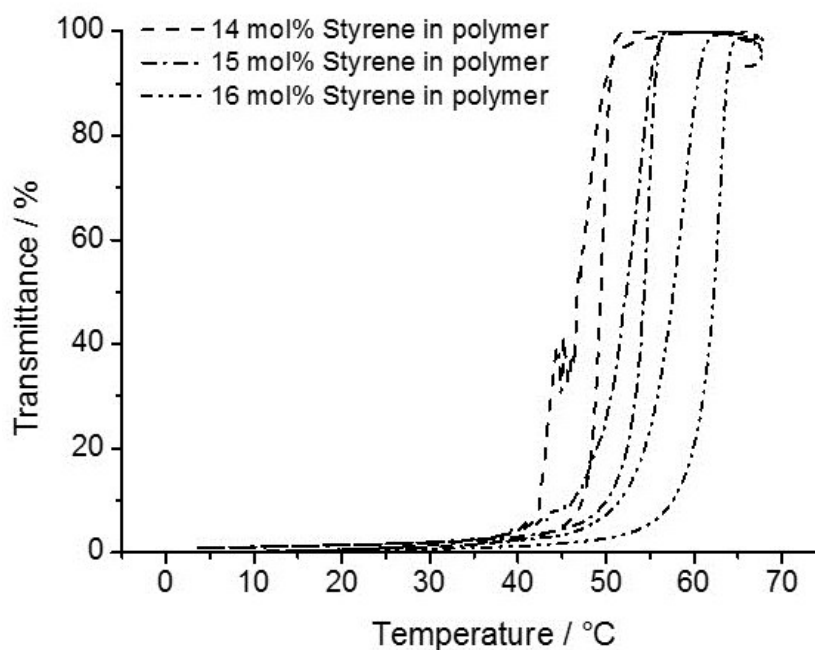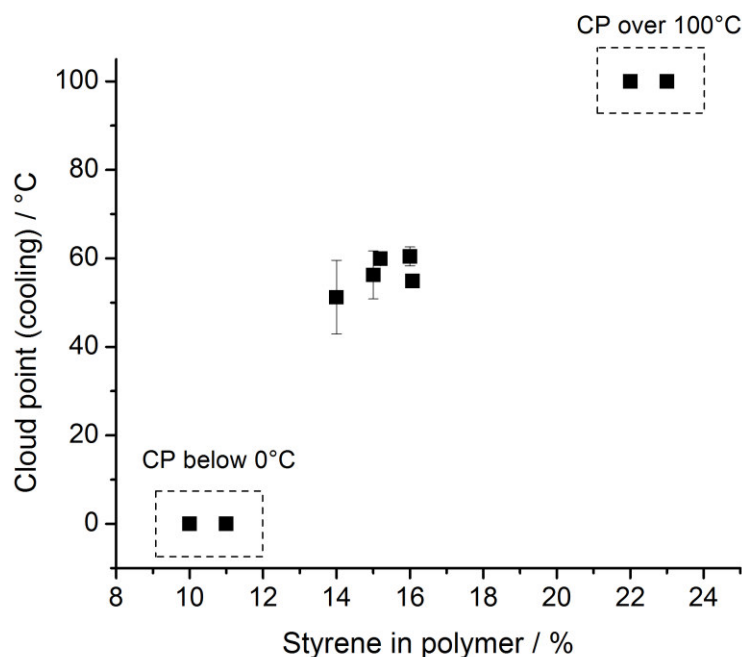Figure 19: Cloud points of 0.5 wt% polymer solutions as a function of St content. The measurement range was 65-3.5°C, with a cooling rate of 1.0 °C/min

The thermoresponsive behavior of the copolymers of AAm and St (Figure 18) could be affected by the used sample preparation method. For example, the applied temperature and the dissolution time in water influence the phase transition, since amide bonds are prone to hydrolysis.[112] The dissolution time (required time to dissolve the polymer) and the dissolution temperature (required temperature to obtain a homogeneous solution) represents important parameters that affect the thermoresponsive behavior of the synthesized copolymers. Therefore, these should be taken into consideration for the sample preparation. For instance, a copolymer sample with 15 mol% of St in copolymer dissolved in aqueous media at 70 °C for 2.5 h was no longer thermoresponsive. A similar behavior was observed by increasing the dissolution temperature from 70 °C to 75 °C over 1.5 h. As previously shown for PNAGA samples, the introduction of ionic groups by hydrolysis of the side chains hindered the observation of cloud points upon cooling and heating.[28] Due to the hydrolysis dependence of the AAm groups to time and dissolution temperature, all samples were prepared under the same conditions at 70°C over 1.5 h for turbidity analysis.

Furthermore, the used cooling and heating rate for turbidity measurements are other important factor that influences the phase transition temperature. In this work, all measurements were carried out with cooling and heating rates of 1 °C/min. The decrease of the measuring rate to 0.1 °C/min induced slight hydrolysis of the polymer samples, due to the prolonged time at temperatures above the UCST. Consequently, the phase transition temperature decreased upon cooling from 57 °C (1 °C/min) to 49 °C (Figure 20). Further, a broad hysteresis was observed, which is the result of larger aggregates formed slowly during the cooling cycle, which could not be dissolved completely in the reversed heating cycle. Therefore, the polymer concentration in solution decreased considerably during the measurement.
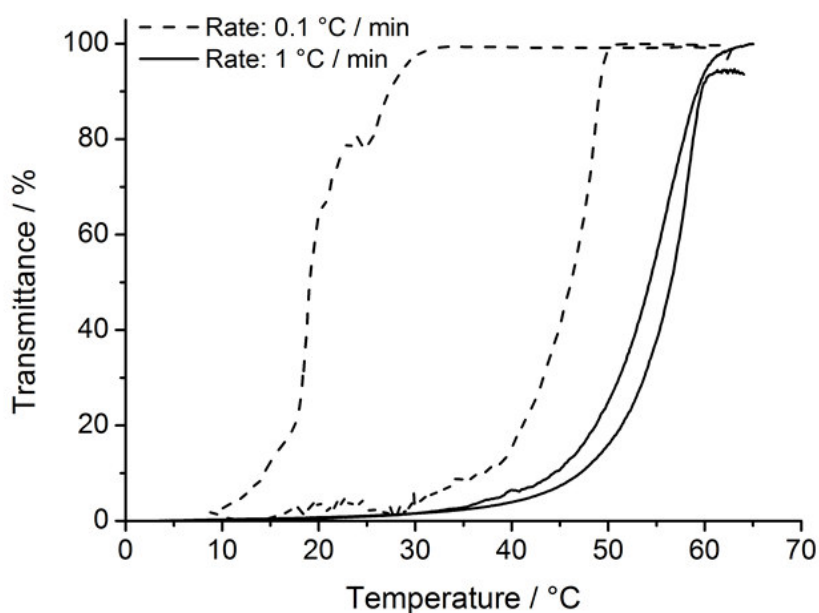


Figure 20: Influence of cooling and heating rates on the UCST behavior of poly(AA-*co*-St) with 15% St in polymer. The measurement range was between 65-3.5 °C. The heating/cooling rate was 0.1 °C/min and 1.0 °C/min, respectively.

As previously mentioned, the cloud point of poly(AAm-*co*-St) samples increased with the St content as well as with the polymer concentration in water. In order to evaluate the responsive behavior of the copolymers in dependence of the concentration, different aqueous polymer solutions were measured (Figure 21). The increase of polymer concentration decreases the entropy of mixing, due to the intensified intermolecular interactions. Therefore, an increase of the phase transition temperature was expected, as observed at the beginning of the curves. Further, it was observed that with polymer solutions between 0.2 wt% and 1.0 wt%, the curves flattened and the cloud points remained stable between 60-66 °C. This indicates that the

polymer-polymer interactions remained almost unchanged by increased polymer concentration. Polymer samples over 1.0 wt% formed "gel-like" structures by physical interactions between the polymer chains, which hindered the analysis by turbidity measurements.

Moreover, turbidity measurements of the different polymer concentrations show sharp phase transition temperatures with small hysteresis from 1.0 wt% until 0.2 wt%, which is an indicative of a homogeneous chain composition. Additionally, the use of lower polymer concentrations (< 0.1 wt%) hinders the fast collapse of the polymer chains, since the polymer-solvent interactions are favored. This leads to a broader phase transition temperatures until complete disappearance of the thermoresponsivity at very low concentrations (0.05 wt%) (Figure 22).
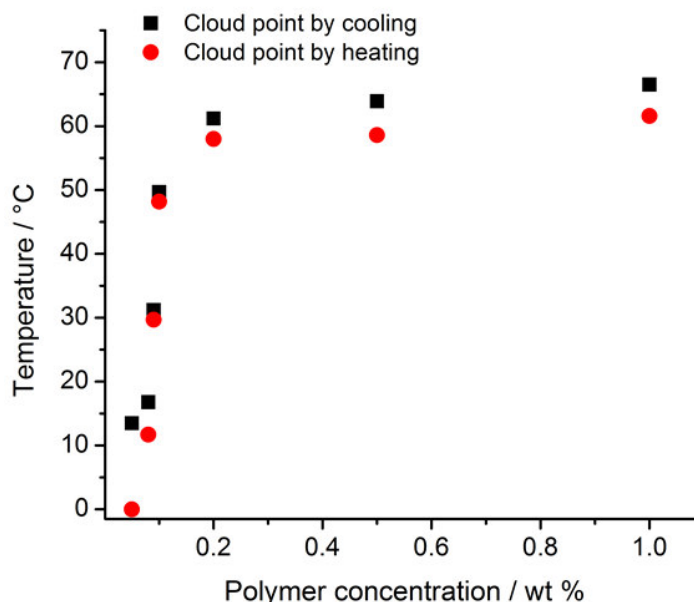


Figure 21: Cloud points of poly(AAm-*co*-St) with 14 mol% of St in polymer as a function of the polymer concentration in water.
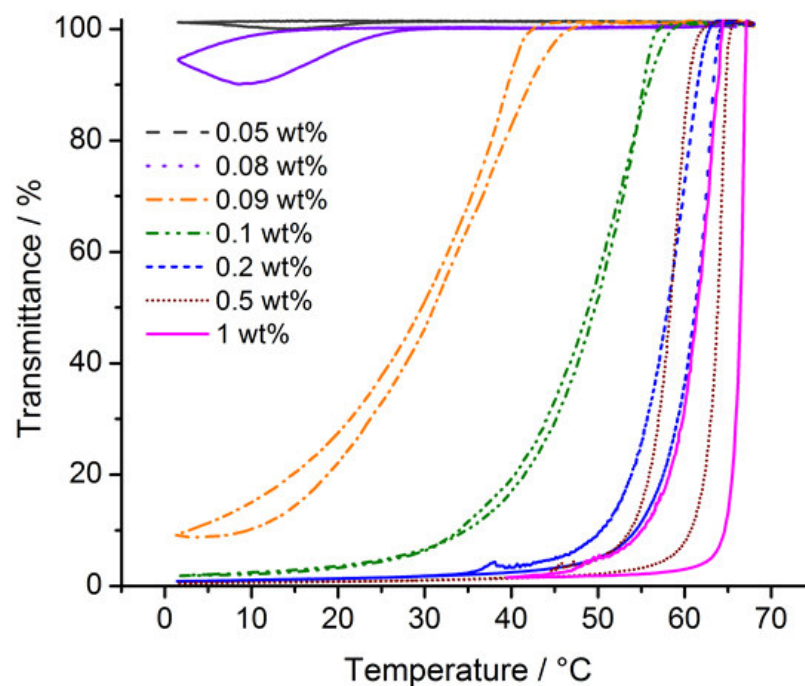
Figure 22: Turbidity curves of different concentrations of poly(AAm-*co*-St) with 14 mol % St content. The measurement range was 65-3.5°C, with a cooling/heating rate of 1.0 °C/min. Figure based on own publication ref.[29], permission not required. Copyright from John Wiley and Sons.

## 3.1.4  Kinetic studies for microstructural characterization

Homogeneous chain growth during polymerization is an important factor for copolymers of AAm and St. The sharpness of the turbidity measurements can be defined as the immediate precipitation of the majority of polymer chains at a specific temperature. Therefore, a homogeneous chain composition is reflected in the observation of a sharp phase transition temperature, which facilitates the manipulation of the cloud points. To get detailed knowledge concerning copolymer composition, kinetic studies were carried out using a monomer : CTA ratio of 200 to 1. The first-order kinetic plots over 600 min confirm the constant rate of growth of the polymer chains (Figure 23), as expected for a controlled RAFT polymerization.
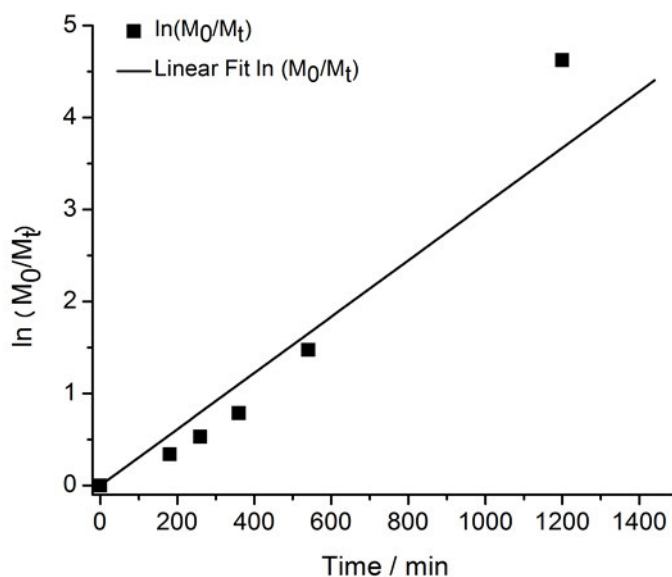
Figure 23: First-order kinetic plots until 600 min of the RAFT polymerization of AAm and St with a monomer : CTA ratio of 200 to 1 and AIBN as initiator. Figure based on own publication ref.[29], permission not required. Copyright from John Wiley and Sons.

Molar masses increased continuously depending on the conversion (Figure 24 A). Number averaged molar masses $M_n$ were lower compared to the theoretical molar masses $M_{n,theo}$. For GPC measurements a calibration with polysaccharides containing maltotriose moieties (Pullulan) were used as standards. Thus, the determined molar masses were not absolute and consequently a deviation of $M_n$ from $M_{n,theo}$ was observed. The copolymer composition and GPC data are listed in Table 3. As expected for a RAFT synthesis, the control of the polymerization increased in course of the reaction time, since the dispersity indices (Đ) decreased from 1.4 to 1.2. The decrease in Đ with ongoing conversion is typical for a Poisson growth. Further, Figure 24 B shows narrow and monomodal GPC curves with increasing the monomer consumption, confirming the controlled character of the polymerization.

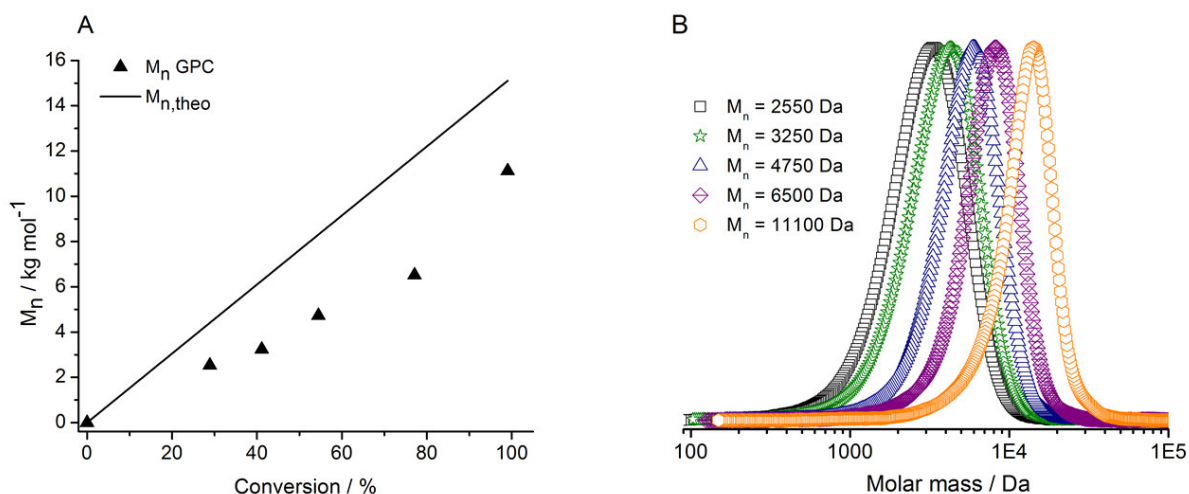Figure 24: (A) Molar masses determined by DMSO-GPC (triangles) as a function of the copolymer conversion. The solid line represents $M_{n,theo}$. (B) DMSO-GPC curves of poly(AAm-*co*-St) synthesized by RAFT polymerization, using a monomer : CTA ratio of 200 to 1 and AIBN as initiator. (B) is based on an own publication ref.[29], permission not required. Copyright from John Wiley and Sons.

Table 3: Summary of reaction times, copolymer composition, number average molecular weights ($M_n$) and molar mass dispersity (Đ) acquired from GPC (DMSO) at different reaction times. RAFT polymerization was carried out with a monomer:CTA ratio of 200:1 and a monomer ratio of AAm:St = 174:26. The concentration was set to 8.0 M with 0.3 equiv. of AIBN as initiator at 70 °C. Table based on own publication ref.[29], permission not required. Copyright from John Wiley and Sons.

| Entry | Time / h | St in polymer / mol % | St in polymer / mg | AAm in polymer / mg | $\ln(M_0/M_t)$ | $M_{n,theo}$ / Da | $M_n$ (GPC) / Da | Yield / % | Đ | CP / °C Cooling |
|---|---|---|---|---|---|---|---|---|---|---|
| 1 | 3 | 21.1 | 676 | 1846 | 0.34 | 4825 | 2550 | 29 | 1.4 | Insoluble |
| 2 | 4 | 21 | 868 | 2372 | 0.53 | 6733 | 3250 | 41 | 1.3 | Insoluble |
| 3 | 6 | 20 | 1267 | 3461 | 0.79 | 8775 | 4730 | 54 | 1.2 | Insoluble |
| 4 | 9 | 15 | 1352 | 5238 | 1.47 | 10942 | 6500 | 77 | 1.2 | 60 |
| 5 | 20 | 12.4 | 1799 | 8591 | 4.62 | 15176 | 11100 | 99 | 1.2 | 55 |

* Initial amounts of monomers: 1.82 g St and 8.88 g AAm

Based on the results listed above, at the beginning of the polymerization process, the microstructure of the copolymers was defined by the fast incorporation of St (37 wt%) in only 3 h, compared to the 21 wt% of AAm. Both comonomers (AAm and St) are integrated in the copolymer structure until the end of the polymerization time. Using the reactivity ratios for St ($r_{st} = 2$) and AAm ($r_{AAm} = 0.2$)[111] combined with the obtained copolymer composition at different reaction intervals, it was possible to predict a possible copolymer microstructure. It

37

suggests that in the early stages of the polymerization long sequences of St units are followed by AAm functionalities. Further, the increasing reaction time favors the continuous incorporation of AAm units, therefore, longer sequences of this monomer are obtained at the end of the polymerization. This type of microstructure is supported by the solubility and thermoresponsive behavior obtained with the copolymers of Table 3 (entries 4 and 5). The samples with low content of St between 15 and 12 mol % were obtained at high yields (77 and 99 %). Therefore, the longer hydrophilic AAm sequences could allow the observation of phase transition temperatures at 60 and 55 °C, respectively.

The importance of a controlled polymerization to obtain sharp phase transition temperatures was demonstrated by increasing the monomer:CTA ratio from 200:1 to 400:1. As observed in Figure 25, poly(AAm-co-St) shows broad phase separation curves when prepared under those conditions. Since the efficiency of the RAFT agent to control the polymerization process decreases at higher monomer:CTA ratios, the compositional homogeneity of the copolymer is reduced. Moreover, the increase of the molecular weight ($M_n$ = 21300 Da) minimizes the influence of the hydrophobic alkyl end group on the UCST behavior. Therefore, copolymers of similar composition but different molecular weight present phase transition temperatures that decreases upon cooling from 30 °C at $M_n$ = 12700 Da to 23 °C at $M_n$ = 21300 Da (Figure 25).
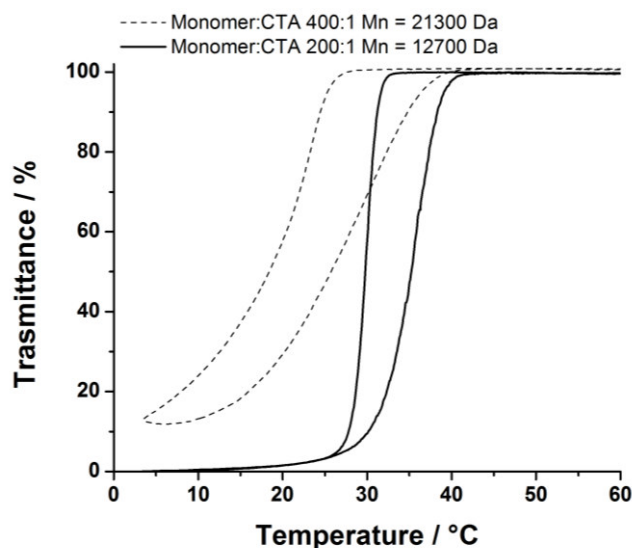


Figure 25: Influence of the monomer:CTA ratio and the molecular weight on the thermoresponsive behavior of poly(AAm-co-St) with 13 mol% St in polymer.

## 3.1.5   Conclusion

Non-ionic UCST copolymers based on AAm and St in different compositions were successfully synthesized *via* RAFT polymerization. The same copolymers prepared *via* conventional free radical polymerization were not thermoresponsive at any temperature. Homogeneous composition of the macromolecular chains represents a key parameter to design thermoresponsive copolymers of UCST type, especially for monomers with highly different reactivity ratios. The copolymers prepared *via* conventional free radical polymerization presented high molar mass dispersities from 1.7 to 2.0, due to the inherent termination and transfer reactions. As comparison, RAFT provided low molar mass dispersities (1.1-1.2) and a homogenous chain composition independent of the polymer conversion, which was proven by kinetic measurements. This indicates that most of the polymer chains grew uniformly with increasing polymerization time.

The studies at different reaction intervals allowed the prediction of possible microstructures of the copolymers, which suggested that St is incorporated very quickly in the copolymer structure, followed by longer AAm sequences towards the end of the polymerization reaction, which increases the solubility in water.

Moreover, the copolymer system of poly(AAm-*co*-St) by RAFT polymerization allowed the manipulation of the UCST behavior in the range of 50-62 °C. The copolymers displayed sharp phase transition temperatures upon cooling and heating. Further, the observed cloud points were dependent of the polymer concentration in water, where the use of low concentrations (0.1 wt%) decreased significantly the cloud point and the sharpness of the turbidity curves.

The present studies showed that the type of polymerization method is very important to synthesize polymers with UCST behavior. The influence of macromolecular compositional homogeneity plays an important role even for LCST polymers, for which sharp phase transition temperatures were only obtained *via* RAFT polymerization in comparison to the broad phase transition observed with conventional free radical polymerization.[76] In the case of UCST copolymers, the compositional homogeneity provided a thermoresponsive behavior of UCST type with a new copolymer system.

## 3.2 Hydrolysis studies and chemical stability of UCST copolymers

(This work has been published in *Polym. Chem.*, 2016, **7**, 1979–1986, with the title: "pH dependent thermoresponsive behavior of acrylamide–acrylonitrile UCST-type copolymers in aqueous media" by Beatriz A. Pineda-Contreras, Holger Schmalz and Seema Agarwal.)

As mentioned in the previous Section (3.1) the reversible thermoresponsive behavior of UCST polymers is based on the hydrogen bonding, which enables in the case of non- ionic polymers an increased stability against changes of pH and salt concentration in the solution. However, there are important criteria to follow in order to assure the successful synthesis and handling of UCST polymers.[27] For instance, the incorporation of ionic groups in the polymer chain during the synthesis or sample preparation can decrease or suppress the observation of the UCST behavior in aqueous media.[28] The hydrolysis process of non-ionic UCST polymers in water represents a main drawback for this type of system, since above the UCST, the polymer is in its soluble state and the functional groups (especially amides) are more prone to be approached by water molecules, which affects the chemical stability of the polymers. The effect of ionic groups on the UCST behavior, formed during hydrolysis, can be counteracted through the addition of electrolytes, as shown by Agarwal et. al., with low molecular weight samples of PNAGA.[28] Nevertheless, there are further issues beyond thermoresponsive and chemical stability in aqueous media, that require improvement in order to increase the possible applications of these materials. For instance, prolonged storage times are often required in implantable devices as well as in the pharmaceutical industry.[113,114] Studies showing the influence of the chemical stability on the thermoresponsive behavior are mostly established in the field LCST systems. For example, copolymers with LCST-pH responsive properties using PNIPAM functionalities, have been studied under varied pH media (pH 3 to pH 10). It was observed, that PNIPAM as homopolymer is unstable in an alkaline environment.[115] Further investigations on the thermoresponsive and chemical stability of LCST systems were carried out by Wang et al.; using PNIPAM BCPs in bleach at different pH media. They observed regenerative thermoresponsive properties after exposure of the samples to NaClO.[116] Otherwise, hydrolysis of polymers can be intentionally carried out to affect the polymer composition. For instance, the controlled hydrolysis of polyacrylamide functionalities to carboxylic acid could possibly form polymers with a pH dependent behavior.[117]

This part of the thesis investigates the effect of pH on the phase transition temperature of UCST copolymers of poly(AAm-*co*-AN). Further, the thermoresponsive and chemical stability of the synthesized copolymers of poly(AAm-*co*-AN) were studied under different conditions. It was
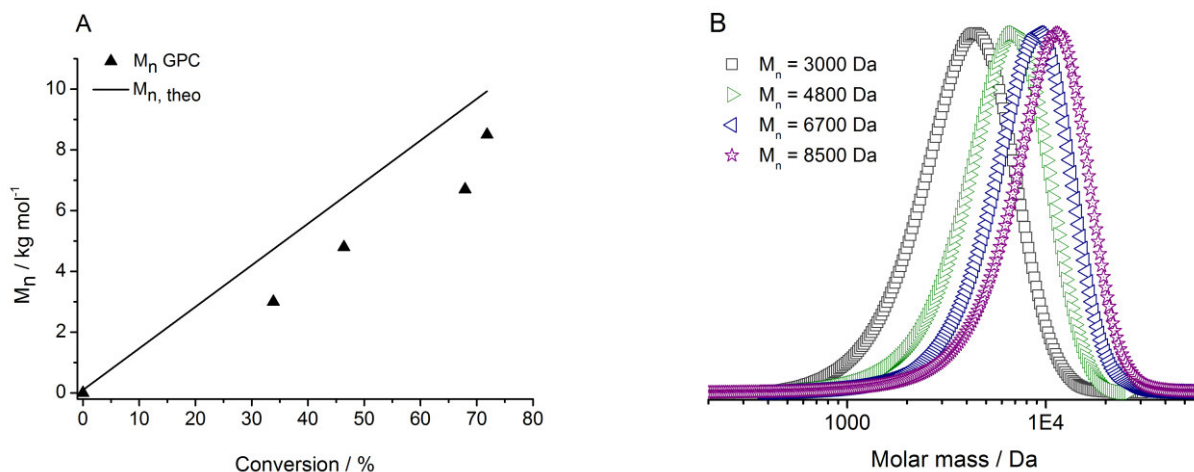
assumed, that this copolymer system should be stable in aqueous media at RT and that relevant changes in the chemical structure or thermoresponsive behavior should appear markedly after the exposure to "extreme" hydrolysis conditions such as high temperatures (> 80 °C) or by the use of acidic (HCl, pH 0) and basic (NaOH, pH 14) environments. Moreover, the effect of formamide as low molar mass additive against hydrolysis was studied under different applied conditions as well.

## 3.2.1 Synthesis and analysis of AAm and AN copolymers

Polymerization of monomers like AAm and AN was successfully carried out using CTAs with high transfer constants. In this regard, trithiocarbonates have been successfully used for controlled polymerizations of AAm and AN to different copolymers (see Figure 26).[73,107]



Figure 26: Reaction scheme of the synthesis *via* RAFT of AAm and AN at 70 °C in DMSO. CMDT was used as RAFT agent.

For the following synthesis, CMDT was used as RAFT agent and the copolymerization process of AAm and AN was followed by kinetic experiments. Figure 27 A shows a continuous increase of the molecular weight with monomer conversion, which is an indicative for a controlled polymerization. The obtained experimental molar masses ($M_n$) were lower than the theoretical expected molar masses ($M_{n,theo}$). This type of deviation is attributed to the standards used for GPC calibration (Pullulan), whereby the GPC values are only relative. Further, whereas the molecular weight distributions were high ($Đ = 1.4$) at the beginning of the polymerization process, with ongoing conversions, these decreased from 1.4 to 1.2, confirming the Poisson growth. The GPC elugrams of all polymers proved to be unimodal with no shoulders or signals of chain aggregation (Figure 27 B). Similar controlled polymerization behavior was observed in UCST-type samples of poly(AAm-*co*-St) (see Section 3.1.4). The RAFT polymerization details of AAm and AN are given in Table 4.

41

## RESULTS AND DISCUSSION



Figure 27: (A) Molar masses determined by GPC (triangles) as a function of the polymer conversion. The solid line represents $M_{n, theo}$. (B) GPC (DMSO) curves of poly(AAm-*co*-AN) synthesized by RAFT polymerization (monomer : CTA ratio of 200 to 1 and monomer ratio AAm : AN = 170 to 30) using AIBN as initiator. Figure based on own publication ref.[10] (open access publication, permission not required).

Table 4: RAFT polymerization of AAm and AN (monomer : CTA ratio 200 : 1 and a monomer ratio AAm : AN = 170 : 30 at 70 °C) with AIBN as initiator and CMDT as CTA. Figure based on own publication ref.[10] (open access publication, permission not required).

| Entry | Time / min | AN / mol % | $\ln(M_0/M_t)$ | $M_{n,theo}$ / Da | $M_n$ (GPC) / Da | Yield / % | Đ |
|-------|-----------|-----------|----------------|-------------------|------------------|-----------|-----|
| 1 | 45 | 15.0 | 0.41 | 5000 | 3000 | 29 | 1.4 |
| 2 | 90 | 13.2 | 0.62 | 6300 | 4800 | 40 | 1.3 |
| 3 | 150 | 12.3 | 1.14 | 9300 | 6700 | 58 | 1.3 |
| 4 | 270 | 11.8 | 1.27 | 9900 | 8500 | 66 | 1.2 |

Figure 28 shows the chemical characterization of the synthesized UCST samples. The FTIR spectrum of poly(AAm-*co*-AN), presented the corresponding bands of AN (C≡N stretching vibration) at 2240 cm$^{-1}$ and AAm (C=O stretching vibration) at 1653 cm$^{-1}$, respectively (Figure 28 A). With regard to the $^1$H-NMR measurements the solvent signal (DMSO) was set at 2.50 ppm and the characteristic peaks of the comonomers were assigned as follow, δ/ ppm: 0.85 (end-group, alkyl-C$H_3$), 1.22 (alkyl), 1.2-1.9 (backbone, -C$H_2$-), 1.9-2.4 (backbone, -C$H$-CONH$_2$), 1.9-2.9 (backbone, -C$H$-CN), 6.7-8 (-N$H_2$) (Figure 28 B).

In order to determine the composition of the polymer samples, a combination of IR data and NMR analysis was required. The determination of the molar content was first carried out using an IR calibration curve, based on the integral ratio from the characteristic bands of AAm (1653 cm$^{-1}$) and AN (2240 cm$^{-1}$) homopolymers, which served as standards. Further, the end

group -C*H₃* (0.85 ppm) from the RAFT agent in $^1$H NMR served as reference signal to obtain the integrals of AAm and AN in the spectrum. Based on the previously determined composition by IR, the content of AAm and AN could be calculated. Further relevant characterization is summarized in Table 5.
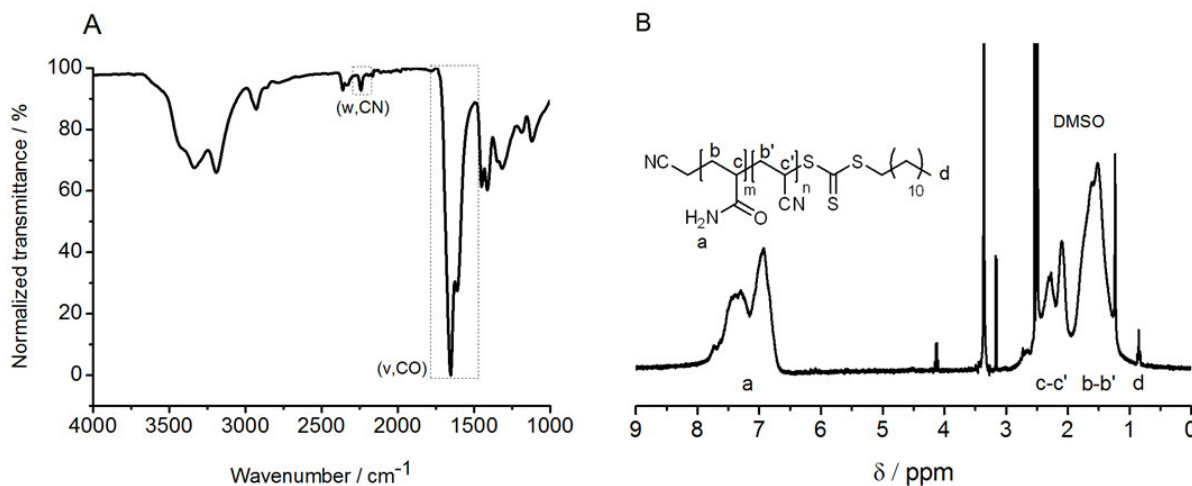


Figure 28: (A) FTIR spectrum of poly(AAm-*co*-AN) with 12 mol% AN content. (B) $^1$H NMR spectrum of the same poly(AAm-*co*-AN) sample in DMSO-*d₆* showing the characteristic signals of AAm and AN. Figure based on own publication ref.[10] (open access publication, permission not required).

Table 5: Samples of poly(AAm-*co*-AN) synthesized *via* RAFT polymerization in DMSO (70 °C). Table based on own publication ref.[10] (open access publication, permission not required).

| Entry | AN in feed / mol% | AN in polymer /mol% | $M_n$[a] /Da | Đ | CP [b] (cooling) / °C |
|---|---|---|---|---|---|
| 1 | 15 | 12 | 20300 | 1.1 | 6 |
| 2 | 20 | 19 | 24700 | 1.2 | 35 |

[a] Values obtained by DMSO GPC; [b] calculated by turbidity measurements at a concentration of 1.0 wt%

Figure 29 shows the dependency of the polymer concentration on the phase transition temperatures. In comparison to the AAm and St system, poly(AAm-*co*-AN) samples were soluble in water even at high concentrations (6 wt%) without observing any gel formation. The solubility of the copolymers in water is dependent on the type of hydrophobic comonomer. Neither PAN nor PS are able to form hydrogen bonds with water molecules. However, the -CN group allows the possible interaction with water as hydrogen acceptor. This behavior classified nitrile moieties not as hydrophilic but as hydroneutral,[118] which explained also the higher solubility of poly(AAm-*co*-AN) copolymers in aqueous media. Moreover, it was observed that the lower hydrophobicity induced by AN in the polymer influenced significantly the sharpness

and phase transition temperature at concentrations lower than 1.0 wt%, since polymer-solvent interactions become strong under these conditions (Figure 29).
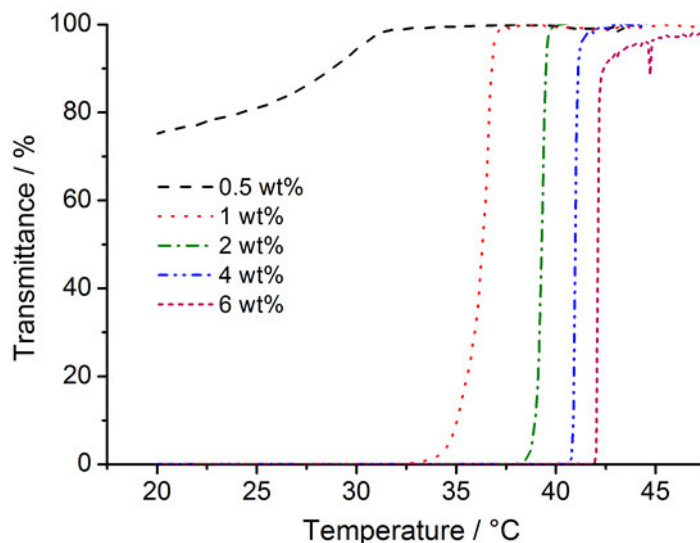


Figure 29: Turbidity curves of poly(AAm-*co*-AN) with 19 mol% of AN in polymer as function of the polymer concentration.

## 3.2.2 Inducing pH dependent UCST behavior

As shown for copolymer samples of poly(AAm-*co*-St), chemical stability is an important issue to be taken into account for non-ionic UCST polymers. The following results show the systematical study of the chemical stability of poly(AAm-*co*-AN) samples under acid and alkaline conditions, as well as the influence of hydrolysis on the thermoresponsive behavior using buffered and non-buffered solutions. Phase transition temperatures of poly(AAm-*co*-AN) are known to remain similar in different pH media (range of pH 5-9).[119] Figure 30 shows the obtained cloud points of a poly(AAm-*co*-AN) sample in different buffer solutions from pH 3 to pH 9. In this case, the observed shifting of cloud points is based on the different ionic strength present in the buffered solutions and not due to the pH media. The influence of ions on the thermoresponsive behavior is well known for LCST and UCST polymers.[33,120] Dependent on the buffer solution different amounts and ion types such as chaotropes and kosmotropes ($Na^+$, $K^+$, $Cl^-$, $OH^-$, citrate ions) are present in the buffer solution. Hence, the variation in ionic strength between 0.1-1 M, present in commercial buffer solutions, was sufficient to influence the phase transition temperatures in a measurable range.[10]
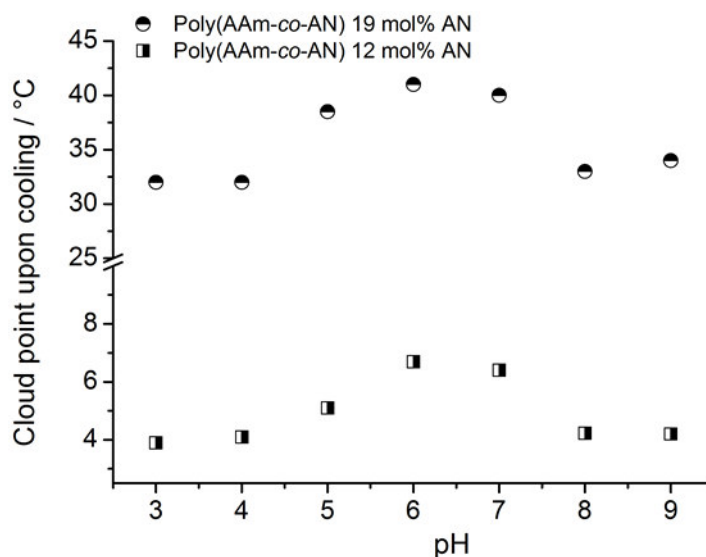
44

Figure 30: Cloud point values for poly(AAm-*co*-AN) with different contents of AN in buffer solutions between pH 3 and pH 9. Figure based on own publication ref.[10] (open access publication, permission not required).

Furthermore, the thermoresponsive stability of poly(AAm-*co*-AN), was dependent on the pH of the chosen buffer solution (Figure 31). For acidic or neutral pH conditions (water or buffer solution) no significant influence on the phase transition temperature of the samples even after 25 days was observed, whereas under basic conditions the UCST behavior was completely inhibited. The hydrolysis of amide groups to carboxylic acid is known to be faster under alkaline conditions.[121,122] Consequently, the disappearance of thermoresponsivity at pH 9 was not surprising. The acidic hydrolysis requires mostly extreme conditions such as high acid concentrations or high temperatures. The possible formation of different intermediates, which is dependent on the protonation of the nitrogen or oxygen atom of the amide, makes this type of hydrolysis very complex.[122] Therefore, basic hydrolysis has been established as preferred method, due to its effectiveness and comparable simple reaction mechanism.
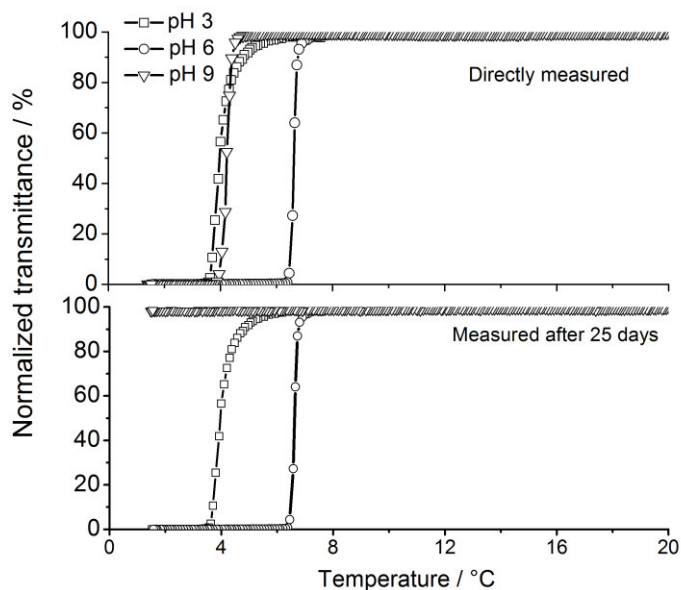
Figure 31: Turbidity curves of poly(AAm-*co*-AN) with 12 mol% AN in polymer in buffer solutions of pH 3, pH 6 and pH 9, after dissolution of the polymer and after 25 days of storage. Figure based on own publication ref.[10] (open access publication, permission not required).

### 3.2.3  Hydrolysis and thermoresponsive stability under acidic conditions

Long term thermoresponsive stability was observed for poly(AAm-*co*-AN) samples under mild acidic conditions (RT and buffer solutions). In order to increase the hydrolysis effect, polymer samples were also analyzed under extreme acidic conditions. Therefore, hydrolysis experiments were carried out in HCl solutions of pH 0 at 40 °C over periods of 1 and 6 h. After 6 h in this type of environment, the thermoresponsivity in water of all tested samples (Table 5) disappeared completely, due to hydrolysis. Only for the polymers with 19 mol% AN, a thermoresponsive behavior after 1 h of hydrolysis could be observed. However, this sample showed a 13 °C decrease of its original phase transition temperature. In this case, the formation of carboxylic groups, due to the hydrolysis of the AAm moieties, was the main factor affecting the thermoresponsive behavior. In water the carboxylic groups are in their ionized form ($pK_a = 4$), therefore, a protonation of the carboxylic ions at pH 3 was necessary to regenerate or increase the thermoresponsivity of the samples, as shown in Figure 32 A and 32 B.

Non-ionic UCST polymers are less influenced by salt addition than ionic or zwitterionic UCST polymers.[11] Hou et al. showed recently that the thermoresponsive behavior of poly(AAm-*co*-AN) samples changed only slightly (decrease of 5 °C) upon addition of different amounts of NaCl.[119] However, after hydrolysis in HCl (1 h), even a low content of ionic groups changed

46

the sensitivity of poly(AAm-*co*-AN) to salt addition. Figure 33, shows that the use of small amounts of NaCl increased the cloud point from 22 to 31 °C (10 mM NaCl). The further increase of salt concentration in the polymer solution improved the solubility and induced a continuous decrease of the cloud points until its complete disappearance.
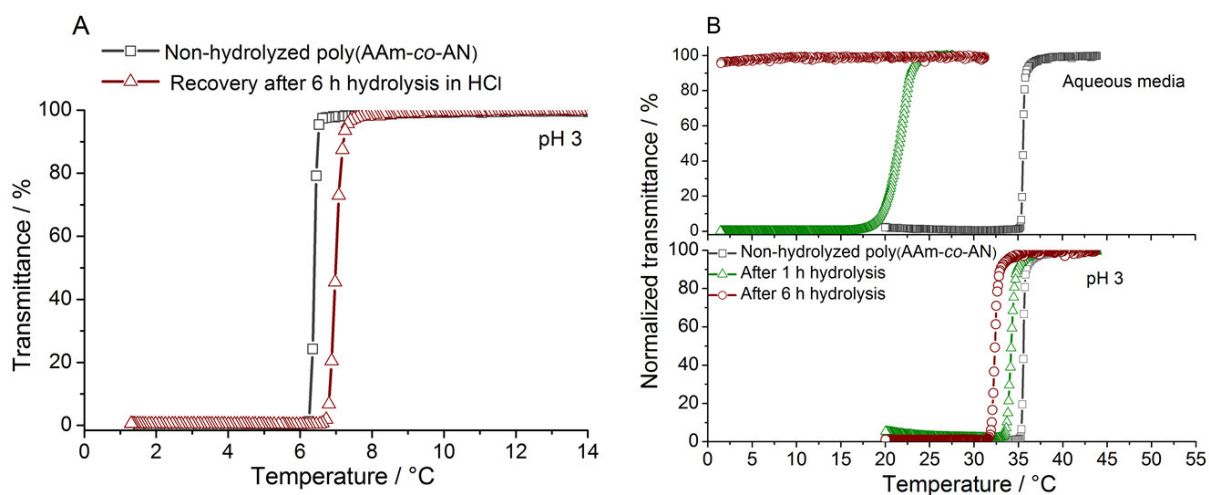


Figure 32: (A) Turbidity curves (upon cooling) of poly(AAm-*co*-AN) with 12 mol% AN before and after hydrolysis in HCl (pH 0) at 40 °C. Measurements were carried out in aqueous solutions of pH 3. (B) Turbidity curves (upon cooling) in aqueous media and at pH 3 (HCl) of poly(AAm-*co*-AN) with 19 mol% AN before and after hydrolysis in HCl (pH 0 at 40 °C). Figure B, is based on an own publication ref.[10] (open access publication, permission not required).
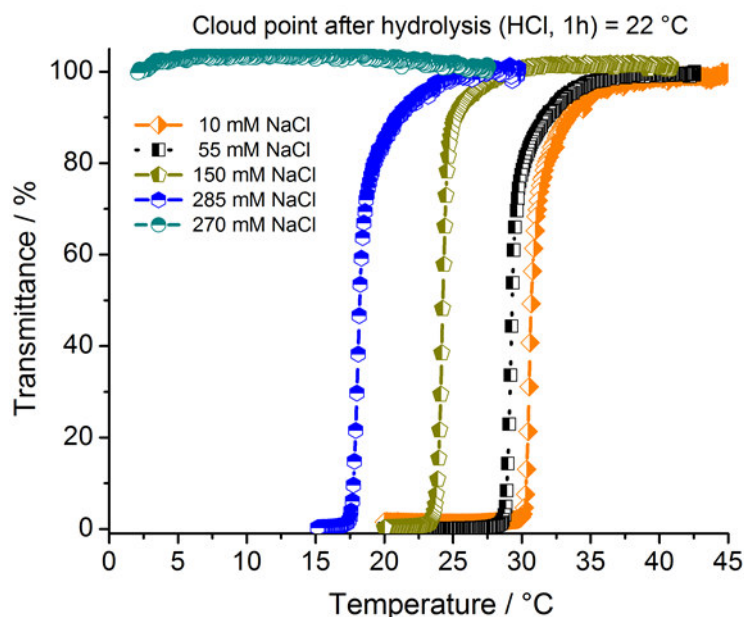
Figure 33: Influence of NaCl addition on the thermoresponsive behavior of hydrolyzed (HCl of pH 0, 1h) poly(AAm-*co*-AN) with 19 mol% AN in polymer.

To confirm the presence of carboxylic groups formed during the hydrolysis process in HCl FTIR and ^{1}H NMR analysis were carried out. After hydrolysis, the FTIR spectra corroborated the typical carbonyl stretching vibration band at 1740 cm^{-1}, which appeared continuously with increasing hydrolysis of the sample as shown in Figure 34 A. The characteristic C≡N peak at 2240 cm^{-1} as well as the amide signals at 1600-1650 cm^{-1} remained without significant changes. Similar results were obtained from the analyzed ^{1}H NMR spectra (Figure 34 B). The hydrolysis of the samples did not affect the characteristic amide signals at 6.5-8 ppm or the RAFT agent end group (–CH$_3$) at 0.85 ppm. Nevertheless, continuous formation of the carboxylic acid proton signal at 12 ppm could be observed by increasing the hydrolysis time. For analysis of the NMR spectra dichloroethane (DCE) (8.6 mg/mL) was used as internal standard. Whereas a strong decrease of the phase transition temperature up to a loss of thermoresponsivity in water was observed by turbidity measurements, the FTIR and NMR spectra remained almost unchanged, indicating that the chemical structure of poly(AAm-*co*-AN) samples remained stable under the applied conditions. Therefore, it was assumed that the content of formed carboxylic groups was too low to be quantified by these techniques.
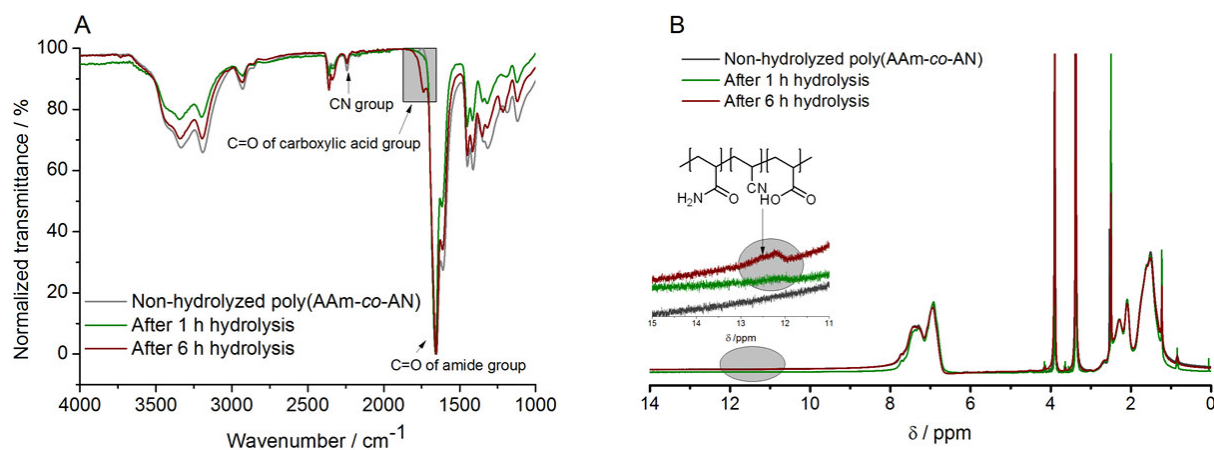
Figure 34: (A) FTIR spectra of poly(AAm-*co*-AN) with 12 mol% AN before and after hydrolysis in HCl (pH 0) at 40 °C. (B) $^1$H NMR spectra in $d_6$-DMSO of non- and hydrolyzed poly(AAm-*co*-AN) with 12 mol% AN, with DCE as internal standard. Samples were hydrolyzed in HCl (pH 0) at 40 °C. Figures based on own publication ref.[10] (open access publication, permission not required).

## 3.2.4 Hydrolysis and thermoresponsive stability under alkaline conditions

The UCST behavior under alkaline conditions (buffer of pH 9) was divergent to the observed thermoresponsive tolerance of poly(AAm-*co*-AN) samples to mild and extreme acidic conditions. The progressive influence of the hydrolysis process on the thermoresponsive behavior is observed in detail on Figure 35. After 14 days, only a decrease of 2 °C was observed on the thermoresponsive behavior of the samples. However, a significant change was obtained with hydrolyzed samples over more than 18 days. At this point the thermoresponsive behavior decreased until a complete disappearance after 25 days.
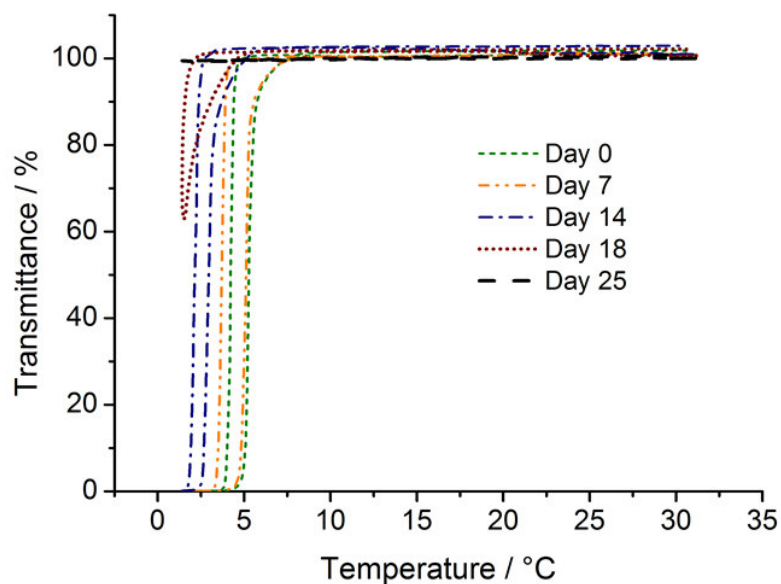
Figure 35: Turbidity curves of poly(AAm-*co*-AN) with 12 mol% AN in polymer showing the progressive hydrolysis of the samples over 25 days under basic conditions (buffer solution). Figure based on own publication ref.[10] (open access publication, permission not required).

As shown for the acidic catalyzed samples, the decrease and loss of the thermoresponsive behavior after treatment at pH 9 (buffer), is an indicative of hydrolysis of the amide moieties to carboxylic acid. In order to investigate the formation of ionic groups as well as structural changes of hydrolyzed poly(AAm-*co*-AN) samples, FTIR and ^{1}H NMR spectroscopy were carried out. Figure 36 A shows FTIR spectra with the characteristic amide bands at 1654 cm^{-1} and 1450 cm^{-1}, respectively, as well as the C≡N stretching vibration band at 2240 cm^{-1}. The measured spectra before and after hydrolysis at pH 9 were almost identical. In the case of the hydrolyzed sample, no C=O stretching vibration of carboxylic acid units appeared. Similar results were obtained from ^{1}H NMR spectra (Figure 36 B), since the proton signals of AAm and AN remained unchanged after hydrolysis. Furthermore, no evidence of the characteristic hydrogen shift of carboxylic acid at ~12 ppm could be observed. The obtained results infer that the content of ionic moieties was too low to be quantified. Figure 37 shows the possible mechanisms occurring during the hydrolysis of poly(AAm-*co*-AN) in buffer solutions of pH 9.
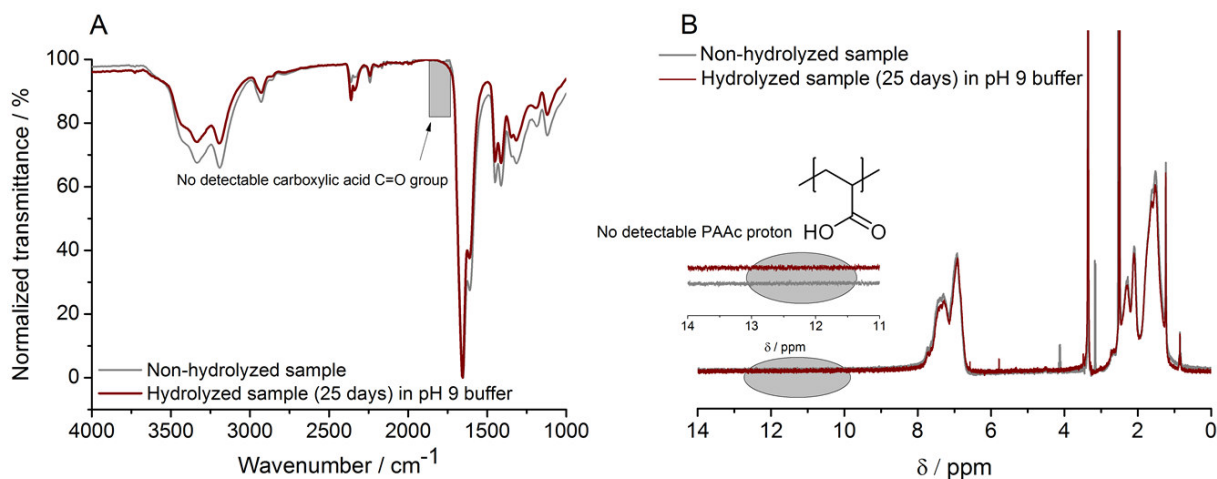
Figure 36: (A) FTIR spectra of poly(AAm-*co*-AN) with 12 mol% AN content before and after hydrolysis in buffer solutions of pH 9. (B) ^{1}H NMR (DMSO-*d₆*) spectra of poly(AAm-*co*-AN) sample before and after hydrolysis in buffer of pH 9. Figures based on own publication ref.[10] (open access publication, permission not required).
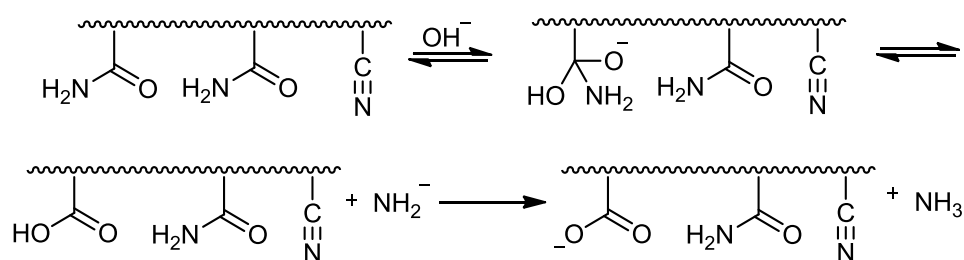


Figure 37: Hydrolysis process of poly(AAm-*co*-AN) at pH 9 (buffer) over long periods of storage (25 days).

The use of buffer medium and RT cause a mild hydrolysis of the samples. Therefore, it was expected that the low content of anionic groups in the polymer could be protonated, using acidic conditions (HCl or acidic buffer), to induce the increase or regeneration of the lost thermoresponsivity in water. Figure 38 shows the progressive decrease of the cloud points of every hydrolyzed sample over 25 days as well as the continuous recovery of the thermoresponsive behavior at low pH.
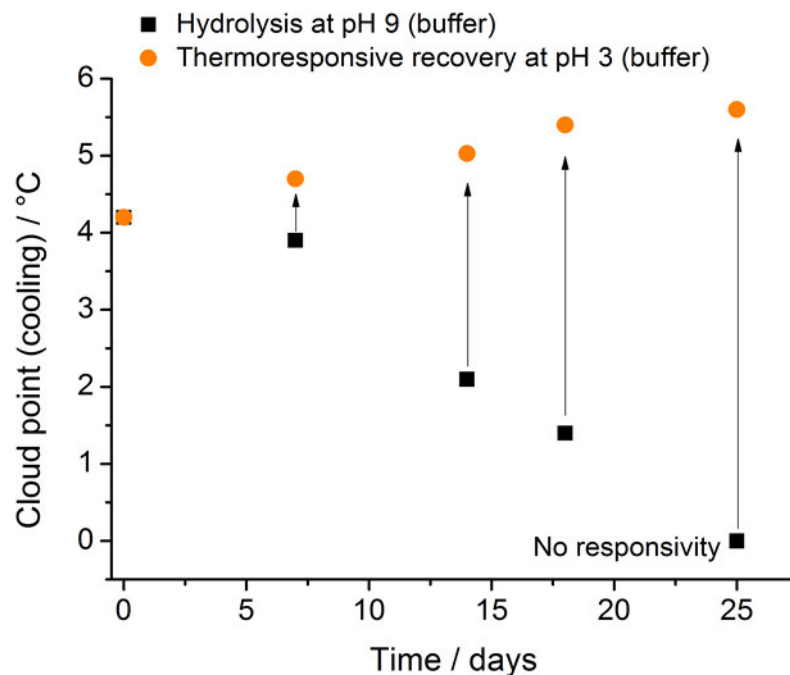
Figure 38: Continuous loss (pH 9) and regeneration (pH 3) of the phase transition temperature of poly(AAm-*co*-AN) samples with 12 mol% AN content. Figure based on own publication ref.[10] (open access publication, permission not required).

In order to increase the hydrolysis of the polymer samples, poly(AAm-*co*-AN) was dissolved in NaOH solutions of pH 9. In comparison to the slow hydrolysis in buffer medium of pH 9, the same sample lost its thermoresponsive behavior already after 10 h of treatment (Figure 39 A). The FTIR and $^1$H NMR analysis revealed that the chemical structure of the polymer sample remained unchanged, as observed for the hydrolysis in buffer at pH 9, which indicated also a very low hydrolysis degree. Therefore, the regeneration of the thermoresponsivity (Figure 39 B) was achieved by adding NaCl (33 mM) as chaotropic salt, which enabled the shielding effect of the formed carboxylic groups. Furthermore, a similar recovery effect was observed by using low pH conditions (HCl and buffer).
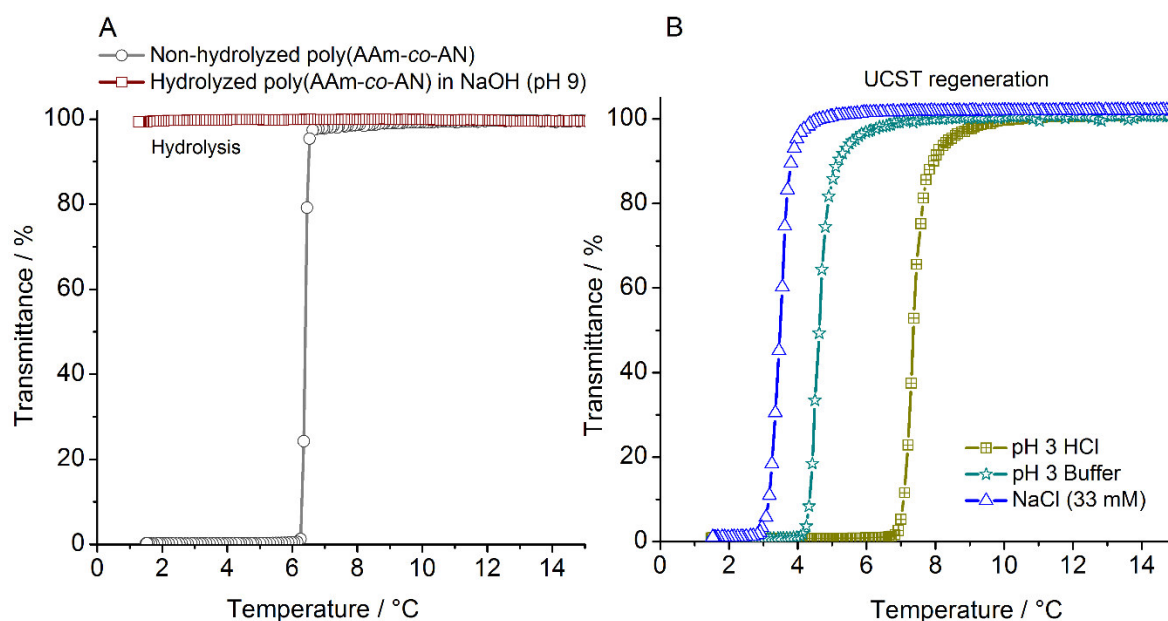
Figure 39: (A) Thermoresponsive behavior of poly(AAm-*co*-AN) with 12 mol% AN before and after hydrolysis over 10 h in NaOH (pH 9). (B) Regeneration of the thermoresponsivity of hydrolyzed poly(AAm-*co*-AN) under acidic conditions and after addition of NaCl (33 mM). Figures based on own publication ref.[10] (open access publication, permission not required).

According to the analytical characterization by FTIR and ^{1}H NMR, the chemical structures of UCST polymers were not strongly influenced either by the use of buffer or mild NaOH hydrolysis at RT. Additionally, this allowed an ease recovery of thermoresponsive behavior under different conditions (Figures 38 and 39 B). To analyze the chemical stability of poly(AAm-*co*-AN) and the impact of higher hydrolysis degrees, harsher alkaline hydrolysis in NaOH solutions (1 M) of pH 14 at 40 °C was carried out. The samples were hydrolyzed under these conditions over 1 and 6 h, respectively. Polymers with lower phase transition temperature (Table 5, entry 1) were hydrolyzed between 39-44 % (determined by elemental analysis). Figure 40 shows the turbidity curves with increasing degree of hydrolysis. Since the content of carboxylic ions increased under these conditions, no thermoresponsivity in pure water could be measured. Therefore, polymer solutions were prepared by adjusting the pH to a value of 3. Thereby, the 1 h hydrolyzed polymer sample increased its phase transition temperature from 6 to 47 °C. Short time settling of the sample at the bottom of the cuvette induced during cooling a slight inhomogeneous turbidity curve at 35 °C. Samples hydrolyzed over 6 h showed a broad phase transition temperature. Moreover, it is important to notice that the thermoresponsive behavior of all polymer samples hydrolyzed under the applied conditions depends not only on the concentration or temperature, but also on parameters like pH and ionic strength.

Table 6 summarizes the dependency between hydrolysis degree and thermoresponsive behavior at pH 3.
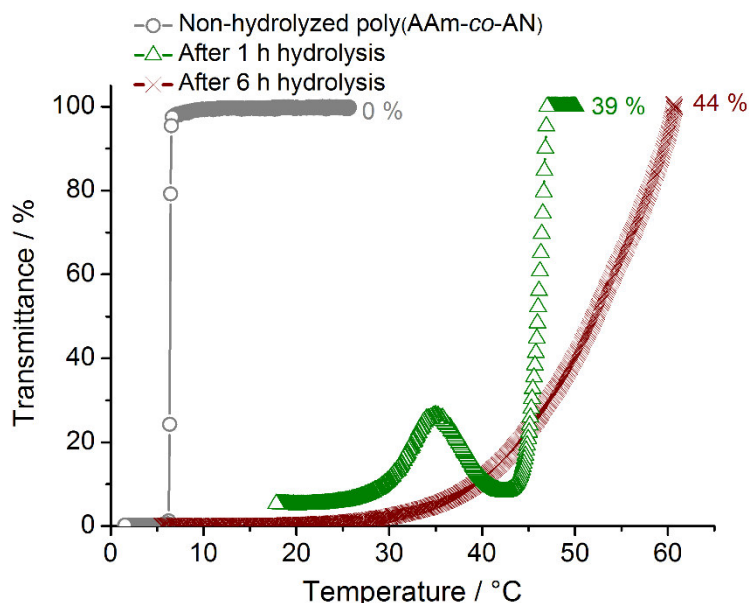


Figure 40: Thermoresponsive behavior (during cooling) measured before and after hydrolysis in NaOH (pH 14 at 40 °C) of poly(AAm-*co*-AN) (12 mol% AN). The analyzed polymer samples were dissolved (1.0 wt%) in water and the pH was adjusted to a value of 3 with HCl. Figure based on own publication ref.[10] (open access publication, permission not required).

Table 6: Hydrolysis degree determined by elemental analysis and the influence on the cloud point of poly(AAm-*co*-AN) samples after hydrolysis in NaOH (pH 14, 40 °C). Table based on own publication ref.[10] (open access publication, permission not required).

| Hydrolysis duration / h | * Degree of hydrolysis / % | * Content of (O) / % | Cloud point (cooling) / °C |
|---|---|---|---|
| 0 | - | 25 | 6 |
| 1 | 39 | 33 | 47 |
| 6 | 44 | 36 | 53 |

*Determined by elemental analysis

The thermoresponsive behavior of the UCST polymers with 19 mol% content of AN (Table 5, entry 2) was modified significantly after hydrolysis in NaOH (pH 14) at 40 °C. As expected, the hydrolyzed polymers were no thermoresponsive in water. Therefore, these polymer solutions were also adjusted to the pH of 3 prior measuring. The turbidity curves shown in Figure 41 A demonstrate the decreased phase transition temperature from 35 °C to less than 10 °C as well as the loss of sharpness of the curves. The decrease of sharpness might be due to the difficult solubility of the sample, leading to a decrease of the total concentration in the solution. Further, for the 6 h hydrolyzed polymer, interpolymer complex "gels" were formed

(Figure 41 B). The obtained physical crosslinked gel was insoluble in acidic media, while it was completely soluble between neutral or basic pH. Therefore, no transition temperatures could be measured.
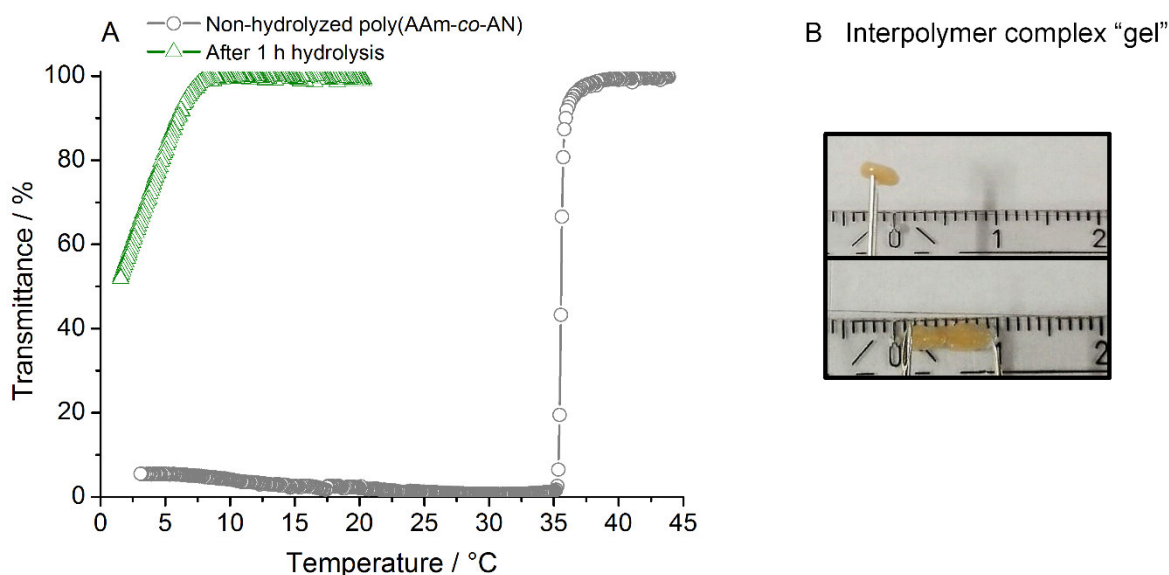


Figure 41: (A) Turbidity curves (during cooling) measured before and after hydrolysis in NaOH (pH 14 at 40 °C) of poly(AAm-*co*-AN) (19 mol% AN). The analyzed polymer sample was dissolved in HCl solutions and adjusted to a pH value of 3 with a total polymer concentration of 1.0 wt %. (B) Images of the formed interpolymer complex "gel" after contact with HCl solution of pH 3 (hydrolysis time of 6 h in NaOH of pH 14, 40 °C). Figures based on own publication ref.[10] (open access publication, permission not required).

The chemical analysis of the hydrolyzed samples in NaOH was focused on the polymers with measurable thermoresponsivity in acidic media (Table 5, entry 1). FTIR spectra of hydrolyzed samples are shown in Figure 42 A. Main differences between the non- and hydrolyzed samples are observed already after 1 h of hydrolysis. The spectra analysis showed an important diminution of the characteristic C≡N stretching vibration band at 2240 cm$^{-1}$ to an almost absence after 6 h. Analogous results were obtained by Kampalanonwat and coworkers by analyzing the hydrolysis of PAN to carboxylic acid moieties in alkaline conditions at 75 °C.[123] The $^1$H NMR analysis confirmed the changes between the spectra before and after hydrolysis (Figure 42 B). The strong basic conditions influenced all signals of the hydrolyzed samples, inclusive the end group signal of the RAFT agent (-CH$_3$) at 0.85 ppm, which was used as reference for previous analysis. For a quantitative analysis, dichloroethane (DCE) was used as internal standard (10 mg/mL). In order to increase the solubility of the samples in DMSO, a specific amount of deutero-HCl (15 µL/mL) was added, since the presence of sodium polyacrylate as side product of the hydrolysis, complicated the dissolving behavior. A decrease

of the amide signal between 6.5-8 ppm was observed with increased hydrolysis. Furthermore, hydrogen-bonding proton signals at lower fields (8.5-10 ppm)[124] were observed as the result of interpolymer complexation between AAm and protonated AAc for hydrolyzed samples, due to the use of deutero-HCl in DMSO-$d_6$.
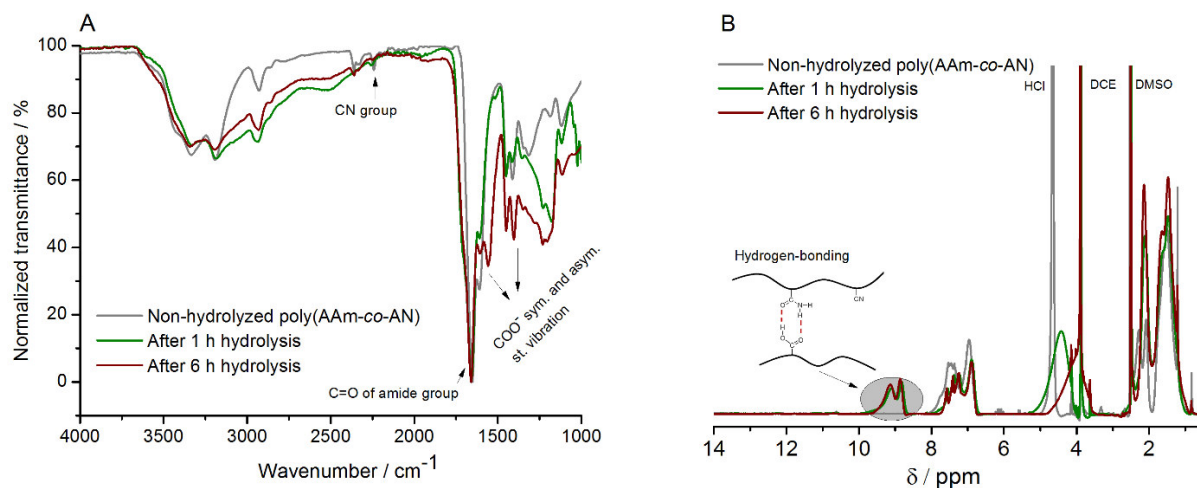


Figure 42: (A) FTIR spectra of poly(AAm-*co*-AN) with 12 mol% AN, before and after hydrolysis in NaOH (pH 14, 40 °C). (B) ^{1}H NMR spectra in $d_6$-DMSO of the non- and hydrolyzed poly(AAm-*co*-AN) with 12 mol% AN using DCE as internal standard. The hydrolysis of the samples were carried out in NaOH (pH 14, 40 °C). Figures based on own publication ref.[10] (open access publication, permission not required).

## 3.2.5  Influence of sacrificial additives on the hydrolysis of UCST polymers

As previously shown, the use of buffers as storage media preserved the responsivity of non-ionic UCST polymers over long periods of time. However, another possible alternative to influence the hydrolysis of UCST samples and the consequent change of the phase transition temperature can be achieved through the addition of sacrificial agents as additive. Particularly, amides with low molar masses, *e.g.* formamide, can hydrolyze faster than the polymer chains of the UCST system. Thus, the responsive behavior can be protected and is not significantly affected by the addition of the sacrificial agent. Thereby, the alkaline hydrolysis of amides yield the corresponding carboxylic acid, based on the nucleophilic attack of the hydroxyl anion at the carbonyl group. The efficiency of this type of hydrolysis reaction depends on the accessibility of the amide moieties. Since the steric hindrance for a polymeric amide moiety is generally higher than for small molecules, the activation energy of the reaction increments inducing a slower hydrolysis of the polymer.[125,126] Therefore, the low molar mass formamide hydrolyzes

under basic conditions or high temperatures more easily and selectively than any AAm or AN unit of the polymer chain, since no steric hindrance or polymer entanglement occurs.

Figure 43 A shows turbidity curves of poly(AAm-*co*-AN) samples with and without addition of formamide as sacrificial agent. Thereby the formamide additive should allow the preservation of the thermoresponsive behavior after NaOH (pH 9) treatment. Therefore, as expected, the sample without formamide additive was no longer thermoresponsive after hydrolysis under basic conditions. However the same sample with formamide showed a sharp phase transition temperature of 4 °C upon cooling, indicating the protection capability of the additive. Furthermore, the addition of formamide could preserve as well the thermoresponsivity of the samples for several hours at high temperatures (85 °C). In comparison, an aqueous solution without sacrificial agent hydrolyzed already after 1 hour at identical temperature (Figure 43 B). This behavior was previously observed for PNAGA exposed to temperatures of 75 °C.[28]
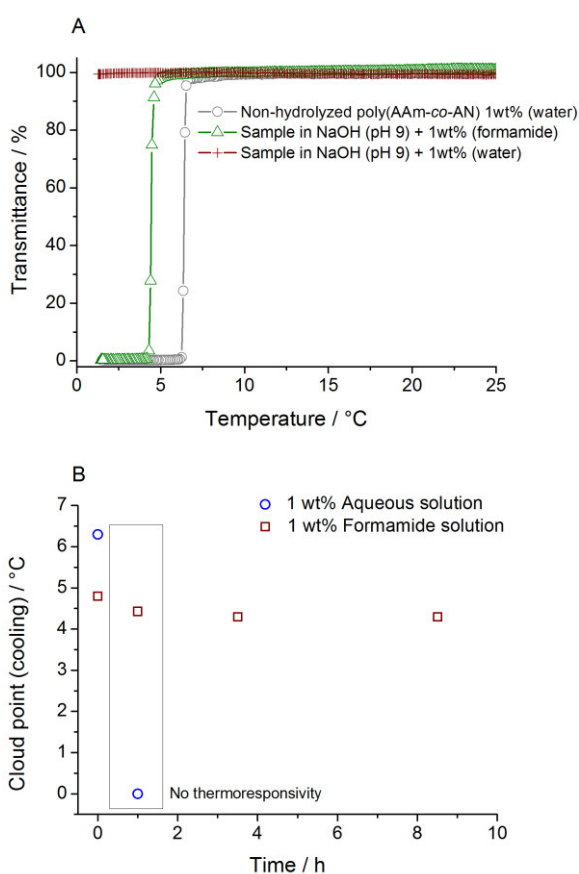


Figure 43: (A) Hydrolysis stability of poly(AAm-*co*-AN) in NaOH (pH 9), with and without sacrificial additive. (B) Stability of the thermoresponsive behavior in aqueous medium of poly(AAm-*co*-AN) at 85 °C in dependence of time, with and without sacrificial additive. Figures based on own publication ref.[10] (open access publication, permission not required).

## 3.2.6   Conclusion

Copolymers based on AAm and AN were successfully polymerized *via* RAFT. The controlled polymerization provided copolymers with low molar mass dispersities and sharp UCST phase transition temperatures in water. The obtained results in this part of the work showed that poly(AAm-*co*-AN) samples present thermoresponsive and chemical stability in neutral as well as in acidic media. The slow hydrolysis process, induced in these environments at RT, allowed the observation of the UCST behavior even after 25 days of storage. In previous studies, it was reported that the incorporation of ionic groups decrease or even hinder the phase transition temperature of polymers of UCST-type like PNAGA.[28] In the case of poly(AAm-*co*-AN), the hydrolysis process induced the formation of a pH dependent UCST behavior. Whereas poly(AAm-*co*-AN) samples remained stable under acidic to neutral conditions, in alkaline medium (buffer or NaOH solutions), the hydrolysis rate of the polymers increased significantly, especially at temperatures of 40 °C. Consequently, the formation of ionic groups induced diminution until complete disappearance of the phase transition temperature in water. However, the increment or recovery of the thermoresponsivity could be achieved by the addition of a chaotropic salt (NaCl) or by the use of low pH aqueous solutions (buffers or HCl), due to shielding effects and protonation of the carboxylic anions, respectively. Moreover, it was observed that the hydrolysis process is importantly decreased by the use of low molar mass amides as chemical additives, especially under alkaline conditions (NaOH of pH 9 at RT) and high temperatures (aqueous solution at 85°C).

The obtained results increased the knowledge on UCST polymers, especially in the field of chemical stability. Moreover, the use of intentional hydrolysis of the poly(AAm-*co*-AN) samples under different conditions (acidic or basic media), enables the exploration of a pH dependent UCST thermoresponsive behavior.

# 3.3 UCST di-block copolymers: From UCST in solution to processability properties

Non-ionic thermoresponsive BCPs with UCST behavior have not been extensively investigated and their processing to films and fibers is at its infancy. Most properties of non-ionic UCST polymers are known in solution. Therefore, the preparation and study of water-stable UCST films and fibers represent a challenging field of investigation, since the material should remain stable in the applied media and at the same time maintain its responsive property. There are different methods to prepare water-stable thermoresponsive materials, such as copolymerization with photo crosslinkable comonomers[98,107] as well as chemical modification methods *e.g.* click chemistry.[109]

Until now, first processable non-ionic UCST copolymers as fiber material have been achieved with post crosslinking under UV-light for long periods of time.[107] However, the use of this type of post treatment method would restrict the use of sensitive components. Since for instance, polymer fibers can be used as carrier material for active agents.[17] A further strategy for water-stable thermoresponsive systems is achieved by BCPs. In this case, a hydrophobic block segment confers the required stability in water without significant influence on the thermoresponsive behavior.

Herein, the focus was set on the modification of water-soluble non-ionic UCST polymers to water-stable and processable UCST materials, which opens new possibilities, due to the vast applicability of polymer films and fibers.

The processing of LCST polymers is well known in the literature.[96,98,105] Therefore, di-block copolymers consisting of a hydrophobic block based on polystyrene (PS) and a hydrophilic PNIPAM thermoresponsive segment, were used as suitable model system for the development of processable non-ionic UCST polymers. The preparation of films and fibers of different surface morphologies increases the probable application fields. Particular interest was focused on the formation of porous materials. In this sense, porous electrospun fibers could serve as carrier for active agents such as catalysts, enzymes, cells, bacteria, etc. For which porosity represents an important parameter to interact with the applied medium.

The implementation of RAFT as controlled polymerization method should serve to design water-stable BCPs with UCST behavior. Fundamental studies in the preparation of non-ionic UCST BCPs *via* RAFT, based on copolymers of AAm and AN as hydrophilic block, offers first tools for processing these polymers.

It was assumed that the incorporation of St as hydrophobic block should induce the required stabilization in water and allow the formation of porous structures, due to the self-assembly properties of the di-block copolymers. The synthesis of BCPs by sequential RAFT polymerization is a common method. Vega-Rios et. al. carried out intensive studies with different monomer sequences for the controlled polymerization of LCST BCPs of NIPAM and St.[127]

Accordingly, it was assumed that the preparation of UCST BCPs should be successful using diverse sequences of monomer addition. Therefore, St as hydrophobic block was polymerized based on two synthetic routes. The first route was based on the use of poly(AAm-*co*-AN) as CTA and the further chain extension with St. The main advantage of this approach is the ability to analyze the thermoresponsivity in aqueous medium before chain extension (Figure 44). The second route implies the use of St as starting macromonomer with a subsequent polymerization of AAm and AN to form the thermoresponsive block. However, this method could influence the homogeneity of the copolymer chains of AAm and AN, since the efficiency of the macromonomer as CTA is assumed to be decreased.
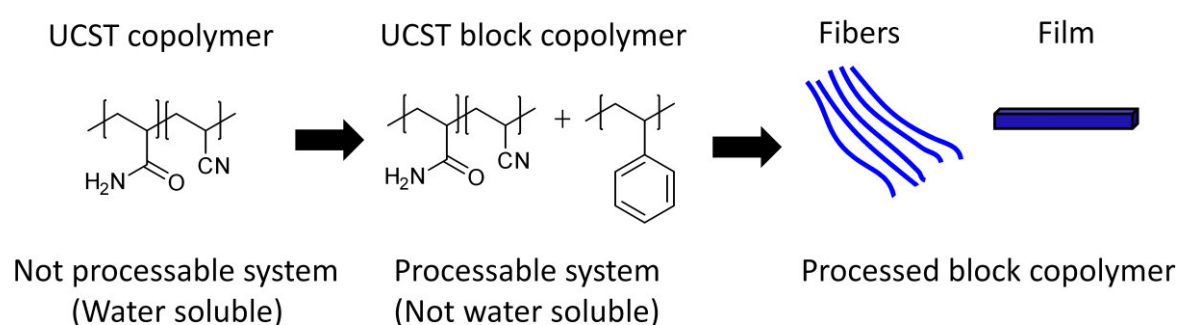


Figure 44: Schematic illustration of the conversion of thermoresponsive water-soluble copolymers to water stable and processable materials.

## 3.3.1 Route I: Synthesis and characterization of BCPs with poly(AAm-*co*-AN) as CTA

UCST BCPs of different cloud points were synthesized using poly(AAm-*co*-AN) as macro CTA to extend the copolymer with St as second hydrophobic block (Figure 45).
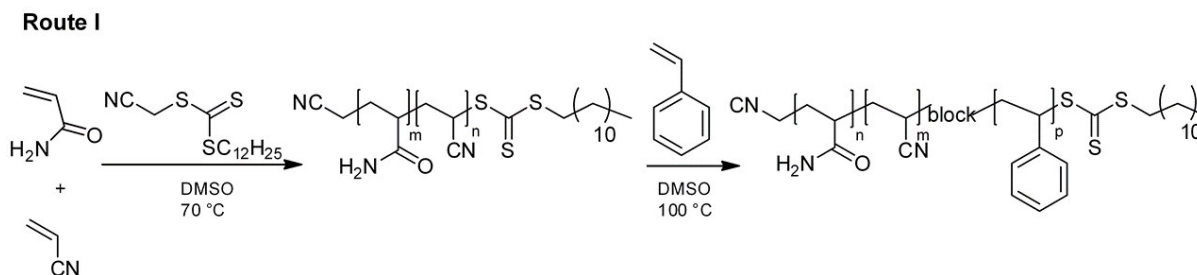
**Route I**



Figure 45: Scheme of the RAFT polymerization of UCST di-block copolymers, with poly(AAm-*co*-AN) as CTA and St as hydrophobic block segment.

The poly(AAm-*co*-AN) CTAs were prepared and characterized as shown in a previous Section (3.2.1). The preparation of UCST BPCs can be influenced by the molecular weight of the used macromonomer, since the addition rate to the RAFT end group is potentially chain-length dependent. This effect was observed by Wong et. al,. in the synthesis of St and *N,N*-dimethylacrylamide (DMA) BCPs. [128]

In the case of UCST BCPs with poly(AAm-*co*-AN) as macromonomer, it could be observed that the incorporation of St led to a tailing and broadening of the GPC curves in DMF (Figure 46). The low molecular weight tailing of the BCP samples suggests the possible presence of dead homopolymer chains produced during the preparation of the macromonomers. This can be due to the oxidizing influence of DMSO used as polymerization solvent on the trithiocarbonate end groups of the RAFT agent.[128,129] Moreover, the broadening of the curves became more noticeable for the macromonomer with the highest molecular weight, showing an increase of the molar mass dispersity from 1.1 to 1.5 (Table 7, entry 2). In this case, the molecular weight of the macromonomer could probably interfere with the approach of the trithiocarbonate end group.[128] In addition, the solvent used for polymerization could also influence the incorporation of St as hydrophobic block, since by increasing chain length the solubility of PS in DMSO tends to decrease. However, DMSO was the only suitable solvent for the synthesized macromonomers.
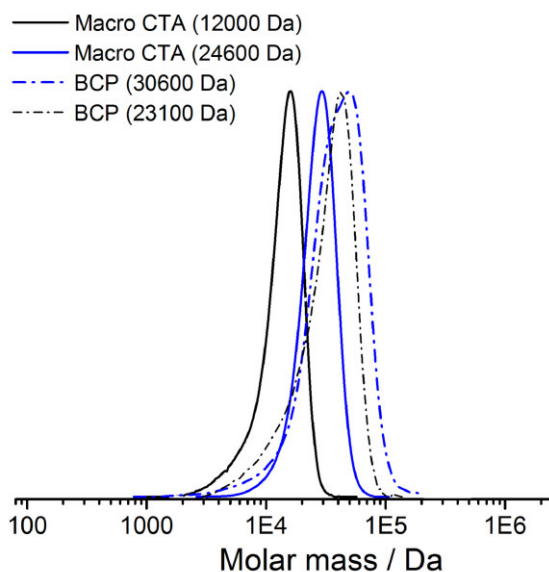
Figure 46: GPC (DMF) curves of poly(AAm-*co*-AN) as macromonomer (Table 7, entries 1 and 2) before and after chain extension with St.

One of the methods to analyze the structure of the synthesized UCST BCPs was ^{1}H NMR at 70 °C in *d₆*-DMSO (Figure 47). The ^{1}H NMR spectra of the synthesized macromonomers showed the characteristic signal at 0.85 ppm of the terminal methyl group –CH$_3$ from the CMDT RAFT agent (Figure 47 A), which was used as reference signal for further analysis of the BCP spectra. Figure 47 B shows the increase of the signals between 6-7.5 ppm, due to the resonances of the aromatic protons, after the chain extension with St. Particularly, the sample of higher molecular weight (Table 7, entry 2), showed the most significant changes. Furthermore, the signals attributed to the CMDT decreased considerably in the region of 0.7-0.9 ppm and 1.2-1.3 ppm, which confirmed the chain extension of poly(AAm-*co*-AN).
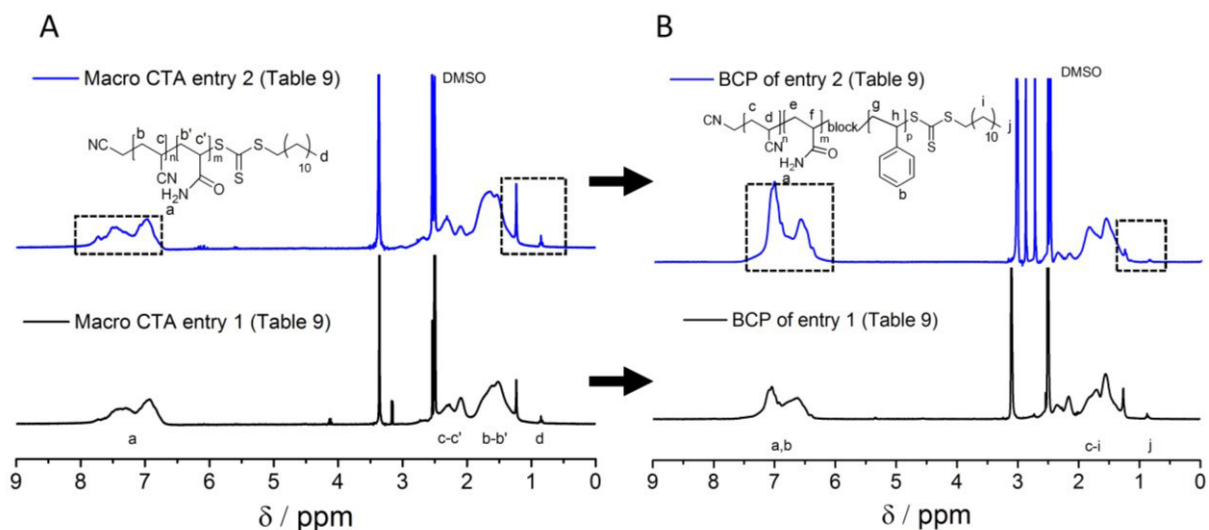
Figure 47: $^1$H NMR of poly(AAm-*co*-AN) as macromonomer (Table 7, entries 1 and 2) before (A) and after chain extension with St (B). The samples were measured in $d_6$-DMSO at 70 °C.

Further, DSC measurements were carried out to analyze the phase separation of the different polymer segments in dry state. The glass transition temperature was evaluated in a temperature range of 25–250 °C with heating rates of 10 °C/min. For the analyzed samples of poly(AAm-*co*-AN-*b*-St) two glass transitions were observed (Figure 48). The first transition corresponds to PS and the second transition to the copolymers of AAm and AN. The increase of St content in the BCP (sample of Table 7, entry 2) induced a slight increment (4 °C) of the exothermal transition temperature from the PS block. Further, as shown in a previous work, the glass transitions of AAm and its copolymers with AN proved the dependence of the chain mobility and the observed hysteresis of the copolymers.[7] The obtained glass transitions of the poly(AAm-*co*-AN) blocks were between ~10 and 30 °C higher than the reported values.[7] This can be explained by the influence of the PS block, which reduced the chain mobility of the samples. The influence was particularly higher for the BCP with the higher content of St.
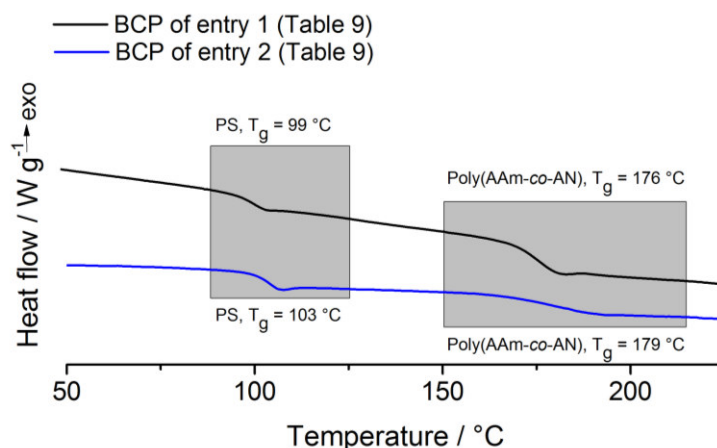
Figure 48: DSC analysis of UCST BCPs. The samples were measured at a temperature range of 25-250 °C at a heating rate of 10 °C/min (Table 7, entries 1 and 2).

Table 7: Summary of synthesized macromonomers of poly(AAm-*co*-AN) and their corresponding di-block copolymers with St.

| Entry | Block [a] 1 (CTA) | Đ | AN in polymer/ mol% | CP point / °C | Block [a] 2 | CP point / °C | St in polymer/ mol% | Đ |
|---|---|---|---|---|---|---|---|---|
| 1 | Poly(AAm-*co*-AN) $M_n$ = 12000 Da | 1.1 | 12 | 6 | Poly(AAm-*co*-AN-*b*-St) $M_n$ = 23100 Da | 8 [b] | 54 | 1.4 |
| 2 | Poly(AAm-*co*-AN) $M_n$ = 24600 Da | 1.1 | 25 | 44 | Poly(AAm-*co*-AN-*b*-St) $M_n$ = 30600 Da | 25 [c] | 61 | 1.5 |

[a] Values obtained by DMF GPC; [b] low concentration (0.1 wt%); [c] low concentration (0.125 wt%) in a water : THF (50:50 % v/v) mixture.

## 3.3.2 Thermoresponsive behavior of BCPs of Route I in solution

Turbidity measurements were carried out to study the responsivity of the synthesized BCPs. Figure 49 shows the thermoresponsive behavior after chain extension with St (Table 7, entries 1 and 2). In both BCP samples, completely reversible curves upon cooling and heating could be observed. The BCP of entry 1 (Table 7), showed a relative broad hysteresis in water. The change of the polymer structure and decreased chain mobility are factors that influence the hysteresis of the samples.[7] Moreover, the concentration is a further parameter affecting the UCST behavior. Due to the increased hydrophobicity, turbidity measurements were only possible by the use of dilute solutions (0.125-0.1 wt%). In this concentration range, the macro CTA based on poly(AAm-*co*-AN) (Table 7, entry 1) is no longer thermoresponsive, since concentrations up to 0.5 wt% in water are required for the observation of the phase transition temperature of this copolymer (Section 3.2.1).

In the case of BCPs with higher hydrophobic content (Table 7, entry 2), the solubility in water decreased considerably. Therefore, turbidity measurements could not be carried out in pure aqueous medium. The solubility of the BCP was achieved in 50 vol% THF-water mixtures. The THF solvent was used to dissolve the PS block selectively, allowing the preparation of homogeneous solutions for turbidity measurements. Due to hydrogen bonding interactions between the amide functional groups and the THF molecules as well as the reduced polymer concentration, the cloud point of the BCP decreased to 25 °C in comparison to the used macromonomer (CP = 44 °C in water). However, the polymer sample showed sharp phase transition temperature curves upon cooling and heating.
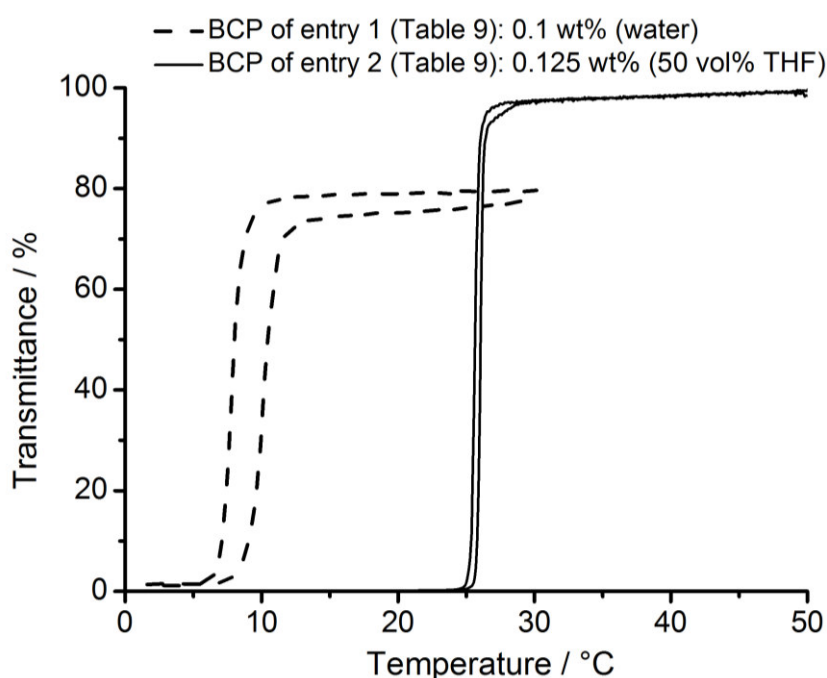
Figure 49: Turbidity curves after chain extension with St, using different polymer concentrations in aqueous medium (sample of Table 7, entry 1) and THF : water mixtures (sample of Table 7, entry 2).

BCPs can form thermoresponsive micelles in aqueous solutions depending on the dissolution process.[103] *Cryo*-TEM imaging of the BCP aqueous solutions through direct mixing with water at RT showed the formation of aggregated micelles (Figure 50 A). The formation of aggregates at temperatures above the cloud point (8 °C) hindered the 100 % transmittance at the beginning of all turbidity measurements. To characterize the collapse of the obtained micelles, SAXS measurements were carried out in dependence of the temperature (Figure 50 B). The polymer solutions utilized for turbidity measurements (0.1 wt%) were used as well for the SAXS experiments. The size of the micelles were in the range of 55 nm at temperatures above the

cloud point (8 °C, measured by turbidimetry). The collapse of the polymer micelles began at 5 °C with a diminution of the micelle diameter to 46 nm. A further temperature decrease induced a major collapse until 36 nm at 1 °C. The continuous decreased size of the micelles is attributed to the collapse of the hydrophilic poly(AAm-*co*-AN) shell. Similar results have been obtained with BCPs of St and NIPAM. SAXS studies showed that the micelle size decreased about 45 % between 20 and 40 °C, due to the collapse of the thermoresponsive block of NIPAM.[103] Moreover, it is important to remark that the contrast of the UCST BCP in water was very low, therefore, deviations of the obtained values are possible. However, as observed for the turbidity measurements, the collapse of the polymer micelles showed a broad hysteresis behavior.
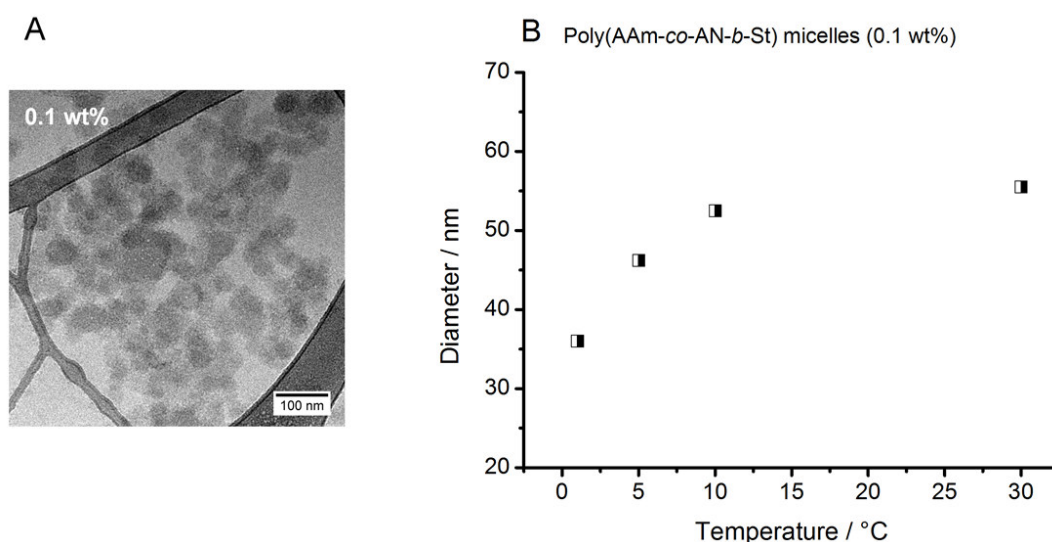


Figure 50: (A) *Cryo*-TEM image of thermoresponsive micelles formed from direct mixing of the BCP with water (0.1 wt%) at RT. (B) SAXS measurements for calculation of the micelle diameter (formed after direct mixing) in dependence of the temperature at a concentration of 0.1 wt%. The sample used for *cryo*-TEM and SAXS measurements is listed in Table 7, entry 1.

The use of dialysis from organic solvents, *e.g.* DMF against water, is a method to decrease considerably the formation of aggregates, since upon dialysis the hydrophobic PS block collapses slowly until an equilibrium in the aqueous medium is reached. The decrease of polymer aggregates induced not only a higher solubility of BCP in water (0.25 wt%), but also improved the sharpness of the obtained turbidity curves. In comparison, the same BCP dissolved by direct mixing in water (0.25 wt%) showed poor solubility and a broad phase transition temperature. Further, the *cryo*-TEM imaging of the dialyzed BCP aqueous solution showed the formation of micelles with less aggregation (Figure 51 A and 51 B).
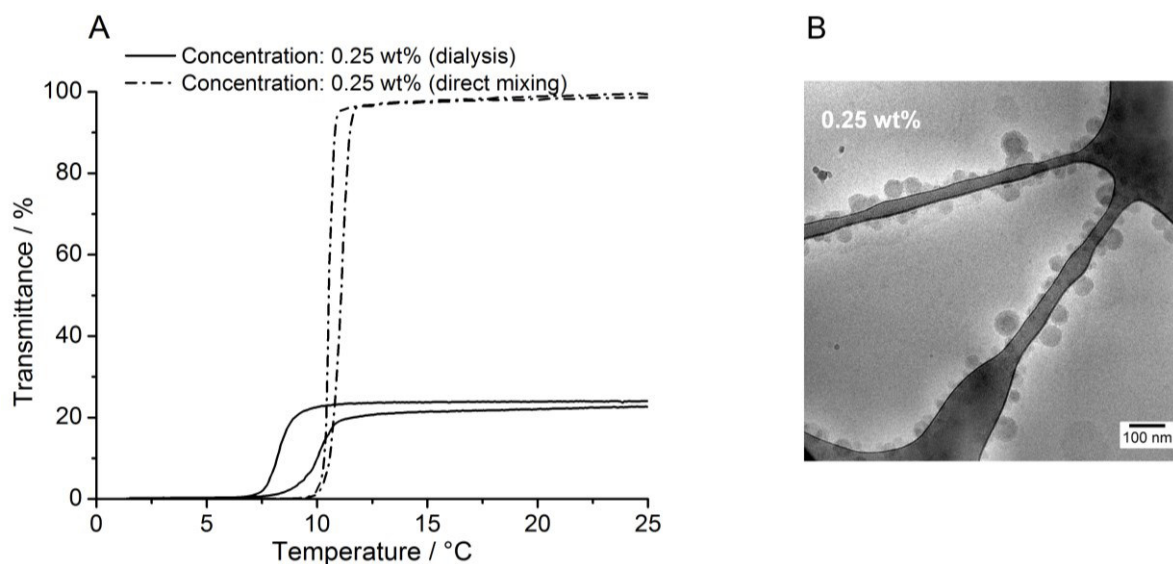
Figure 51: (A) Turbidity curves of UCST BCP samples (Table 7, entry 1), dissolved by direct mixing in water and by dialysis from DMF against water. (B) *Cryo*-TEM image of thermoresponsive micelles formed by dialysis (0.25 wt%).

### 3.3.3  Processing thermoresponsive BCPs to films and fibers

Processable polymers are of important value for today's industry. Therefore, there is an interest for the development of processable polymers with additional features, such as thermoresponsivity, *e.g.* for selective filtration under different temperatures. In this respect, the preparation of porous materials increases the accessible surface area, which as mentioned in Section 3.3, could be used for the design of thermoresponsive carriers with interchange properties.

PNIPAM is often present in copolymers and blends for the preparation of thermoresponsive films and fibers. However, in the case of fiber materials, these tend to lose their shape and functionality after various cooling and heating cycles.[100,130–133] Contrary observations have been report in the field of PNIPAM based BCP fibers, since these type of materials are more stable in the applied media.[96,99,134]

Since there is a background for the preparation of films and fibers with different types of structural morphologies using LCST polymers, in the following section LCST BCPs synthesized *via* RAFT were used as model system to transfer the knowledge to non-ionic UCST BCPs and establish first tools for the development of processable films and fibers. Based on the methods: NIPS, electrospinning, as well as the combination of both. It was assumed that it should be possible to prepare markedly different morphologies. In particular, porous structures

67

should give rise to special features. The synthetic procedure of the prepared LCST BCPs is described in detail in Section 4.3.8.

### 3.3.3.1 Processing LCST BCPs *via* NIPS for film formation

LCST BCPs of poly(St-*b*-NIPAM) can be compared to the polystyrene-*b*-poly(4-vinylpyridine) (P4VP) system employed by Peinemann and coworkers, to produce films of different structures by NIPS,[50] since an analogue preparation method was employed for the LCST BCP samples. Processing studies were carried out with two different polymers as shown in Table 8.

Table 8: Summarized content for the synthesis of LCST BCPs with different PS macro CTAs.

| Entry | Block [a] 1 (CTA) | Đ | $[M]_0 : [CTA]_0$ | Block [a] 2 | Đ |
|-------|-------------------|---|-------------------|-------------|---|
| 1 | PS<br>$M_n$ = 7000 Da | 1.1 | 400:1 | Poly(St-*b*-NIPAM)<br>$M_n$ = 64000 Da | 1.2 |
| 2 | PS<br>$M_n$ = 30600 Da | 1.1 | 400:1 | Poly(St-*b*-NIPAM)<br>$M_n$ = 84700 Da | 1.3 |

[a] Values obtained by DMF GPC

The BCP samples for film formation *via* NIPS were prepared using a solvent mixture of DMF : THF in a ratio of 1:1. Water was used as non-solvent at different temperatures. To induce both, the collapse of PS as well as the collapse of the PNIPAM segment, the temperature should be above the LCST.

SEM analysis were carried out to investigate the effects of different film processing methods and conditions on the film morphology. For instance, the temperature of the coagulation bath is an important factor that affects significantly the porous morphology of the films.[79,135–137] Therefore, the coagulation bath was equilibrated at 40 °C (above the LCST of NIPAM) before immersing the polymer solution. Figure 52 shows the surface and cross-section at different magnifications of the obtained film. The images of the surface show a non-ordered porous structure. Furthermore, an inhomogeneous porosity was observed, since some parts presented more dense porous structures than others. This could be due to the collapse of the PS and NIPAM segment as well. Considering that PNIPAM is not completely hydrophobic above its LCST,[35] hydrophilic-hydrophobic instabilities of this block segment during the film formation could lead to this type of inhomogeneity. Moreover, under this condition probably a higher affinity between the solvent mixture (DMF : THF) and water was achieved.[136] The cross-

section showed the formation of a porous thin skin layer and a sponge-like structure beneath it. Further, the obtained porous sub-structure presented void spaces, which are typical for this type of film preparation.[79,138]
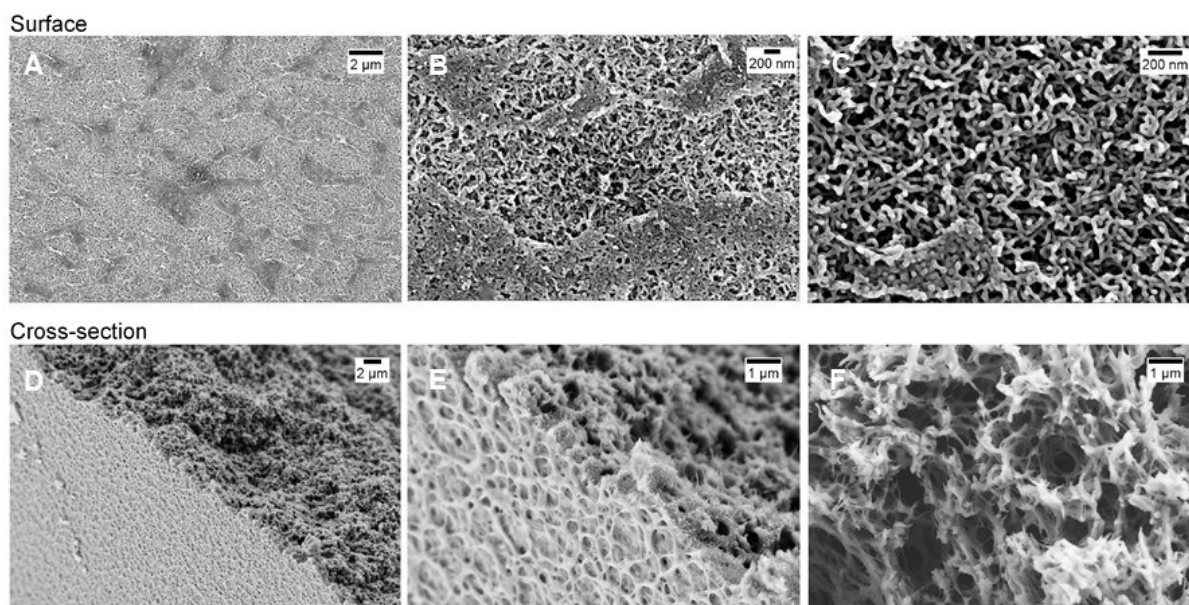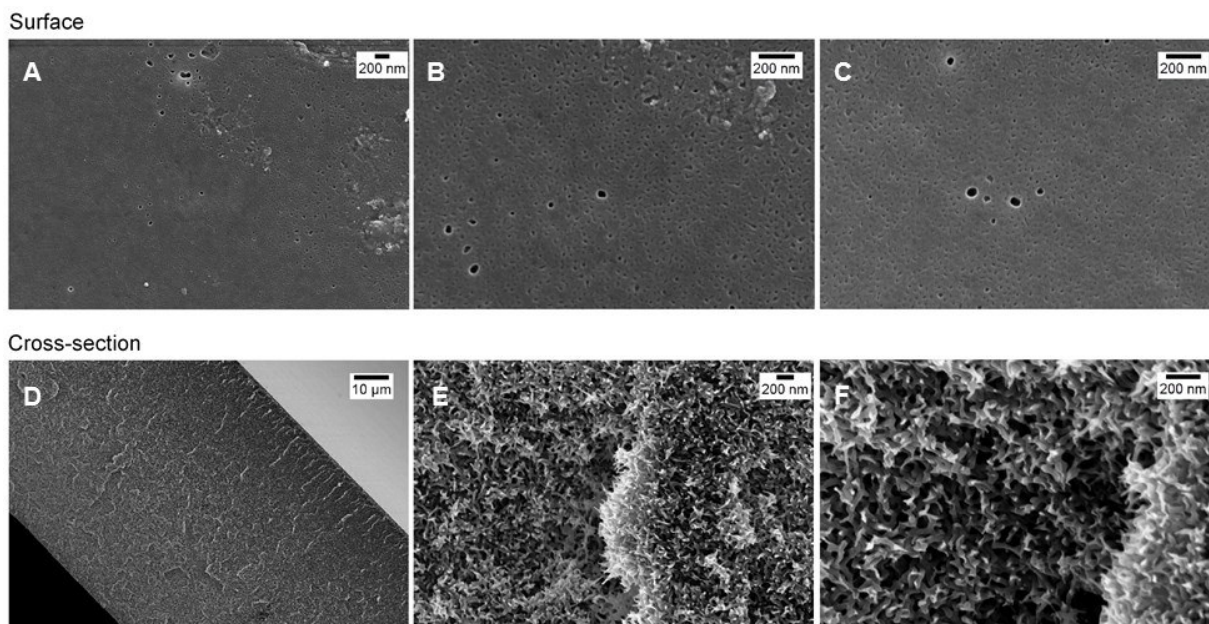


Figure 52: SEM images of the surface at different magnifications (A-C) and cross-sections (D-F) of LCST BCP films prepared *via* NIPS with an equilibrated coagulation bath at 40 °C, (sample of Table 8, entry 1).

Film formation using the coagulation bath at RT (below the LCST of PNIPAM), induced the formation of a porous skin layer and a sponge like substructure (Figure 53). However, under this coagulation conditions, the PS block collapsed and the PNIPAM domain remained in its hydrated state, which reduced the fast interaction between non-solvent and solvent. Consequently a more dense smooth porous structure on the surface with some void spaces was formed. This indicates the higher compatibility of the hydrophilic PNIPAM block with the non-solvent at 20 °C. Wang and coworkers have demonstrated similar results with LCST PVDF membranes prepared *via* NIPS at different coagulation temperatures.[137] The images of the cross-section do not showed significant differences between samples prepared at 40 °C or 20 °C. The sponge like structure remained similar in both cases. This indicates that the BCP structure is not the dominating factor in this part of the film formation process.[50]

Figure 53: SEM images of the surface at different magnifications (A-C) and cross-sections (D-F) of LCST BCP films prepared *via* NIPS with an equilibrated coagulation bath at 20 °C, (sample of Table 8, entry 1).

To compare the influence of the film preparation method on the obtained structure, LCST BCP films were prepared *via* conventional solvent casting method, using a solvent mixture of DMF : THF (1:1). Thereby, the volatile THF evaporated faster from the polymer solution as DMF. Therefore, the film formation took longer as compared to the NIPS method. Figure 54 shows a smooth surface and cross-section of the film without pores. Thus, the self-assembly of the two block segments did not influence the morphology of the film. Consequently, the films with porous structures obtained *via* NIPS are the result of different factors, *e.g.* solvent-non-solvent interactions, self-assembly of the BCP at water contact and temperature of the coagulation bath.
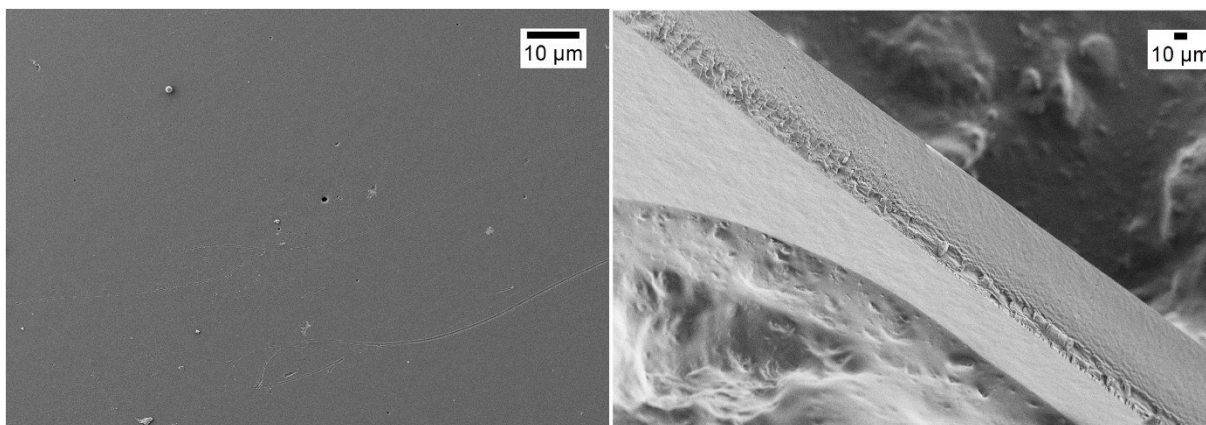
Figure 54: SEM images of a LCST BCP film (sample of Table 8, entry 1) prepared *via* film casting from DMF : THF solvent mixtures. Left-side, smooth polymer surface without pores and right-side, sealed cross-section without any sponge like pores.

In order to prove that the films prepared *via* NIPS were continuously porous with interconnected structures (Figure 55 scheme), capillary flow porometry measurements were carried out, using Topor as low surface tension liquid. The bubble point of the thermoresponsive film was determined at a pressure of 48 mbar (9 µm). Further, distribution of the pore size was obtained through the increment of the gas flow (1057 mbar). Figure 55 (left-side) shows the mean flow pore distribution at a mean flow pore size of 0.5 µm. The formation of smaller pores could not be measured due to limitations of the used equipment. However, bigger pores in the range of 3 µm were observed, which are typical for the NIPS process[79] (see SEM image on the right side of Figure 55).
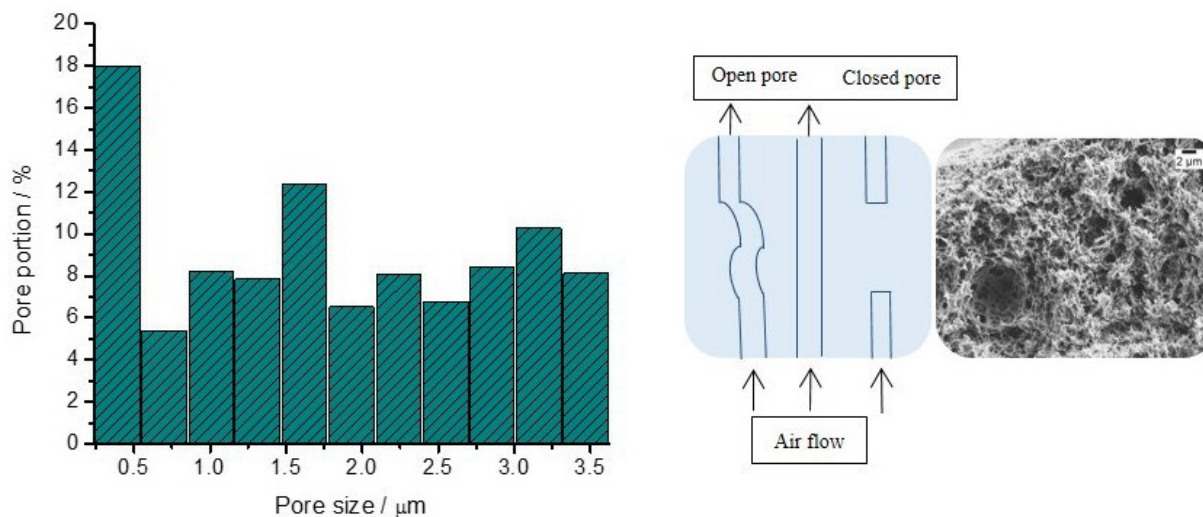
Figure 55: On the left-side, capillary flow porometry measurements with the pore size distribution for a poly(St-*b*-NIPAM) film (sample of Table 8, entry 1) prepared *via* NIPS. Right-side, scheme with the possible porous morphology inside the prepared film (SEM image).

### 3.3.3.2 Processing of LCST BCPs *via* electrospinning and characterization

Based on the obtained results of film formation *via* NIPS, the further processing of the LCST BCPs was carried out by electrospinning. Different strategies were followed to prepare varied fiber morphologies. The first strategy was based on the optimization of the electrospinning process of LCST BCPs as well as the stability of the obtained fibers in water. The electrospinning process and characterization was carried out with two BCP samples listed in Table 8. The solvent mixture DMF : THF in a ratio of 1:1 was used to electrospin all polymers. First characterizations were carried out using the BCP with the shortest PS block (Table 8, entry 1). Figure 56 A shows LCST fibers of different diameters (0.5-3.0 μm) with a smooth homogeneous surface. Furthermore, the prepared fibers showed a bead free structure. To test the stability in aqueous media, the fibers were immersed in water over 1 h at RT (below the LCST). As shown in Figure 56 B, most of the fibers lost their cylindrical shape and formed a compact film structure. Hence, the 7000 Da PS block does not confer enough hydrophobicity to hinder the deformation.
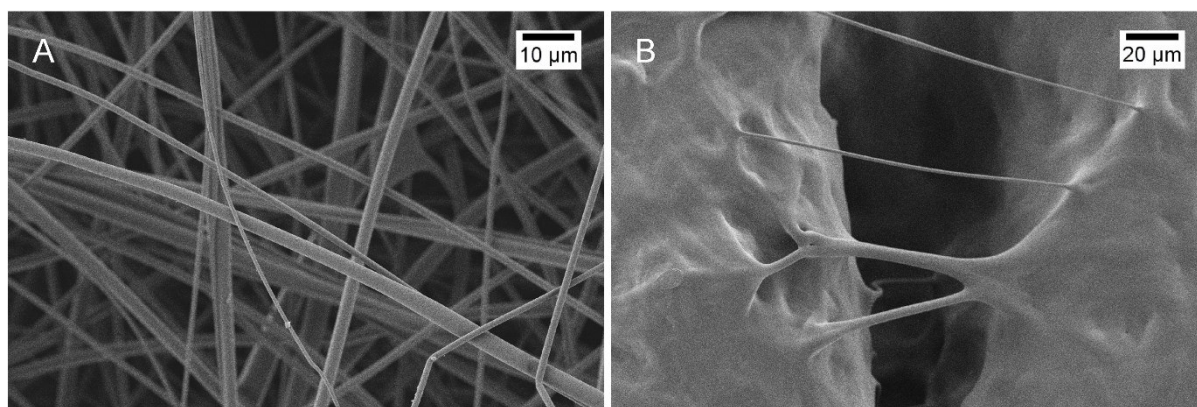
Figure 56: (A) SEM image of poly(St-*b*-NIPAM) (Table 8, entry 1) fibers in their dry state. (B) Deformed structure of the LCST fibers after treatment in water at RT over 1 h.

Considering these results, further analysis were carried out using a BCP sample with a longer PS block (Mn = 30600 Da). Thereby, the obtained surface fiber morphology remained smooth and without beads. However, due to an increase of the flow rate during electrospinning, the fiber diameter was increased to a range of 4-4.5µm (Figure 57 A). The fiber shape was stable in water over several heating and cooling cycles, since no signs of deformation could be observed (Figure 57 B). Further, micro DSC allowed the analysis of the thermoresponsive behavior of the LCST BCP fibers. Figure 57 C, shows a broad phase transition behavior at 28 °C. The decreased LCST of PNIPAM (~32 °C) is attributed to the introduction of PS as hydrophobic block, since the hydrogen bonding interactions are restricted in this type of materials.[139,140]
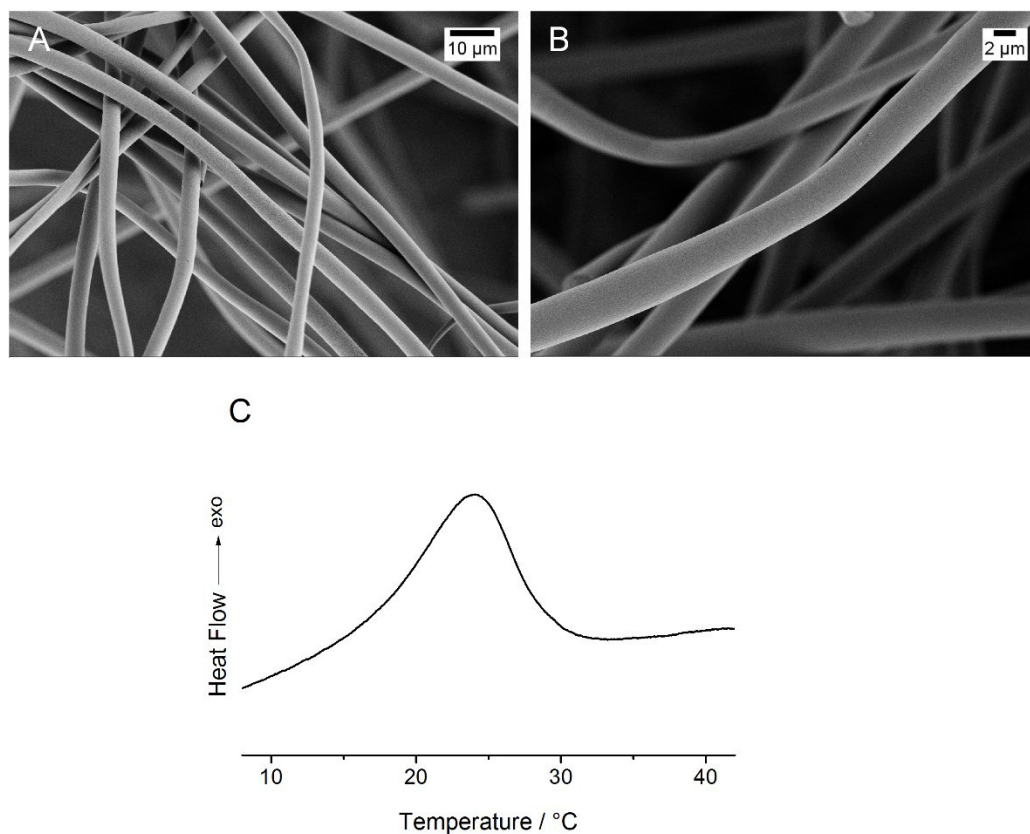
Figure 57: (A) SEM analysis of poly(St-*b*-NIPAM) (Table 8, entry 2) fibers in their dry state. (B) SEM images of the stable fiber structure after treatment in water. (C) Micro DSC thermogram of the LCST BCP fibers, measured at a heating/cooling rate of 2 °C/min (5-50 °C).

The electrospinning process induces a fast solidification of the polymer. Therefore, in the case of BCPs, the block segments do not have enough time to self-assemble in organized morphologies before fiber solidification.[96,141–143] On the contrary, during the film formation well-ordered BCP structures are obtained by the slow evaporation of solvent, since the polymer domains are able to adopt the best polymer chain conformation to decrease the total free energy of the system.[41] The observed darker domains in all TEM images of Figure 58 correspond to the PS segments, which were selectively stained with $RuO_4$. Figure 58 A-B shows a self-assembled lamellar structure for block copolymer films, formed by slow evaporation (7 days) of $CHCl_3$. In comparison, TEM images of the electrospun fibers showed an unordered micro phase separation, due the fast solvent evaporation (Figure 58 C-D). These results are comparable to the self-assembled morphologies obtained with BCP systems of PS-*b*-P4VP, processed as fibers and in bulk.[141]
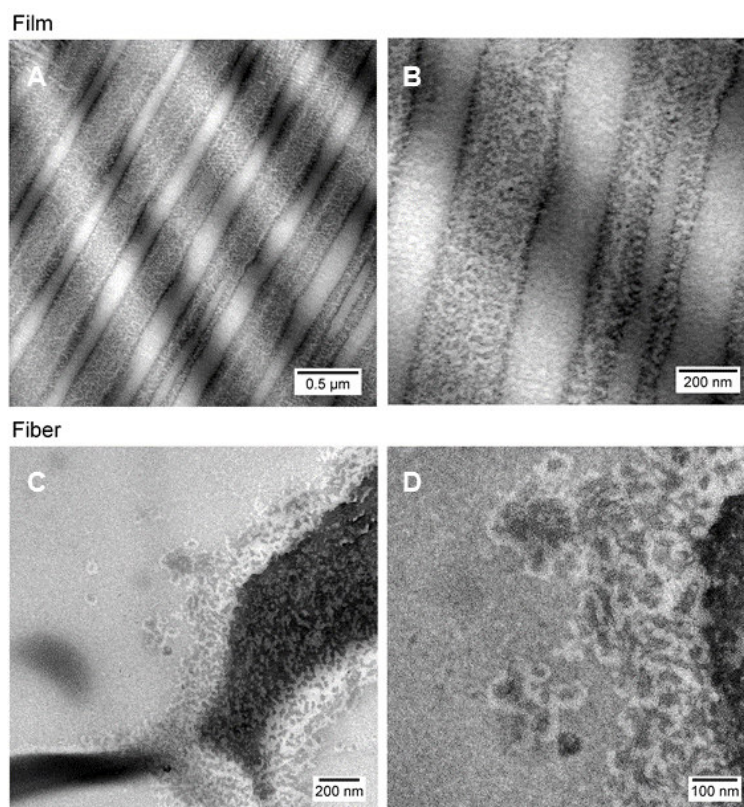
Figure 58: TEM images of films (A-B), showing micro phase separation of the BCP domains (sample of Table 8, entry 2). The film morphology, showed ordered structures due to slow solvent evaporation, whereas an unordered morphology was observed for the electrospun fibers (C-D).

### 3.3.3.3 Formation and characterization of porous fiber structures

To achieve additional fiber morphologies, high humidity conditions during electrospinning were applied.[144] Moreover, the combination of electrospinning and NIPS method represents a further alternative to influence the fiber structures.[144–146]

The impact of the humidity on the fiber morphology depends on the solvent used. In this context a mixture of DMF : THF (1:1) allowed the condensation of water droplets at the fiber surface, directly after the evaporation of THF. On the contrary, DMF could induce the formation of internal pores through the exchange of solvent and non-solvent (humidity) in the electrospinning jet.[144] Figure 59 (A-B) shows SEM images of the nano-porous surface of LCST BCP fibers at different magnifications. The obtained pore sizes were in the range of 13-17 nm. Moreover, a significant increase of the fiber diameter was observed (4.5-9.5 $\mu$m). This can be explained by the decreased dielectric constant $\varepsilon$ of the solvent system under the applied humid conditions at the charged jet.[144,147] The fiber cross-sections presented in Figure 59 (C-D)

showed a compact porous structure, which is similar to the morphology obtained with LCST BCP films *via* NIPS.
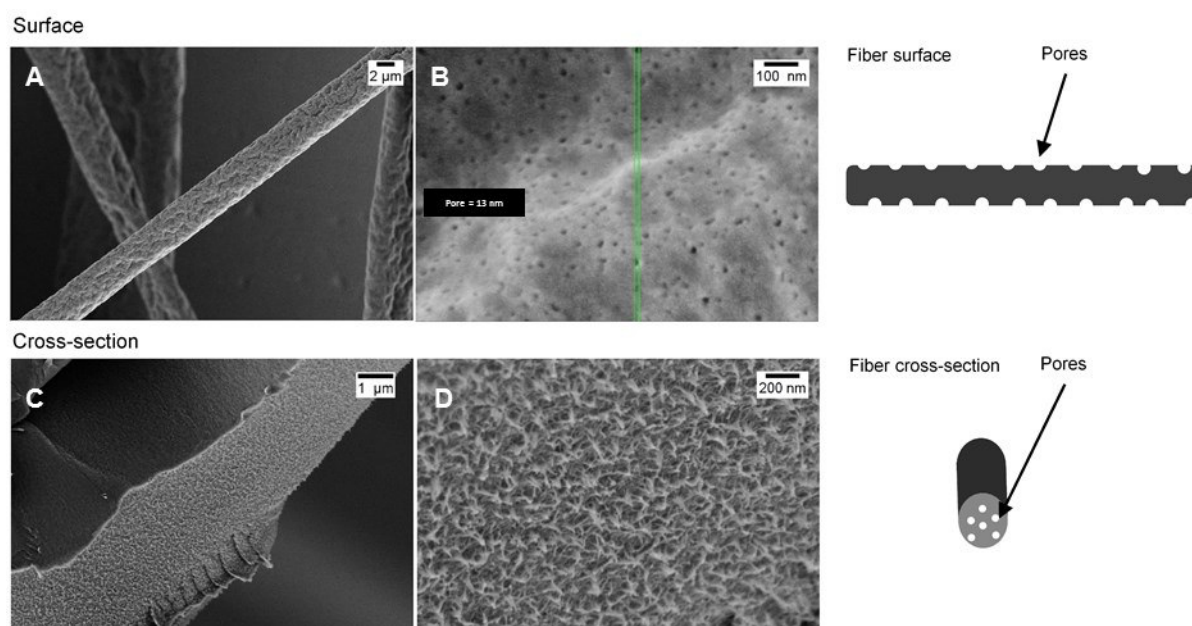


Figure 59: (Left-side) SEM images of LCST BCP fibers prepared under high humidity conditions (~ 60 %). (A-B) Porous surface of LCST BCP fibers, (C-D) sponge-like cross-section of the fibers (sample of Table 8, entry 2). (Right-side) Scheme of the porous structure of the formed fibers.

The morphology of LCST BCP fibers was further modified by the combination of NIPS and electrospinning methods. In this type of processing, the formed fibers were collected in a coagulation bath as counter electrode. Nayani et. al., reported this combined method to produce highly porous polyacrylonitrile (PAN) fibers from DMF. The authors used the combined method to induce porosity in other polymeric fibers as well.[145] One important remark made by these authors was the relevance of residual solvent in the formed fibers to allow phase separation after contact with the coagulation bath. Therefore, the electrospinning process was carried out using a short distance between needle and collector (6 cm). Figure 60 A, shows the wet collected fibers after the electrospinning process. As expected, the hydrophilic segment of PNIPAM induced swelling of the fibers. After drying, a rough surface morphology of the fibers is observed from the SEM images (Figure 60 B). Unlike the morphology obtained under high humidity conditions, no measurable pore structures were obtained. It is assumed that the absence of bigger pores on the polymer surface is due to the fast precipitation of the fibers in the coagulation bath, which might induce a re-deformation of the pore structures. However, the cross-section in Figure 60 C exhibit a porous morphology. This results are expected for low

volatile solvents such as DMF,[148–150] where the solvent and non-solvent interactions are responsible for the formation of internal porous structures.
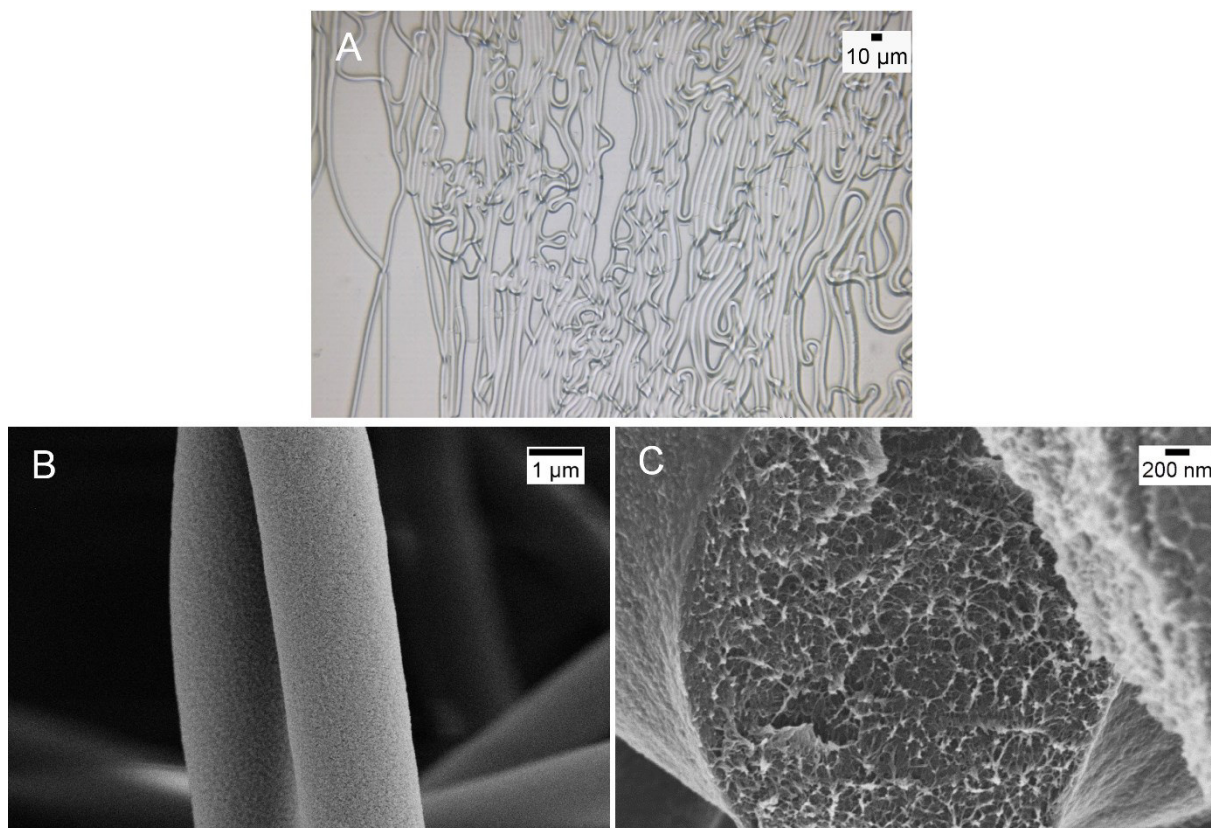


Figure 60: (A) Microscope image of the collected LCST fibers after electrospinning in the aqueous coagulation bath. (B-C) SEM images of the fiber surface and cross-section respectively after drying. (Sample of Table 8, entry 2).

### 3.3.4 Processing non-ionic UCST BCPs of Route I

Based on the previous results for the processing of LCST BCPs, film casting from organic solvents, was the first method to process UCST BCPs. In this case solvent mixtures of DMF : THF (85:15) with a 10 wt% concentration were used to produce polymer films (200 μm thickness). The thermoresponsivity was analyzed using turbidimetry and micro DSC measurements of the wet films. However, no thermoresponsive behavior could be observed. The cause is probably based on the orientation of the two block segments during film casting. Since for the observation of thermoresponsivity (H-bonding interactions) functional groups of the poly(AAm-co-AN) should be able to interact with the aqueous media. Therefore, it was assumed that the hydrophobic domains of St, which represent the block segment with smaller $M_n$ magnitude ($M_n = 6300$ Da), segregated at the film surface to decrease interfacial free

energy. Further, the possible orientation of St polymer chains towards surface induced less conformational entropy loss in the system, compared to the thermoresponsive segment ($M_n = 24000$ Da). This assumption is based on several studies, which referred the direct dependence of $M_n$ and conformational entropy on the structural morphology of formed polymeric films. The authors point out that polymer chains with high $M_n$ at the film surface are not favorable, due to significant conformational entropic penalty.[50,151–153]

To induce the orientation of the thermoresponsive segment or hydrophilic part of the BCP to the surface of the film, NIPS was used as processing method. Thereby, the same solvent mixture as for film casting and a concentration of 15 wt% was used. White films were obtained after immersion of the polymer solution in the non-solvent bath (water, below phase transition temperature). The immersing step in water as non-solvent induced the orientation of the thermoresponsive segment of the block copolymer to the outer side of the film, due to the high affinity of this segment to water in comparison to St, even at temperatures below the phase transition temperature. Similar results were obtained with BCP membranes of P4VP and PS prepared *via* NIPS by Peinemann and coworkers. They claimed that the compatibility of the hydrophilic block (P4VP) with water allowed the formation of a P4VP upper layer on the asymmetric porous membranes.[50]

Since the obtained UCST films were non-transparent and presented a white color, conventional turbidity measurements could not be used as analysis method. Therefore, to prove the thermoresponsivity, micro DSC measurements of the wet film were carried out. As shown in the thermogram of Figure 61, a peak maximum could be measured at 36 °C. The obtained collapse transition of the thermoresponsive segment was very broad (~45-30 °C). However, a similar broad phase transition behavior (~40-29 °C) was observed for poly(AAm-*co*-AN) in water, which was used as macro CTA (CP = 44 °C measured by turbidimetry). The detection of phase transition temperatures of UCST polymers by DSC or micro DSC is known to be difficult since the hydrophobic effect in these type of polymers is very small compared to LCST polymers, like PNIPAM. Furthermore, the enthalpy changes due to hydrogen bond formation is very low for primary amides, such as PAAm, which difficult even more the detection of a phase transition.[11] In comparison, PNAGA exhibits a broad phase transition temperatures already in a 1.0 wt% polymer solution,[28] whereas for poly(AAm-*co*-AN) samples 20 wt% solutions were required (Figure 61 lower graphic).

Poly(AAm-*co*-AN-*b*-St) wet film

Poly(AAm-*co*-AN) macro CTA in aqueous media

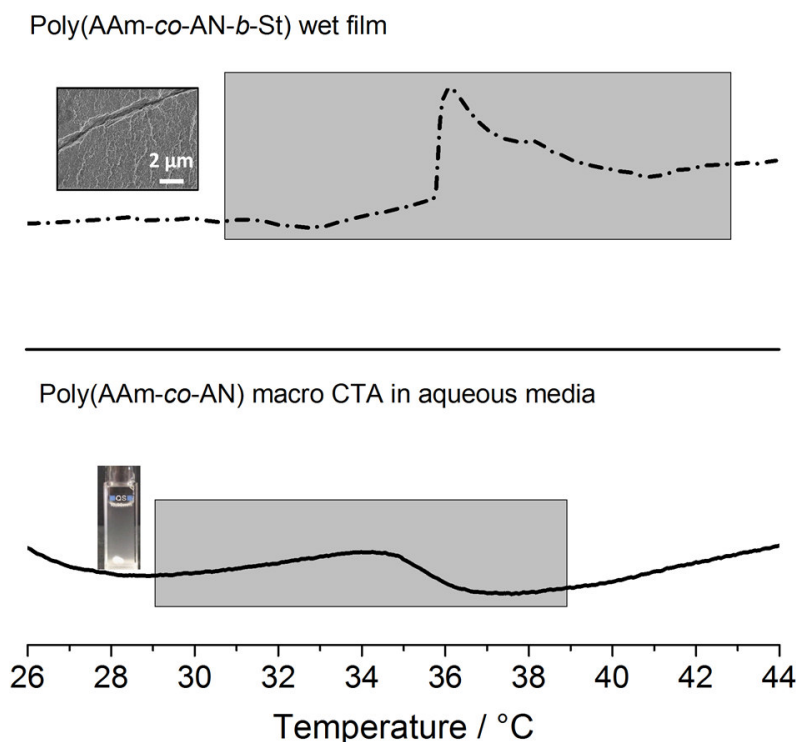26 28 30 32 34 36 38 40 42 44
Temperature / °C

Figure 61: Micro DSC thermogram curves (Table 7, entry 2) of poly(AAm-*co*-AN-*b*-St) as wet film (54 wt%) prepared *via* NIPS (see SEM picture above) and poly(AAm-*co*-AN) as CTA in aqueous media (picture on the left-side below) at a concentration of 20 wt%. Heating rate of 1 °C / min.

## 3.3.5 Morphology and characterization of BCP films and fibers (Route I)

The use of NIPS as processing method, not only allowed the orientation of the thermoresponsive segment of the BCP to the outer side of the films, but also allowed the preparation of a porous material. The formation of a specific porous structure in polymer films is based on the interaction of the non-solvent and the polymer solution. Sponge-like morphologies for example, are formed in the case of slow penetration rate of the non-solvent inside the polymer solution.[79] Based on the obtained SEM images (Figure 62), the morphology of the films indicated the formation of a sponge-like structure. Thereby, Figure 62 A shows an irregular rough aspect of the film surface. However, at higher magnification the non-ordered porous structure did not exhibit the formation of larger pores (Figure 62 B). Nevertheless, a typical sponge-like structure was observed at high magnification below the unordered skin of the polymer film (Figure 62 C). In this case, no evidence of macrovoids was observed. Especially for polymer membranes, these type of structural defects represent an issue, since the membranes are used in filtration processes where high pressure is requiered.[79]

The described formation of porous structured BCP films is a complex process, which is influenced by the NIPS method itself (kinetic and thermodynamic) as well as by the self-assembly of the BCPs.[50,79,154]
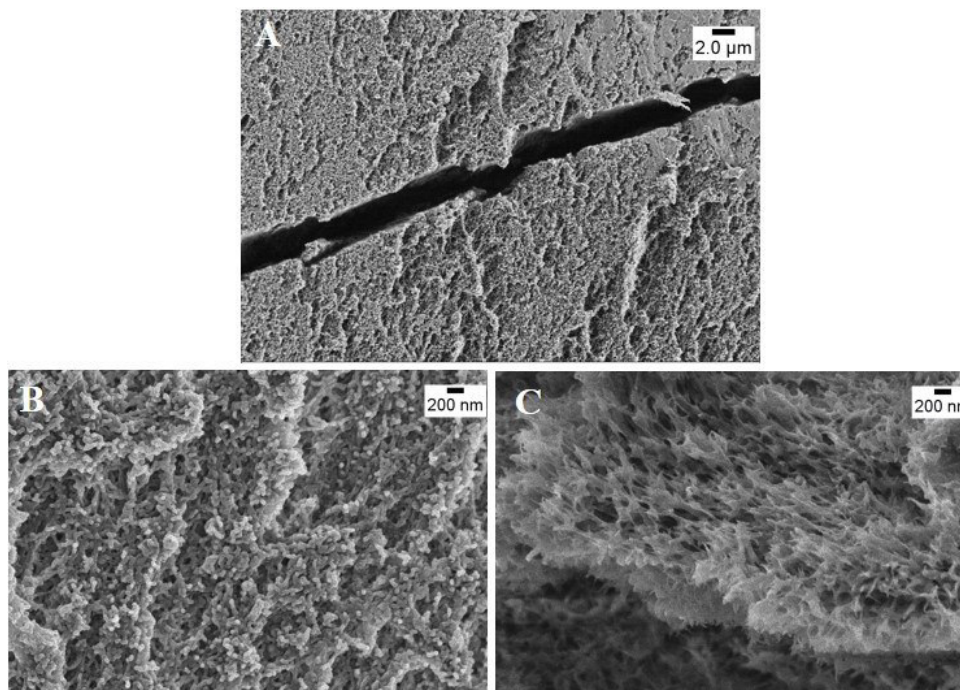


Figure 62: SEM images of the surface (A and B) and cross-section (C) of the formed BCP film (sample of Table 7, entry 2) *via* NIPS, with a coagulation bath of water.

The orientation of the polymer chains in dependence of the film preparation method was also evident in the obtained TEM micrographs. The image observed in Figure 63 A shows an unordered micro-phase separation of the microdomains of the di-block copolymer after solvent casting. Thereby, the dark domains correspond to the St block, as it was selectively stained with RuO$_4$ to enhance the contrast. The lighter domains correspond to the thermoresponsive poly(AAm-*co*-AN) block. Figure 63 B shows the magnification of the non-ordered micro-phase separated structure.

In the case of films prepared *via* NIPS method, the TEM micrographs showed a uniform aligned micro-phase separation of the block segments (Figure 63 C). The St block (dark domains) was again stained with RuO$_4$. The ordered arrangement of the two segments in the BCP film is clearly observed at higher magnification in Figure 63 D. The orientation of the poly(AAm-*co*-AN) segment towards surface was of significant importance to allow the thermoresponsivity of the obtained film.
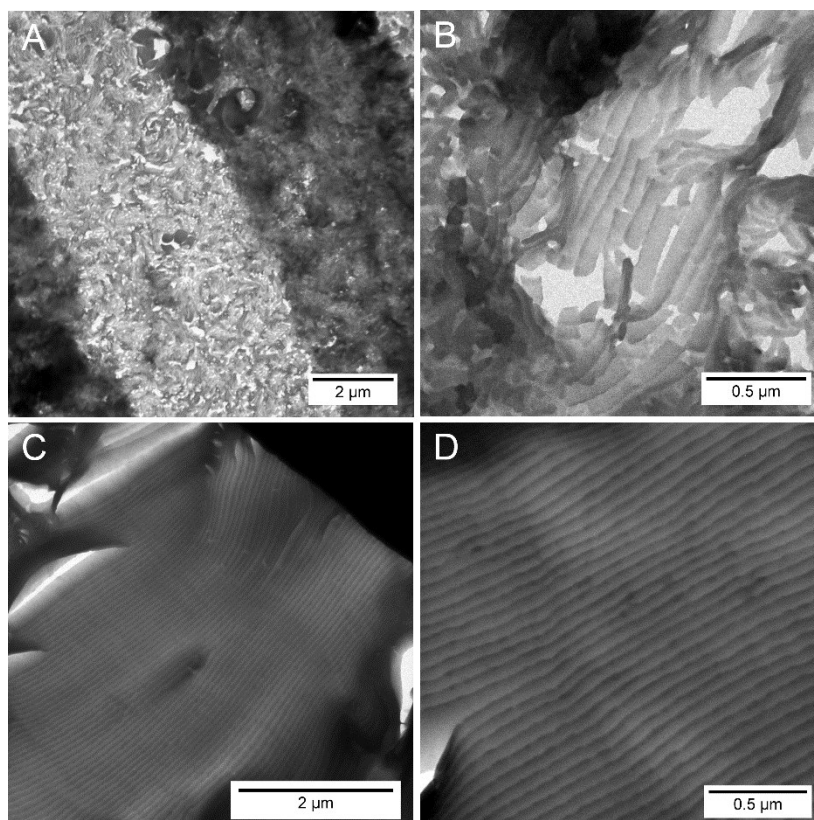
Figure 63: TEM images of UCST BCP films prepared by different methods. (A) BCP film prepared by solvent casting method, after staining with $RuO_4$ to enhance contrast of the St block. (B) Magnification of the obtained morphology after film casting. (C) Well aligned micro-phase structure after film preparation *via* NIPS. (D) Magnification of the BCP film (*via* NIPS).

The stability and thermoresponsivity of UCST BCPs as thin films was used as reference system to process the same BCP as fiber material *via* electrospinning. In order to obtain a continuous electrospinning process with no defects, different process parameters were taken into account, *e.g.* molecular weight of the polymer and solution concentration. To compensate the "low molecular weight" (30600 Da) of the synthesized UCST BCP, concentrations of 35 wt% were required for the formation of fibers. Thereby, an electrospraying of the samples was avoided. However, due to the high concentration an average fiber diameter of $2.2 \pm 0.3$ μm (from SEM measurements) was obtained.

As observed with the UCST films, the orientation of the thermoresponsive segment towards surface is very important. Therefore, the electrospinning process was carried out under high humidity conditions (45-55 %). Moreover, the used of humid conditions should serve as a tool for the formation of fibers of different morphology, *e.g.* with porous structures.[90] In the case of UCST BCPs, electrospinning from organic mixtures (DMF : THF, ratio 85:15) and a humid

environment could induce a surface chain orientation in the fibers, before solidification. Figure 64 A-B shows that the concentration of the polymer solution affected de morphology of the fibers. Lower concentration (29 wt%) induced the formation of many beads of different sizes (Figure 64 A). Therefore, the concentration of the polymer solution was increased until 35 wt%, which significantly improved the fiber formation process (Figure 64 B). Moreover, after immersion in water at 60 °C (above the phase transition temperature over 30 min), the fibers were measured again in their hydrated state (Figure 64 C). The measurements showed an increase of the fiber diameter from ~2.4 to 4.3 μm. It is important to notice that the fibers remained stable in water without dissolving at the used temperature (60 °C), which prove that the hydrophobic domain of the BCP confer enough hydrophobicity to hinder deformation and dissolution.
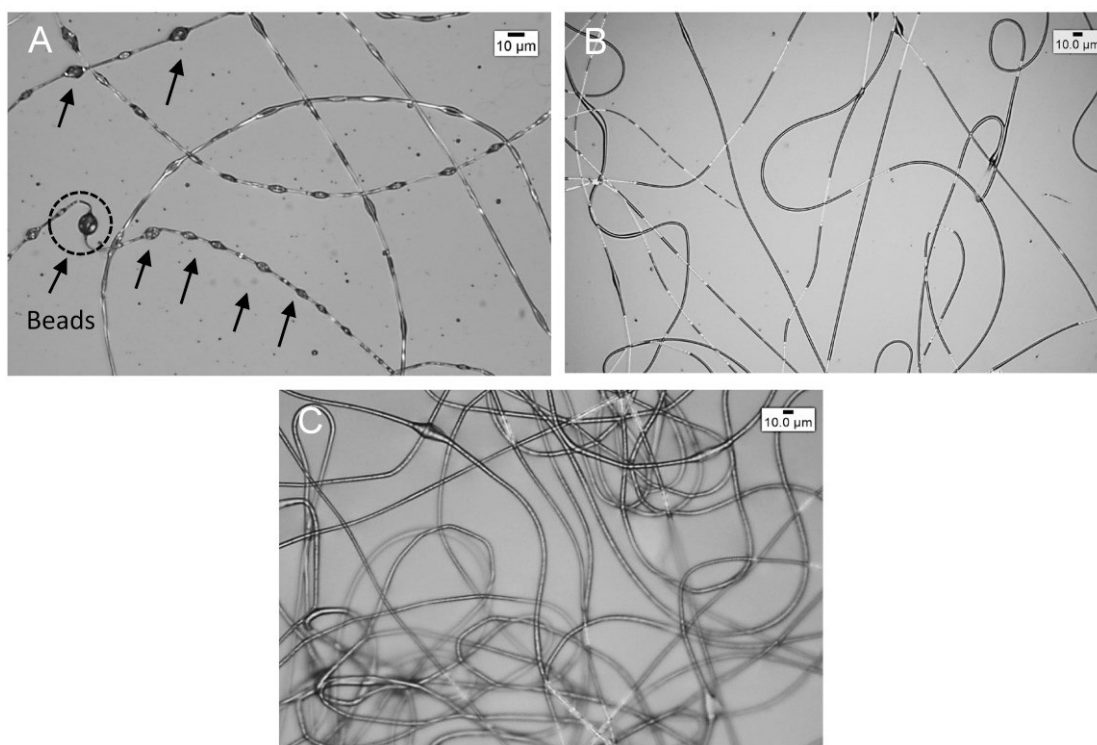


Figure 64: Optical microscope images (light field) of UCST BCP fibers. (A-B) Dry fibers prepared from DMF : THF (85:15) at a concentration of 29 and 35 wt%, respectively (under high humidity conditions, 45-55 %). (B) Wet fibers after equilibration (30 min) at 60 °C in water.

The morphology of the fibers was analyzed in detail using SEM micrographs (Figure 65). The measurements of the fiber diameter showed no changes after immersion below and above the phase transition temperature (4 °C and 60 °C). Since the fibers were carefully dried before SEM analysis, there is no formation of hydrogen bonds in dependence of temperature. Therefore, it

is difficult to prove changes in the morphology or a swelling-deswelling behavior after immersion at different temperatures by SEM images. Further, it was important to avoid the immersion in water at very high temperatures over long time, in order to prevent hydrolysis of the thermoresponsive segment poly(AAm-*co*-AN), as shown in previous results (see Section 3.2). Therefore, the fiber samples were immersed in water at 60 °C for 30 min. In the case of samples equilibrated at 4 °C (below the phase transition temperature), the fiber diameter showed only minor changes after short or long time of equilibration (30 min and 4 h). Figure 65 A shows the SEM images of the polymer fibers without treatment in water and after water contact at 4 °C and 60 °C (Figure 65 B and C), respectively. The prepared fibers showed a rough morphology, without porosity.
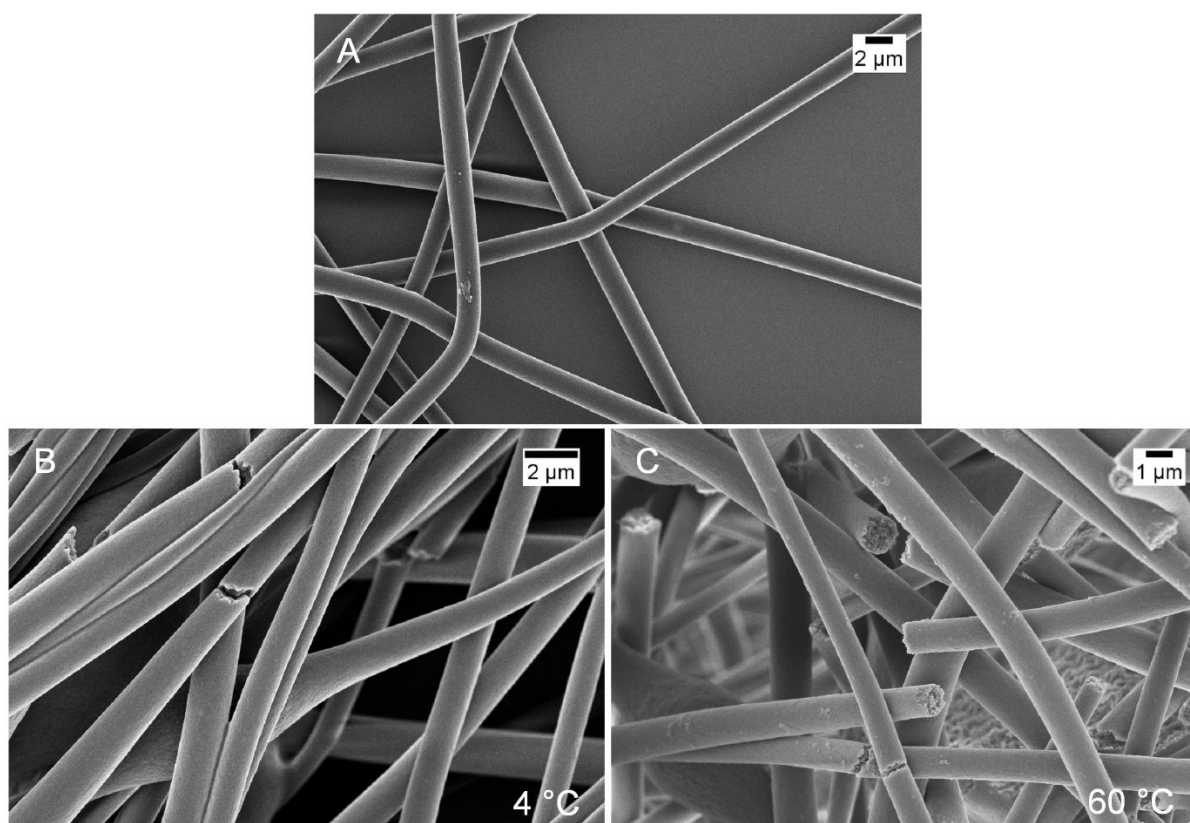


Figure 65: SEM images of UCST BCP fibers. (A) Fiber morphology without immersion in water. (B and C) Dry fibers after equilibration in water at 4 °C and 60 °C, respectively.

Extensive heating of the fibers at 70 °C over 4 h was carried out as "extreme" condition to induce a significant fiber diameter change. However, after drying the samples, no important diameter changes were observed. Nevertheless, the samples presented a different morphology as observed in Figure 66 A and B. Since the samples remained over long time at high temperature in water, the drying process under vacuum induced a fast evaporation of the

absorbed water inside the swollen fibers. Thereby, the SEM analysis at higher magnification, showed the formation of "porous" fiber structures (Figure 66 B). The distribution of these type of morphology was however random.

Nykänen and coworkers obtained similar results using LCST BCP fibers based on PNIPAM. SEM images of the PNIPAM BCPs showed that swollen fibers were transformed in "porous skeletons" after freeze-drying process, due to the sublimation of ice.[96]
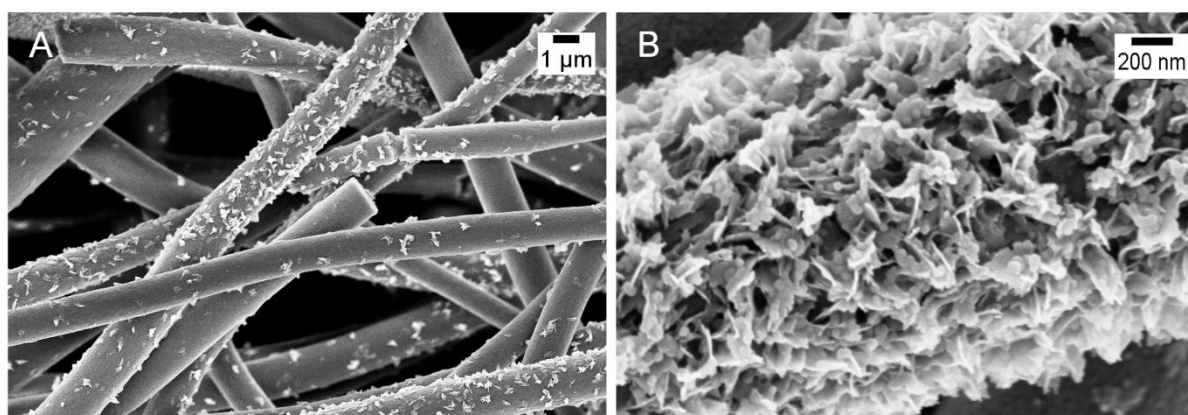


Figure 66: SEM images of the BCP fibers after immersion in water over 4 h at 70 °C.

## 3.3.6  Route II: Synthesis and characterization of BCPs with PS as CTA

The second approach for the synthesis of UCST BCPs *via* RAFT polymerization began with PS as macro CTA and the subsequent synthesis of copolymers of AAm and AN as second block (Figure 67). The obtained results are summarized in Table 9.
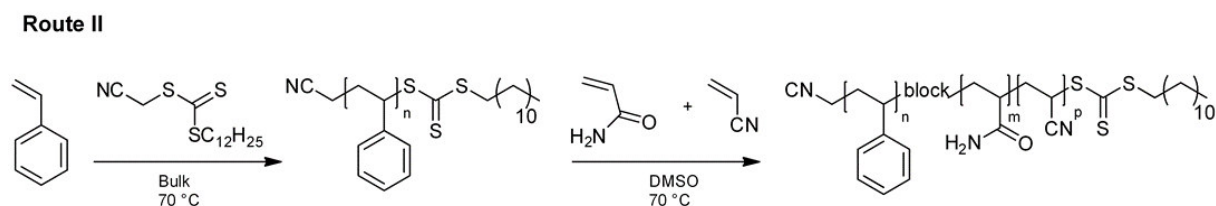


Figure 67: RAFT polymerization scheme for the synthesis of UCST BCPs, using PS as macro CTA. AAm and AN were used to polymerized the second block segment.

The chain extension of PS with a second block of AAm and AN copolymers, induced a broadening of the GPC curve (Đ = 1.1-1.5), as observed for the BCPs obtained with Route I. The increased polydispersity and the low molecular weight tailing are shown in Figure 68 A, indicating the presence of unreacted PS macromonomer.[128,155]

Moreover, for the successful chain extension of the PS block, repulsive effects between the hydrophobic- and the forming hydrophilic-segment should be taken into consideration, since a phase separation of the polymer during polymerization can lead to an inhomogeneous polymerization. In the case of UCST BCPs this type of inhomogeneity could take place at molecular level, inducing the decreased control of the polymerization.[128,156]

For further structural characterization ^{1}H NMR spectroscopy was carried out. Figure 68 B (above) shows the NMR spectrum with the characteristic signals of aromatic protons of PS used as macro CTA at 6.3-7.3 ppm, as well as the signals of the polymer backbone at 1.3-2.3 ppm. After chain extension with the copolymer of AAm and AN additional defined signals were observed in the backbone region, as well as a broader signal between 6.3-7.8 ppm, which is attributed to the aromatic and amide protons. Furthermore, the decrease of the end group signals (alkyl-$CH_3$) at 0.85 ppm and (alkyl) at 1.25 ppm was considerable after chain extension (Figure 68 B, below).

Table 9: Synthesis of poly(St-*b*-AAm-*co*-AN) *via* RAFT polymerization with PS as macro CTA. Polymerizations were carried out in DMSO at 70 °C (24 h).

| Entry | Block[a] 1 (CTA) | Đ | Block[a] 2 | Đ | CP point / °C | AN in polymer/ mol% |
|-------|------------------|-----|------------|-----|---------------|---------------------|
| 1 | PS Mn = 2000 Da | 1.1 | Poly(St-*b*-AAm-*co*-AN) Mn = 11800 Da | 1.5 | 44 [b] | 14 |
| 2 | PS Mn = 9000 Da | 1.2 | Poly(St-*b*-AAm-*co*-AN) Mn = 15400 Da | 1.3 | - | 10 |

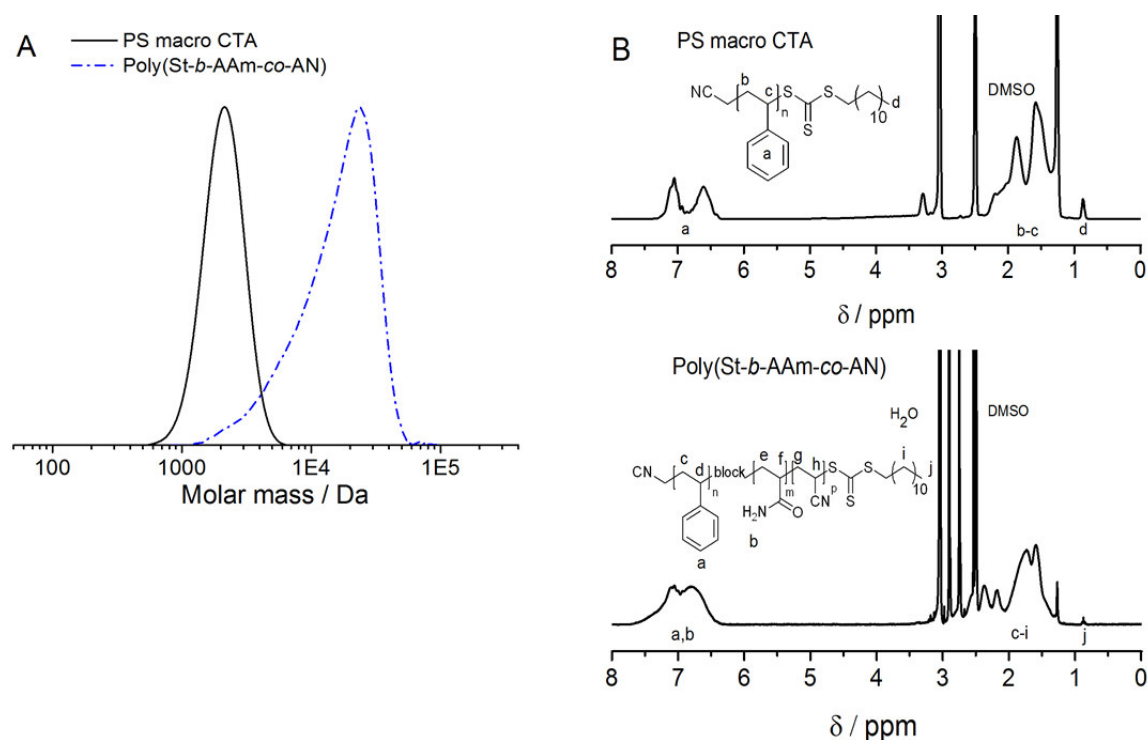[a] Values obtained by DMF GPC, [b] low concentration (0.5 wt%) in a water : THF mixture.

Figure 68: (A) GPC (DMF) curves of PS macro CTA ($M_n$ = 2000 Da, Đ = 1.1) before chain extension and after polymerization with AAm and AN (di-block copolymer $M_n$ = 11800 Da, Đ = 1.5). (B) $^1$H NMR spectra of PS and poly(St-*b*-AAm-*co*-AN) in $d_6$-DMSO at 70 °C.

Additional characterization was carried out by DSC measurements. The observed endothermic glass transition for PS, used as macro CTA at 64 °C is shown in Figure 69 A. The thermal behavior of PS is well known to be molecular weight dependent. Therefore, the obtained glass transition was expected to be low for PS with a molecular weight of 2000 Da, and is in concordance with reported literature.[157,158] In case of the BCP sample, no glass transition of PS could be observed within the DSC thermogram, probably due to its low molecular weight in respect to the poly(AAm-*co*-AN) segment. Thereby, neither higher sample amounts, to increase the enthalpic signal, nor higher heating rates up to 30 °C/min, to reduce the thermal diffusion, could provide enhanced thermograms. However, the broad endothermal glass transition at 172 °C (Figure 69 B) was similar to the observed transition (179 °C) for BCPs, synthesized by Route I (Section 3.3.1).
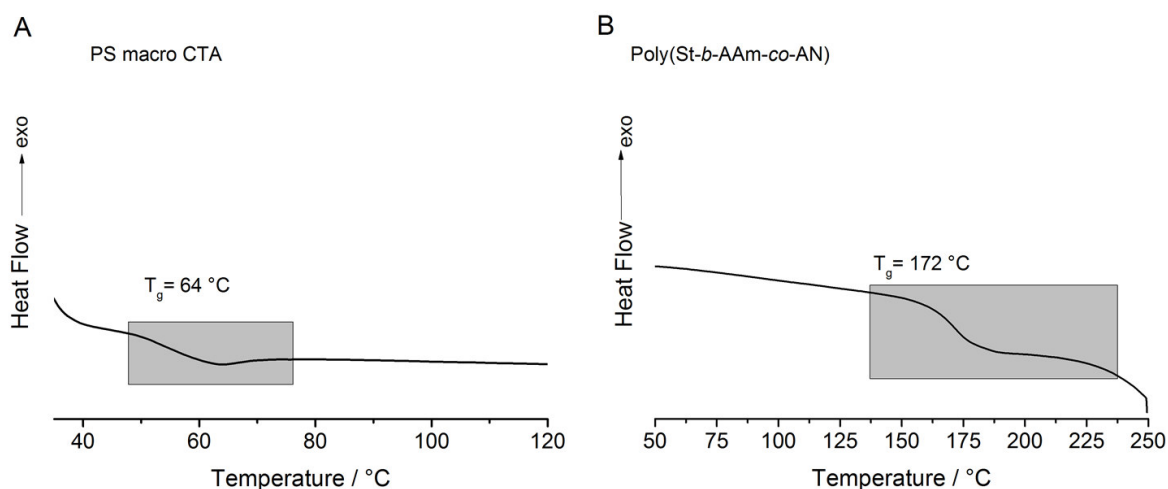
A

PS macro CTA

Heat Flow ⟶ exo

$T_g$ = 64 °C

40　60　80　100　120

Temperature / °C

B

Poly(St-*b*-AAm-*co*-AN)

Heat Flow ⟶ exo

$T_g$ = 172 °C

50　75　100　125　150　175　200　225　250

Temperature / °C

Figure 69: (A) DSC curve of PS used as macro CTA ($M_n$ = 2000 g/mol) at a temperature range of 25-50 °C. (B) DSC curve of poly(St-*b*-AAm-*co*-AN) at a temperature range of 25-250 °C. The polymers were measured at heating rate of 10 °C/min, respectively (Table 9, entry 1).

In case of the PS macromonomer with a molecular weight of 9000 Da (Table 9, entry 2), the observation of a phase transition temperature was entirely inhibited, even in water : THF mixtures. As mention in Section 3.3.1, the chain extension of the first block segment is influenced by the molecular weight of the macro CTA. Therefore, in order to assure high chain reactivity and availability of the trithiocarbonate group, often low molecular weight macro CTAs are required.[159,160] Hence, the analysis of the obtained BCPs was focused on the PS macro CTA with lower molecular weight (2000 Da). Regarding this, thermoresponsivity of the polymer sample could be observed in mixtures of water : THF. Figure 70 shows the turbidity curves upon cooling and heating. In comparison to the BCPs synthesized by Route I, a broad phase transition temperature at 44 °C was observed. Moreover, due to the difficult solubility of the polymer, "noisy" turbidity curves were obtained. Due to lower polymerization control, the sharpness of the phase transition decreased, when PS was used as macro CTA, as the homogeneity of the chain composition from the thermoresponsive block was decreased as well.[11,29]
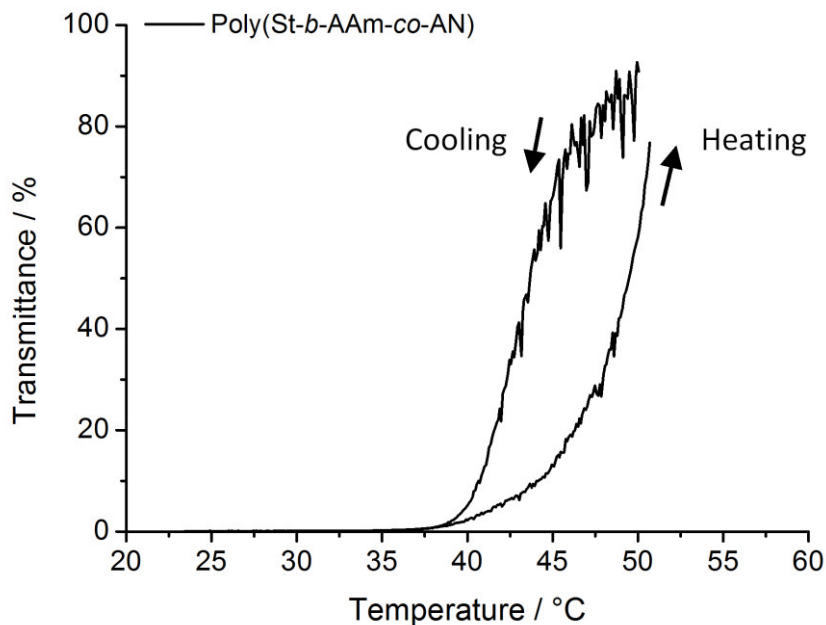
Figure 70: Turbidity curve after chain extension of PS with the copolymer of AAm and AN, using 33 vol% THF in water (0.5 wt%) (sample of Table 9, entry 1).

### 3.3.7  Processing non-ionic UCST BCPs of Route II

Based on the results obtained for the processing of the BCPs by Route I, film preparation was carried out *via* solvent casting from organic mixtures of DMF:THF (90:10) and *via* NIPS method. Films prepared *via* solvent casting did not show a thermoresponsive behavior even after equilibration at different temperatures. However, the successful chain orientation towards surface of the AAm-AN functional groups was achieved again by film preparation *via* NIPS. The high DMF content allowed the selective dissolution of the poly(AAm-*co*-AN) domain, whereas the PS block was preferably dissolved in THF. Self-assembly in solution is often observed for amphiphilic BCPS, which has an important impact on the structure of the obtained film.[161,162] In this type of UCST BCP, the impact of the PS block was significantly lower than for BCPs of Route I. Therefore, during the phase inversion process and after the collapsed of the small hydrophobic PS block, the formed film was mostly influenced by the hydrophilic poly(AAm-*co*-AN) block, which induced the formation of a hydrogel film due to its affinity to water. The colorless films were analyzed by conventional turbidity measurements. Figure 71 A shows a qualitative thermoresponsive behavior using wet films at different temperatures. Semi-transparent films were obtained at 50 °C, whereas a significant turbidity was induced in the film after equilibration at 10 °C. Moreover, the thermoresponsive behavior was analyzed

quantitatively, using turbidity measurements of the wet films. As shown in Figure 71 B, the sample was not completely transparent (17 % transmittance) at 50 °C (above the UCST), due to scattering and diffraction effects caused by the wrinkled morphology of the sample. However, a reversible broad phase transition temperature was observed between 50 and 10 °C.
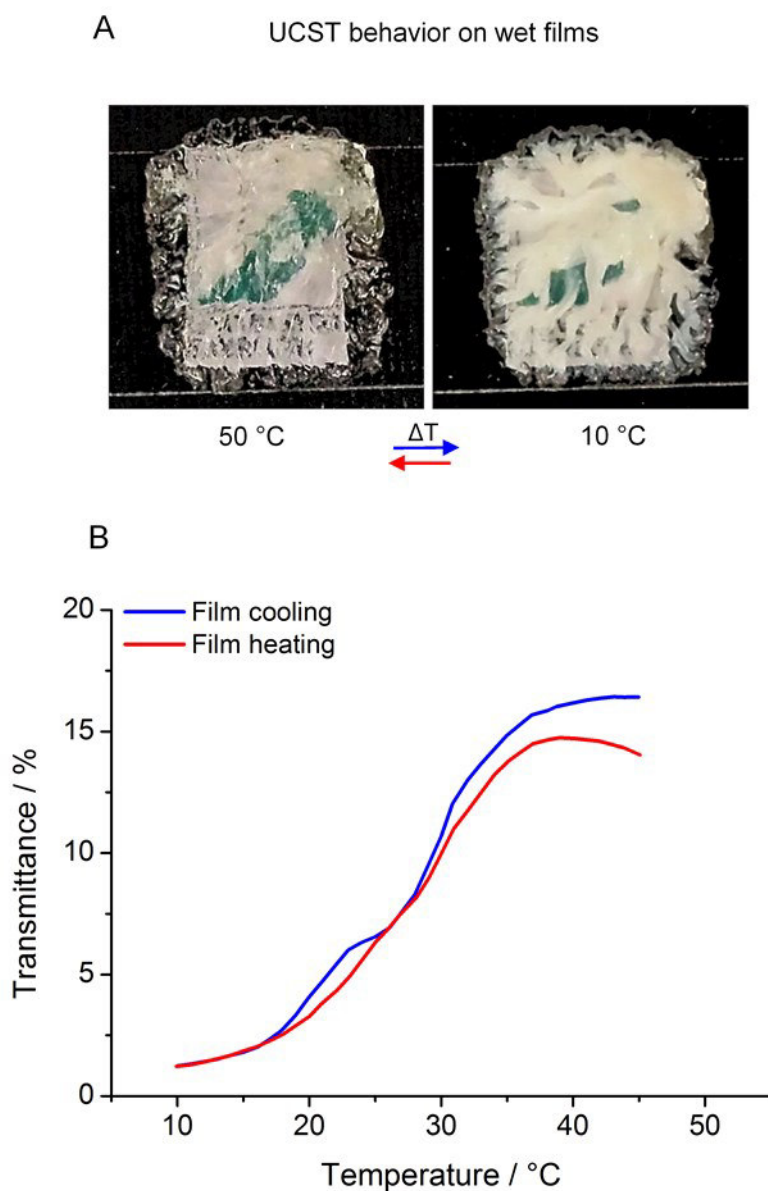


Figure 71: (A) Qualitative thermoresponsive analysis of UCST BCP hydrogel films prepared *via* NIPS at different temperatures (50-10 °C). (B) Turbidity curves upon cooling and heating of BCP wet hydrogel films prepared *via* NIPS. (Sample for both analysis, Table 9, entry 1).

### 3.3.8 Morphology and characterization of BCP films and fibers (Route II)

The surface morphology of the hydrogel films was analyzed using SEM. The pictures revealed a macroscopic wrinkled and smooth surface structure (Figure 72). Since the larger poly(AAm-*co*-AN) segment is compatible with water, it is assumed that the solvent exchange between DMF : THF and the non-solvent (water) occurred rapidly, "freezing" the obtained structure. The short PS block did not induce retardation on the demixing process or alignment of the segments. For further analysis, selective staining of the PS block for TEM measurements was carried out. However, no successful staining of the short PS block could be achieved. Therefore, no comprehensive analysis could be made.
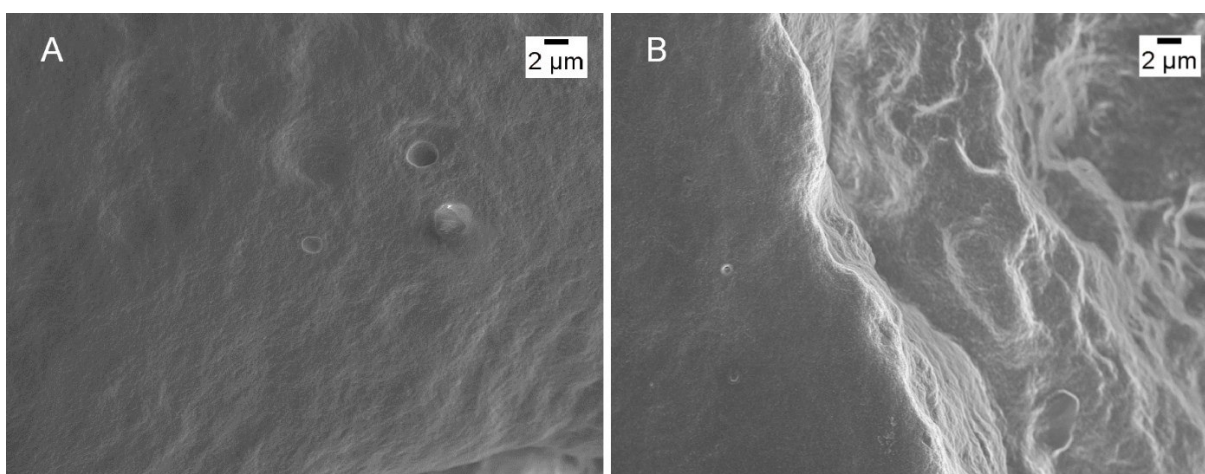


Figure 72: SEM micrographs of the hydrogel film surface (A and B) (sample of Table 8, entry 1). Sample prepared *via* NIPS method.

Subsequently this BCP was used for electrospinning. As mentioned in Section 3.3.5, the low molecular weight of the synthesized BCP was compensated with high concentrations (40-45 wt%) to avoid electrospraying. In order to induce an orientation of the hydrophilic functionalities towards the fiber surface, high humidity conditions (~ 55 %) were applied. Figure 73 A, shows the formed fibers using a concentration of 40 wt% DMF : THF, ratio 85:15. In this case, a continuous jet was formed during the electrospinning process. However, the fibers showed spherical beads, which are commonly formed with polymer solutions of low viscosity and low molecular weight. This means that the used UCST BCP presented low entanglement interactions during electrospinning. Therefore, the concentration was increased to 45 wt%. Further, high molecular weight PS (1 million Da) was blended with the solution as 1.0 wt% matrix-additive. The use of a blend solution reduced the bead formation considerably.

Nevertheless, an inhomogeneous fiber morphology was observed (Figure 73 B). In order to test the stability and responsivity of the blended fibers, these were immersed in water at 50 °C for 10 min. As shown in Figure 73 C, the fiber morphology in the hydrated state was not stable, since most of the fibers tend to lose their form after swelling. In this case, the entanglement of the hydrophobic polymer chains was not enough to keep the shape of the fibers. Thus, the balance between the entanglement of the polymer chains (dynamic effect) and the temperature swelling behavior (thermodynamic effect) of thermoresponsive BCPs is crucial to achieve stable fibers.[96] Due to the low entanglement of these UCST BCP fibers and their instability in water, no further studies were carried out with this material.
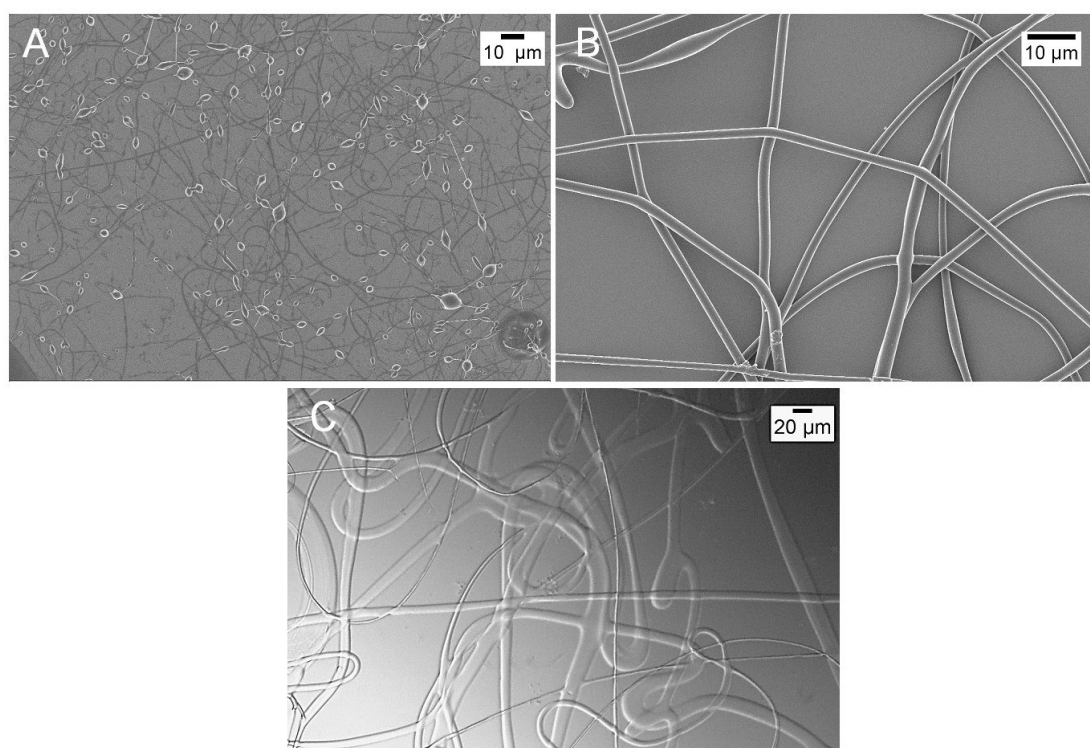


Figure 73: SEM images of UCST BCP fibers without PS blend (A) and (B) after blending with PS (1 million Da) (1.0 wt%). (C) Microscope image of blended fibers after immersion in water at 50 °C.

### 3.3.9 Conclusion

UCST block copolymers were prepared by sequential RAFT polymerization. The obtained samples were characterized in solution as well as in the solid state. The synthesis of these materials was achieved by two different synthetic routes. The first route based on the use of poly(AAm-*co*-AN) as macro CTA, demonstrated the successful incorporation of St as hydrophobic second block. Thereby, the introduction of St in the BCP reduced the solubility in water. For BCP samples with a low phase transition temperature (8 °C) spherical micelles in the range of 55 nm (above the cloud point) in aqueous media were observed. The thermoresponsive behavior of these micelles was, highly dependent on the dissolution process. The direct mixing of the polymer sample with water produced large micelle aggregates, decreasing the sharpness of the phase transition temperature. In contrast, the dissolution through dialysis from DMF against water increased the solubility of the polymer (less aggregation) and sharpened the turbidity curves.

To set the fundament for UCST BCP samples, prepared LCST BCPs were processed using different methods. The first one was based on the formation and characterization of porous films, prepared *via* NIPS. Thereby, it was observed that the temperature of the coagulation bath influenced the film morphology, especially the surface. As second method, electrospinning was applied. By changing the electrospinning conditions, the fiber morphology was significantly modified. For instance, after increasing the humidity to ~60 %, porous fiber structures on the surface and in the cross-section were obtained. Further, the combination of NIPS and electrospinning allowed the formation of fibers with a compact rough surface morphology and a sub-porous structure. Similar results have been obtained as well for other electrospinning systems.[148]

As observed for the processing of LCST BCPs, an enhanced hydrophobicity was required for the preparation of water-stable films and fibers. Therefore, for the preparation of non-ionic UCST films *via* NIPS method, it was important to use samples with higher content of hydrophobic moieties of AN and St. Moreover, this method proved to be fundamental to achieve an orientation of the poly(AAm-*co*-AN) segment at the surface of the film. Thermoresponsive analysis of wet samples showed broad phase transition temperatures of ~ 45-30 °C. The induced orientation of the polymer chains was proven by TEM, where an alignment of the block segments was evident.

Further processability of the samples was achieved by electrospinning. For this method, elevated polymer concentrations (35 wt%) were required, since RAFT polymerization difficult

the synthesis of high molecular weight polymers.[70] Moreover, humidity was used (~55 %) to influence the block orientation during the electrospinning process. SEM analysis of the fibers in dry state did not allow the observation of changes in the morphology or fiber diameter even after equilibration in water at different temperatures. Therefore, the swelling behavior was observed merely under an optical microscope in hydrated state, where an increase of the fiber diameter from ~2.4 to 4.3 μm at 60 °C was observed. Besides the swelling, the fiber morphology was stable in water even at 70 °C.

In a second strategy PS was used as macro CTA to synthesize UCST BCPs. In this opposite polymerization sequence, a low molecular weight PS macro CTA was required to produce thermoresponsive polymers. The increase of the PS block length (9000 Da), limited the incorporation of AAm and AN copolymers, due to steric effects. Therefore, the responsive behavior of these samples was hindered. First analysis of the UCST thermoresponsivity was carried out by turbidity measurements, these showed a reversible broad phase transition temperature at 44 °C, which was obtained after dissolution in water : THF mixtures. Further investigations on the thermoresponsive behavior were carried out on films prepared *via* NIPS. As mention above, this method allowed the orientation of the thermoresponsive functional groups, which induced reversible turbidity of the films between 50 and 10 °C. The low entanglement of the polymer during the electrospinning process, even at high concentrations (40-45 wt%), was improved by the addition of PS (1 million Da) as blending polymer (1.0 wt%). However, the obtained fibers were not homogeneous and deformed irreversibly in water.

In general, the successful polymerization of UCST BCPs, using two different synthetic routes, represent a relevant advance for UCST polymers. The new synthetic approach using PS as macro CTA also demonstrated the potential to polymerize AAm and AN copolymers, which enhances even more the possible applications of UCST systems in the competitive field of thermoresponsive polymers. Moreover, the introduction of a hydrophobic block enabled the processability of these polymers by important techniques such as electrospinning and NIPS. These results set the fundament for the future development and processing of non-ionic UCST BCPs.

# 4 Experimental part

## 4.1 Chemicals

| | |
|---|---|
| Acrylamide | Fisher Scientific ≥ 99.9 % (electrophoresis grade), used as received |
| Acrylonitrile | Sigma-Aldrich, ≥99.9%, distilled |
| Azobisisobutyronitrile | Fluka, recrystallized from ethanol |
| Buffer solutions | VWR, used as received |
| Cyanomethyl dodecyl trithiocarbonate | Aldrich 98 %, used as received |
| Dimethyl sulfoxide | University supply p.a. grade |
| Methanol | University supply (technical grade), distilled |
| *N*-isopropylacrylamide | Aldrich, recrystallized from cyclohexane |
| *N*, *N'*-dimethylformamide | University supply p.a. grade, used as received |
| Polystyrene | BASF, used as received |
| Styrene | BASF, distilled prior used |
| Tetrahydrofurane | University supply (technical grade), distilled |

## 4.2 Characterization methods

### 4.2.1 Turbidity measurements

Turbidity analysis was carried out on a JASCO V-630 UV/VIS-spectrometer equipped with an ETCS-761 Peltier thermostat single cell holder at $\lambda = 670$ nm wavelength. The measurements were performed using heating/cooling rates of 1.0 °C min$^{-1}$ (if not otherwise mention), which was constant for all measurements under magnetic stirring. The cloud point was defined as the maximum of the first derivative of the transmittance curve. The turbidity of samples of poly(AAm-*co*-St) were measured in a Tepper turbidity photometer (TP1-D) at $\lambda = 670$ nm with a cell path length of 10 mm under magnetic stirring. The cloud point was defined as well as the maximum of the first derivative of the transmittance curve.

## 4.2.2 Gel-Permeation Chromatography (GPC)

GPC measurements were carried out in DMSO as solvent for the determination of the molecular weights and respective molecular weight distributions of the synthesized copolymers. The used columns (PLGel Mixed-D) presented the following properties: particle size 5.0 μm and dimension of 7.5 mm × 300 mm. Pullulan standards were employed for the GPC calibration. Measurements were performed at a flow rate of 1.0 mL min$^{-1}$.

To measure UCST and LCST BCPs, GPC measurements in DMF (containing lithium bromide as additive) were carried out with PSS-SDV gel columns, using following properties: particle size 10 μm and dimensions of 8 mm x 300 mm at 30 °C. GPC calibration was based on narrow polystyrene standards. All measurements were performed at a flow rate of 0.5 mL min$^{-1}$.

The obtained data was analyzed with a WinGPC7 software.

## 4.2.3 Infrared Spectroscopy (IR)

FTIR spectroscopy measurements were performed on a Digilab Excalibur Series FTS 3000 spectrometer, equipped with a ZnSe crystal with attenuated total reflection technique. To analyze the spectra, the software Win-IR Pro 3.3 was used. The content of AN of the polymers was determined using a calibration curve, which was obtained by mixing homopolymer powders of PAAm and PAN as standards in specific compositions (see Figure 74).
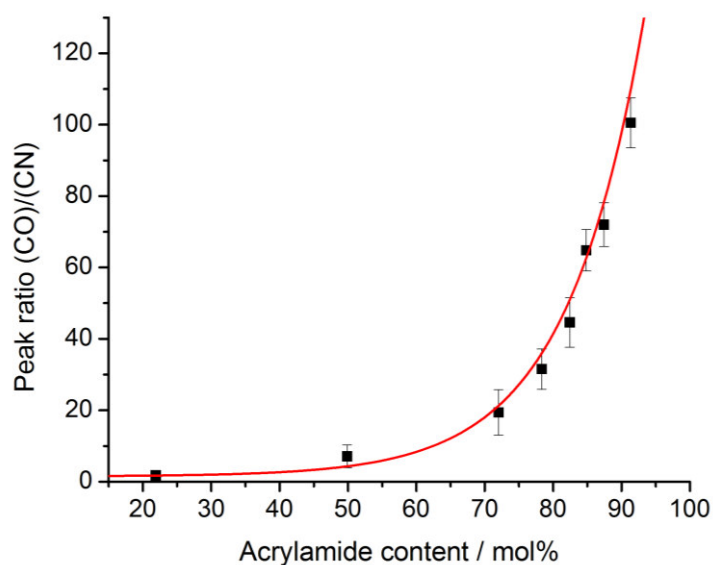


Figure 74: Calibration curve obtained *via* FTIR measurements of the AAm and AN homopolymers.

## 4.2.4 Nuclear Magnetic Resonance (NMR) spectroscopy

^{1}H-NMR measurements were performed on a 300 MHz Bruker Ultrashield 300 spectrometer using different deuterated solvents in dependence of the solubility of the sample to be measured.

## 4.2.5 Differential Scanning Calorimetry (DSC)

The thermal behavior of synthesized polymers was analyzed using a DSC from Mettler Toledo, which was calibrated with indium and zinc. The measurements were carried out with ~ 10 mg samples in aluminum pans using nitrogen atmosphere. The heating and cooling rates varied in dependence of the type of sample from 10 to 20 K·min$^{-1}$. The glass transition temperature of the samples was obtained from the second heating curve using a Mettler Toledo STAR$^e$ software.

## 4.2.6 Micro-Differential Scanning Calorimetry (micro-DSC)

The thermal analysis of sensitive phase transition temperatures of thermoresponsive samples were performed in solution and solid (wet film and fibers) samples. Measurements were carried out on a SETARAN micro-DSC III at a heating/cooling rate of 1 °C min$^{-1}$ (if not otherwise mention). The samples were measured in closed batch cells and water was used as reference.

## 4.2.7 Elemental Analysis

To analyze the hydrolysis degree of polymer samples, carbon, hydrogen and nitrogen (CHN) elemental analysis was measured in an element analyzer EA 3000 (HEKAtech). The measurements were carried out in the department of chemical engineering of the University of Bayreuth.

## 4.2.8 Small-Angle X-ray Scattering (SAXS)

SAXS measurements on aqueous samples were carried out in a temperature range from 30-1 °C on a "Double Ganesha AIR" (SAXSLAB), equipped with a rotating copper anode (MicoMax 007HF, Rigaku Corporation, Japan) as x-ray source, which provided a focused beam at $\lambda = 0.154$

nm. The measurements were performed with a PILATUS 300K (Dectris) position-sensitive detector. SAXS analysis were carried out in the department of physical chemistry I of the University of Bayreuth.

### 4.2.9 Transmission Electron Microscopy (TEM)

TEM images of film and fibers were carried out on a Leica EM FC7 Ultramicrotome below the glass transition temperature of the samples. For cutting, the knife was cooled to -30 °C. Samples with thickness of 50 to 60 nm were obtained and prepared onto copper grids. The hydrophobic PS domains were selectively stained by exposing the sample to $RuO_4$ vapor for 1 min at a reduced pressure of 200 mbar. Bright-field TEM was carried out on a Zeiss CEM902 electron microscope operated at an acceleration voltage of 80 kV. Zero-loss filtered images were registered digitally by a side mounted CCD camera system (Orius SC200W, Gatan) and processed with a digital imaging processing system (Gatan Digital Micrograph 2.3, Gatan).

### 4.2.10 Cryogenic-Transmission Electron Microscopy (Cryo-TEM)

Cryo-TEM studies were carried out using a drop (~2 mL) of the aqueous micellar solution, which was placed on a copper TEM grid (200 mesh, Science Services). Most of the liquid was carefully removed with blotting paper, to form a thin film over the grid holes. The samples were shock vitrified by a rapid immersion into liquid ethane in a temperature-controlled freezing unit (Zeiss Cryobox, Zeiss NTS GmbH). Afterwards, the samples were inserted into a cryo-transfer holder and were further transferred to a Zeiss EM 922 OMEGA EF-TEM instrument. Analysis was carried out at temperatures of 90 K. The obtained images could be registered using a bottom-mounted CCD camera system (Ultrascan 1000, Gatan), combined, and processed with a digital imaging processing system (Gatan Digital Micrograph 3.10).

### 4.2.11 Scanning Electron Microscopy (SEM)

Film and fiber surface morphology was analyzed with SEM, using a Zeiss LEO 1530 equipment (EHT= 3 kV) with an SE2 detector. Prior imaging, the samples were sputter-coated with a thin platinum layer of 2.0 nm. To measure the obtained fiber diameters, ImageJ (Version 1.44p) was used.

## 4.2.12  Digital Microscopy

Digital and fluorescence microscopy images were obtained with a DMRX polarization-fluorescence microscope (Leica), equipped with a CCD-camera (Leica) and different fluorescence filters. Analysis of fiber diameter were performed with ImageJ (Version 1.44p).

## 4.2.13  Capillary Flow Porometry

Porosity of processed films was analyzed with a Topas Pore Size Meter (PSM 165) with an accuracy for pores of > 10 μm. Topor was used as water insoluble liquid for the determination of the pore size distribution. The obtained data were analyzed with a PSMwin-Sofware.

# 4.3  General Synthesis Procedures

## 4.3.1  Copolymers of AAm and St *via* RAFT polymerization

The synthesis of these type of copolymers was performed in different compositions. RAFT polymerization was carried out with a total monomer concentration of 200 equivalents. In a typical reaction for a particular composition, the monomers were weighed in a 25 mL nitrogen flask, using 30 equiv. (1.25g) of St and 170 equiv. (4.83g) of AAm and dissolved in 10 mL of DMSO (prior distilled). In the previous homogeneous solution 1 equiv. (126.8mg) of CMDT was also dissolved. In order to degas the monomer solution, a freeze−pump−thaw procedure (three cycles) was used. Further, 0.3 equiv. of AIBN (19.7 mg) as initiator was separately degassed in DMSO (500 μL) and added to the monomer solution. The flask was placed into a preheated oil bath at 70 °C. The polymerization was finished after 20 h. The polymer was precipitated in methanol, and rinsed again with methanol over three centrifugation wash cycles using a 10 min (10.000 rpm) centrifugation program. The obtained yellowish polymer was dried under vacuum for 24 h at 70 °C. Using similar procedure, several copolymers were made by changing the feed compositions. In dependence of the St content the yields varied from 40 to 99 % (determined gravimetrically).
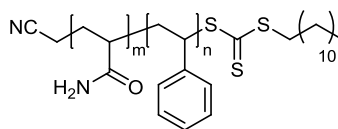
Figure 75: Chemical structure of the synthesized AAm and St copolymer *via* RAFT polymerization.

$^{1}$H NMR: 500 MHz, $D_2O$ (80°C): $\delta$ / ppm = 1.43 (3H -$CH_3$ end group CMDT), 1.7-1.9 (20H -$CH_2$- CMDT), 1.8−2.6 (4H -$CH_2$-backbone of PS and AAm), 2.6−3.0 (2H -CH-backbone of St and AAm), 7.2-8.0 (5H -$C_6H_5$ phenylic protons of St). Reference set to 4.79 ppm. (NMR signal assignment in Figure 16).

## 4.3.2 Copolymers of AAm and St *via* free radical polymerization

The free radical polymerization of AAm and St was carried out in different compositions. In a typical reaction for a particular composition, 11 equiv. (42.55 mg) of St and 89 equiv. AAm (235 mg) were weighed into 10 mL nitrogen-flask and dissolved with 1.2 mL of DMSO (prior distilled). The homogeneous monomer solution was degassed by the freeze−pump−thaw procedure (three cycles). 0.02 mmol (3.05 mg) of AIBN as initiator were separately degassed (100 µL) and added to the previously degassed solution. Then the flask was placed into a preheated oil bath at 70 °C. After the reaction was finished (different reaction times were used, see Table 1), the polymer was precipitated in methanol and rinsed with methanol over three centrifugation wash cycles using a 10 min (10.000 rpm) centrifugation program. The obtained white polymer was dried under vacuum for 24 h at 70 °C. Using similar procedure, several copolymers were made by changing the feed compositions (Table 1). The yield for a sample with 8 mol% of St in polymer was 80 % (determined gravimetrically).

$^{1}$H NMR: 500 MHz, $D_2O$ (80°C): $\delta$ / ppm = 1.3−1.9 (4H -$CH_2$-backbone of PS and AAm), 2.0−2.4 (2H -CH-backbone of St and AAm), 7.0-7.5 (5H -$C_6H_5$ phenylic protons of St). Reference set to 4.79 ppm.

## 4.3.3  Copolymers of AAm and AN *via* RAFT polymerization

RAFT polymerization of AAm and AN was carried out using a total monomer concentration of 400 equivalents. In a typical reaction for a particular composition, the monomers were weighed into a 25 mL nitrogen flask, using 340 equiv. (2.4 g) of AAm and 60 equiv. (0.318 g) of AN and further dissolved in 8 mL of DMSO (prior distilled). CMDT used as RAFT agent was also dissolved 1 equiv. (31.8 mg) in the previous monomer solution. Which was degased with a three freeze−pump−thaw cycles procedure. Further, 0.3 equiv. of AIBN as initiator was separately degassed in DMSO (500 μL) and added to the previously degassed monomer solution. The flask was placed into a preheated oil bath at 70 °C over 3.5 h. The obtained polymer was precipitated in 10-fold excess volume of methanol and rinsed again with methanol over three centrifugation wash cycles using a 10 min (10.000 rpm) centrifugation program. The obtained yellowish polymer was dried under vacuum for 24 h at 40 °C. Using similar procedure, several copolymers were made by changing the feed compositions. The yield was 57 % (determined gravimetrically).
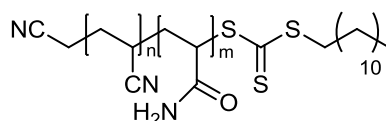


Figure 76: Chemical structure of the synthesized AAm and AN copolymer *via* RAFT polymerization.

$^1$H-NMR: 300 MHz, DMSO-$d_6$ (70 °C): δ / ppm = 0.7-0.9 (3H -CH$_3$ end group CMDT), 1.2-1.3 (20H -CH$_2$- CMDT), 1.2-1.9 (4H -CH$_2$-backbone of AAm and AN), 1.9-2.4 (1H -CH-CONH$_2$ backbone of AAm), 1.9-2.6 (1H -CH-CN backbone of AN), 6.7-7.8 (2H -NH$_2$ amide protons). For NMR signal assignation see Figure 28 B.

FTIR: ν / cm$^{-1}$= 3800-3000 (mb, NH), 2990-2840 (w, CH), 2240 (w, CN), 1649 (vs, CO), 1458 (m), 1410 (m), 1344 (m), 1316 (m), 1120 (w).

The composition of the poly(AAm-*co*-AN) samples was based on the combined analysis of FTIR and $^1$H NMR. Using the calibration curve presented in Section 4.2.3, the integral ratio (CO/CN) from the characteristic bands of PAAm (1653 cm$^{-1}$) and PAN (2240 cm$^{-1}$), could be calculated. From the $^1$H NMR analysis, the end group -C*H$_3$* (0.85 ppm) served as reference signal to obtain the integrals of AAm and AN in the spectrum between 1.2-2.4 ppm (Figure 28 B). Using the determined composition by IR and the content of AAm and AN units in the NMR analysis, the composition of each polymer could be calculated.

## 4.3.4 Hydrolysis and purification of copolymers of AAm and AN

The hydrolysis process of poly(AAm-*co*-AN) was carried out as follow: the samples were dissolved in 2 mL of HCl (1 M) or NaOH (1 M), respectively. After the polymers were completely dissolved, the samples were heated at 40 °C in a thermo-shaker at 250 rpm using different times for the hydrolysis reactions (1 and 6 h). Afterwards, the samples were cooled to RT and the pH of the hydrolyzed solutions was shifted to a pH of 4. The samples were purified by dialysis against water over 3 days. To dry the hydrolyzed polymer samples, freeze-drying was carried out over 24 h.

## 4.3.5 Synthesis of UCST BCPs with poly(AAm-*co*-AN) as macro CTA (Route I)

The synthesis of di-block copolymers was carried out with poly(AAm-*co*-AN) as CTA (synthesis and characterization in Section 4.3.3). The St content in feed was varied in order to obtain higher molecular weights and more hydrophobic polymers. In a typical polymerization *via* RAFT for a particular composition, 1 equiv. of poly(AAm-*co*-AN) as macro CTA (0.244 g) was weighed into a 25 mL nitrogen flask and dissolved in 6 mL DMSO before adding 600 equiv. of St (0.748 g) as monomer. AIBN ($6 \cdot 10^{-3}$ equiv.) was added to the previous solution. To degas the solution, freeze−pump−thaw cycles procedure was used and the flask was placed into a preheated oil bath at 100 °C. The polymerization was stopped after 24 h. The polymer was precipitated in 10-fold excess volume of methanol and rinsed again with methanol over three centrifugation wash cycles using a 10 min (10.000 rpm) centrifugation program. The obtained yellowish polymer was dried under vacuum for 24 h at 40 °C. Using similar procedure, several copolymers were made by changing the feed compositions. The obtained yield was 43 % (determined gravimetrically).
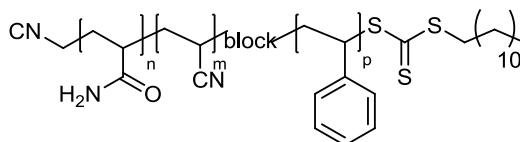


Figure 77: Chemical structure of the synthesized BCP *via* RAFT polymerization, using poly(AAm-*co*-AN) as CTA and St as hydrophobic segment.

$^1$H-NMR: 300 MHz, DMSO-$d_6$ (70 °C): δ / ppm = 0.7-0.9 (3H -CH$_3$ end group CMDT), 1.1-1.3 (20H -CH$_2$- CMDT), 1.2-2.0 (6H -CH$_2$-backbone of AAm, AN and St), 2.0-2.6 (3H -CH-backbone of AAm, AN and St), 6.2-7.6 (7H -NH$_2$ amide and -C$_6$H$_5$ phenylic protons). For NMR signal assignation see Figure 47 B.

To obtain the BCP composition, it was assumed that the poly(AAm-$co$-AN) macromonomer composition should remained the same after chain extension (FTIR analysis, see Section 4.3.3). Since the amide and aromatic protons overlapped in the region between 6.5-8 ppm, the integral difference between the polymer before and after chain extension enabled to calculate the content of St in the polymer. For all NMR analysis the end group -C$H_3$ (0.85 ppm) served as reference signal.

## 4.3.6  Synthesis of PS as macro CTA *via* RAFT polymerization

To prepare BCPs with PS as macro CTA, St was first polymerized in bulk *via* RAFT. In a typical polymerization *via* RAFT for a particular composition, a total monomer concentration of 200 equivalent was used. In a 25 mL nitrogen flask St (5.5 g), CMDT 1 equiv. (0.083 g) and 0.2 equiv. (8.6 10$^{-3}$ g) of AIBN as initiator were weighed. To degas the monomer, freeze−pump−thaw cycles procedure was used. Afterwards the flask was placed into a preheated oil bath at 70 °C. The polymerization was stopped after 3 h, and the polymer was precipitated in 10-fold excess volume of methanol and rinsed again with methanol over three centrifugation wash cycles using a 5 min (8.000 rpm) centrifugation program. The obtained yellowish polymer was dried under vacuum for 24 h at 40 °C. The obtained yield was 18 % (determined gravimetrically).
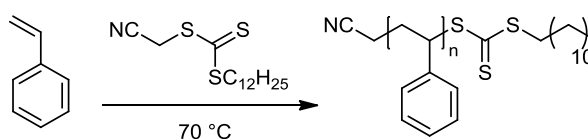


Figure 78: Chemical reaction for the synthesis of PS *via* RAFT polymerization, using CMDT as CTA.

$^1$H-NMR: 300 MHz, DMSO-$d_6$ (70 °C): δ / ppm = 0.8-0.9 (3H -CH$_3$ end group CMDT), 1.2-1.3 (20H -CH$_2$- CMDT), 1.3-1.7 (2H -CH$_2$-backbone of St), 1.7-2.3 (1H -CH-backbone of St), 6.3-7.3 (5H -C$_6$H$_5$ phenylic protons of St).

## 4.3.7 Synthesis of UCST BCPs with PS as macro CTA (Route II)

The synthesis of di-block copolymers was carried out with PS as macro CTA. In a typical reaction for a particular composition *via* RAFT, 1 equiv. of PS as CTA (0.097 g) were weighed into a 50 mL nitrogen flask and dissolved in 20 mL DMSO before adding 300 equiv. of AAm (1.09 g) and 100 equiv. of AN (0.3 g) as monomers. AIBN (0.5 equiv.) was added to the previous solution. To degas the solution, freeze−pump−thaw cycles procedure was used. The flask was placed into a preheated oil bath at 70 °C. The polymerization was stopped after 7 h. The obtained polymer was precipitated in 10-fold excess volume of methanol and rinsed again with methanol over three centrifugation wash cycles using a 10 min (10.000 rpm) centrifugation program. The obtained yellowish polymer was dried under vacuum for 24 h at 40 °C. The obtained yield was 72 % (determined gravimetrically).
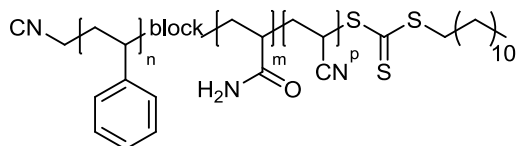


Figure 79: Chemical structure of the synthesized BCP *via* RAFT polymerization, using PS as CTA and AAm-AN copolymer as hydrophilic thermoresponsive segment.

^{1}H-NMR: 300 MHz, DMSO-$d_6$ (70 °C): δ / ppm = 0.7-0.8 (3H -$CH_3$ end group CMDT), 1.1-1.2 (20H -$CH_2$- CMDT), 1.2-1.8 (6H -$CH_2$-backbone of AAm, AN and St), 1.8-2.4 (3H -CH-backbone of AAm, AN and St), 6.1-7.9 (7H -$NH_2$ amide and -$C_6H_5$ phenylic protons).

FTIR: v / cm$^{-1}$= 3700-3000 (mb, $NH_2$), 3026 (w), 2950-2800 (w, CH), 2241 (w, CN), 1665 (vs, CO), 1493 (w), 1447 (m), 1414 (w), 1349 (w), 1314 (w), 1022 (m).

To obtain the BCP composition, similar procedure was followed as described in Sections 4.3.3 and 4.3.5. For all NMR analysis the end group -C$H_3$ (0.85 ppm) served as reference signal.

## 4.3.8 Synthesis of LCST BCPs with PS as macro CTA and NIPAM as hydrophilic block

The synthesis of LCST BCPs was carried out *via* sequential RAFT polymerization as sketched in Figure 80. In a first step, St was polymerized in bulk with CMDT as RAFT agent. The obtained PS macro CTA was used for the controlled polymerization of NIPAM in a second step with AIBN as initiator. Table 8 presents the summary of the synthesized samples (see Section 3.3.3.1).

The successful chain extension of the PS block with the thermoresponsive segment of NIPAM is shown in the GPC and $^1$H NMR analysis (Figure 81). The obtained GPC curves were monomodal with narrow molar mass distributions (Đ 1.2-1.3) (Figure 81 A). The obtained $^1$H NMR spectrum before chain extension showed the characteristic signals of the aromatic protons of PS at 6.3-7.3 ppm. After the chain extension with NIPAM, the NMR spectrum showed the typical proton signal of PNIPAM (CON-C$H$) at 4.04 ppm, as well as the formation of new signals in the backbone range 1-2.5 ppm (Figure 81 B).
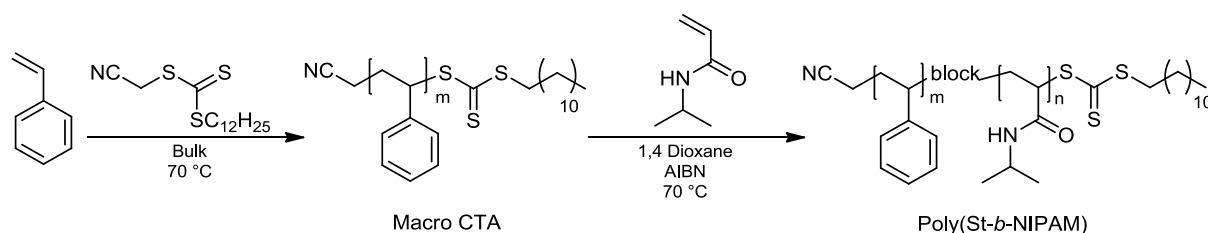


Figure 80: Sequential RAFT polymerization for the synthesis of poly(St-*b*-NIPAM). PS was used as macro CTA and AIBN as initiator.
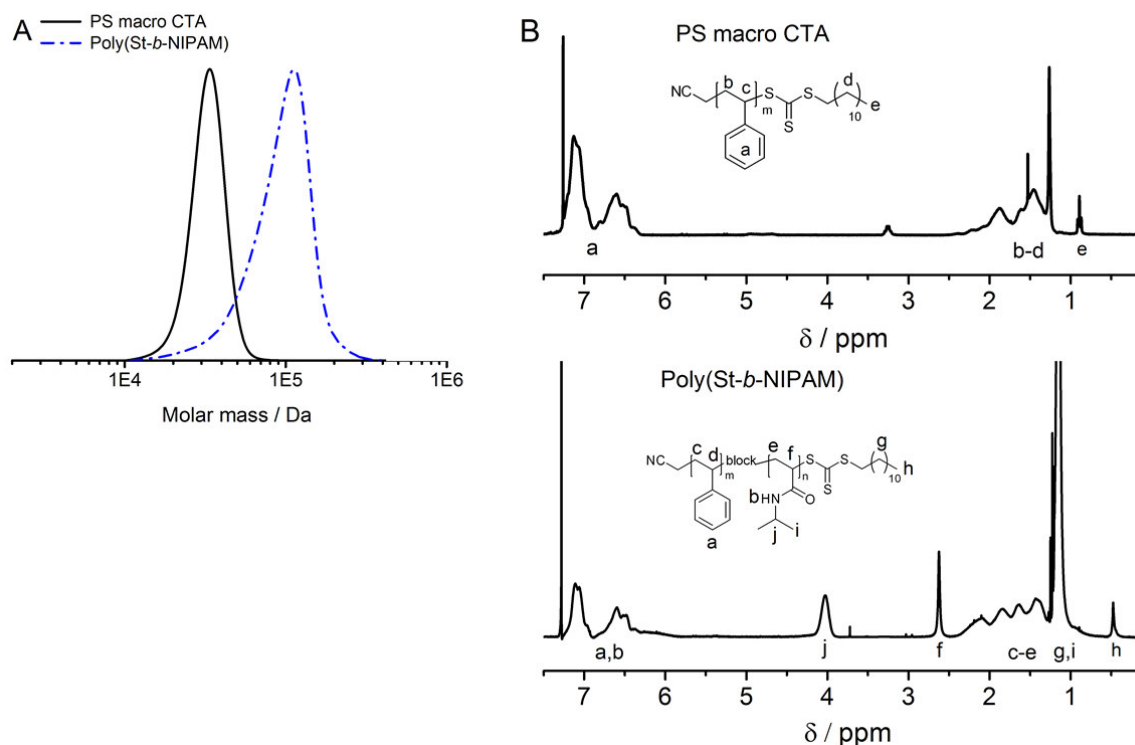
Figure 81: (A) GPC curves (DMF) of the PS macro CTA ($M_n$ = 30600 Da, Đ = 1.1) before and after chain extension with NIPAM ($M_n$ = 84700 Da, Đ = 1.3). (B) $^1$H NMR spectra in CDCl$_3$ of PS and poly(St-b-NIPAM) (Table 8, entry 2).

The synthesis of the BCPs was carried out following the synthetic process showed in a previous Section (4.3.7). In a typical reaction for a particular composition, 1 equiv. of PS as macro CTA (0.63 g) were weighed into a 25 mL nitrogen flask and dissolved in 6 mL dioxane before adding 400 equiv. of NIPAM (0.9 g) as monomer. AIBN (0.25 equiv.) was added to the previous solution. To degas the solution, freeze−pump−thaw cycles procedure was used. The flask was placed into a preheated oil bath at 70 °C. The polymerization was stopped after 14 h, and the obtained polymer was precipitated in 10-fold excess volume of diethyl ether and rinsed again with diethyl ether over three centrifugation wash cycles using a 10 min (10.000 rpm) centrifugation program. The obtained yellowish polymer was dried under vacuum for 24 h at 40 °C. The obtained yield was 70 % (determined gravimetrically).

$^1$H-NMR: 300 MHz, CDCl$_3$: δ / ppm = 0.8-0.9 (3H -CH$_3$ end group CMDT), 0.9-1.1 (20H -CH$_2$- CMDT), 1.2-1.5 (4H -CH$_2$-backbone of NIPAM and St), 1.6-2.3 (2H -CH-backbone of NIPAM and St), 3.8-4.1 (1H -CH- isopropyl group of NIPAM), 6.2-7.4 (6H -NH and -C$_6$H$_5$ phenylic protons).

105

## 4.4 Processing methods and preparation of samples

### 4.4.1 Sample preparation for turbidimetry measurements

For the preparation of aqueous polymer samples of poly(AAm-*co*-St), the polymers were dissolved in polypropylene (PP) tubes (0.5 wt%) over 90 min at 70 °C. The obtained polymer solution was filtered with a preheated PET filter (1.2 µm) in the measuring cuvette.

Samples of poly(AAm-*co*-AN) were dissolved in water at a concentration of 1 wt% above the UCST by direct mixing in PP tubes (dissolution time 5 min).

### 4.4.2 Dialysis of UCST samples

Dialysis of UCST BCPs (DMF against water) was carried out with 50 mg of sample dissolved in 3.5 mL DMF. Dialysis tubes (Spectra/Por 6) from regenerated cellulose (MWCO 3.500 g mol $^{-1}$) were used. The tubes for dialysis were carefully washed with water for opening the pores. Same dialysis tubes were used for the purification of hydrolyzed samples of poly(AAm-*co*-AN). In this case, 2.5 mL of the hydrolyzed polymer solution (40 mg mL $^{-1}$) was used. All polymers were dialyzed against water (1 L) over 3 days at RT.

### 4.4.3 Non-solvent induced phase separation (NIPS)

The general procedure for the preparation of films via NIPS was performed as followed: the polymer solution was casted on a glass slide and with a laboratory blade (200 µm gap) a thin film was formed and allowed to evaporate for 120 s. Afterwards, the substrate was immersed into a water bath (non-solvent) over 1 h. Subsequently, the water-organic solvent mixture of the coagulation bath was replaced with pure water, in order to eliminate rest of organic solvents. The formed film remained in the coagulation bath over 24 h at RT. Further details are given in in Table 10.

Table 10: Details for the preparation of films using thermoresponsive BCPs of UCST and LCST type *via* NIPS

| Polymer sample | Concentration / wt% | Solvent mixture (% v/v) DMF:THF ratio | Water (non-solvent) temperature / °C |
|---|---|---|---|
| Poly(AAm-*co*-AN-*b*-St) | 16 | 90:10 | 20 |
| Poly(St-*b*-AAm-*co*-AN) | 17 | 90:10 | 20 |
| Poly(St-*b*-NIPAM) | 14 | 50:50 | 20 |
| Poly(St-*b*-NIPAM) | 14 | 50:50 | 40 |

## 4.4.4  Formation of nanofibers by electrospinning

For electrospinning of monolithic fibers based on BCPs, different concentrations and solvent mixtures were required. The electrospinning procedure was carried out using a conventional one needle set-up under high voltage as describe in Section 2.4.2. The fibers were collected on different materials such as stainless steel mesh and aluminum foil. Further details are given in the Table 11.

Table 11: Details for the preparation of electrospun fibers of thermoresponsive BCPs of UCST and LCST type

| Polymer sample | Concentration / wt% | Solvent mixture (% v/v) DMF:THF ratio | Voltage / kV | Relative Humidity / % | Flow rate |
|---|---|---|---|---|---|
| Poly(AAm-*co*-AN-*b*-St) | 35 | 85:15 | 14 | 55 | 0.4 mL h$^{-1}$ |
| Poly(St-*b*-AAm-*co*-AN) | 40[a] | 85:15 | 12 | 55 | 0.1 mL h$^{-1}$ |
| Poly(St-*b*-NIPAM) | 30 | 50:50 | 14 | 70[b] | 0.6 mL h$^{-1}$ |

[a] Fibers with bead formation, [b] For electrospinning under high humidity conditions

## 4.4.5  Formation of nanofibers combining electrospinning and NIPS method

LCST monolithic fibers prepared by the combination of electrospinning and NIPS (Figure 82), were fabricated using a concentration of 30 wt% and solvent mixture 1:1 (DMF:THF). The electrospinning procedure was carried out using a conventional one needle set-up under high voltage (16 kV). In this type of combined electrospinning method, the distance between the needle and the collector (water) was 6 cm. The fibers were collected in water and were dried under vacuum for further characterization.
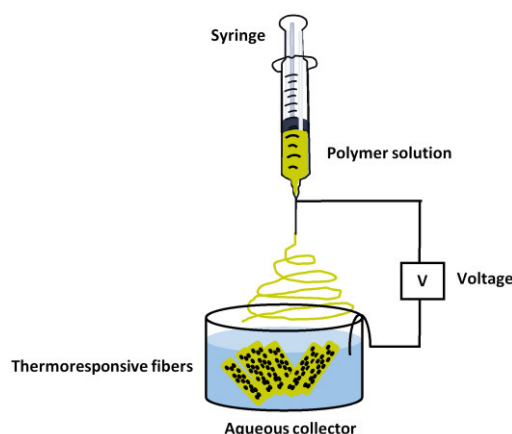


Figure 82: Combination of electrospinning and NIPS as processing methods of LCST BCPs.

# 5  Summary

In the present work, novel Upper Critical Solution Temperature (UCST) polymer systems and fundamental tools for the processing of thermoresponsive polymers *via* Non-Solvent Induced Phase Separation (NIPS) and electrospinning have been achieved. The main aim was the design and characterization of thermoresponsive polymers, particularly of non-ionic UCST type and investigating the effect of important parameters, such as compositional chain homogeneity and pH on the UCST behavior. The fabrication of water-insoluble thermoresponsive systems for processing applications represented the main challenge. Therefore, the processing of UCST polymers to water-stable porous films and fibers, that retained thermoresponsivity and shape in the applied media, was a further goal. Porous morphologies were of particularly interest, due to the possible applications as scaffold and carrier material with interpenetration properties.

There is a growing demand to develop new UCST systems and explore their stability for possible applications. Therefore, the investigation of the thermoresponsive and chemical stability of UCST systems was one important issue in this work. Hence, commercially available and cost-effective monomers, *e.g.* acrylamide (AAm), acrylonitrile (AN) and styrene (St) were applied for the fabrication of UCST type polymers. Thereby, the synthesis method was decisive to obtain a reversible responsive behavior in water. While copolymers of AAm and St prepared *via* free radical polymerization were non-thermoresponsive at all temperatures and concentrations, the same copolymers prepared *via* Reversible Addition-Fragmentation Chain Transfer (RAFT) showed sharp phase transition temperatures in the range from 50-62 °C. These results underlined the importance of chain homogeneity for the preparation of UCST polymers, especially for monomers that differed significantly in their reactivity parameters.

In addition, important stability studies of the chemical and thermoresponsive behavior towards intentional hydrolysis were carried out with poly(AAm-*co*-AN) as model polymer system. The use of acid or alkali aqueous media induced different hydrolysis rates of the polymer. Under neutral to mild acidic conditions, the thermoresponsive behavior could be maintained, whereas an alkali environment decreased or even hindered the phase transition completely. Further, under mild hydrolysis conditions, *e.g.* using buffer solutions at room temperature (RT), decreased hydrolysis rates were observed. The carboxylic groups formed during hydrolysis induced a pH dependent thermoresponsive system. However, in the presence of ionic groups, protonation or shielding of the ions was required, in order to achieve a switchable pH-thermoresponsive behavior. Previously the introduction of ionic groups was seen as undesirable for non-ionic UCST polymers; however, these results showed the potential of a new feature for

a dual responsive behavior in aqueous media. Further development of the UCST systems could be achieved by the transformation of UCST water-soluble systems into processable and water-stable polymers. To achieve this aim, UCST block copolymers (BCPs) were prepared based on two synthetic routes *via* sequential monomer addition by RAFT. In the first route, poly(AAm-*co*-AN) was used as macromonomer, which was chain extended with St in a second polymerization step. In dependence of the St content different BCPs were prepared, which were subsequently applied as UCST responsive micelles as well as processable films and fibers, using NIPS and electrospinning methods, respectively. The prepared films were analyzed using μ-DSC measurements. A broad phase transition temperature between ~45-30 °C (cooling cycle) was observed. Moreover, SEM analysis of the film morphology revealed highly porous structures on the surface as well as of the cross-section. Further, the type of method used for film formation was critical to obtain responsive polymer films. For instance, the NIPS method induced an orientation of the thermoresponsive groups towards surface, which was crucial for obtaining responsivity in BCP films. Moreover, the processing BCPs of Route I to electrospun fibers was also successful. However, the molecular weight in the range of 30600 Da, required high polymer concentrations (35 wt%) for a continuous electrospinning process. The prepared fibers showed a swelling behavior upon heating (60 °C) by increasing the fiber diameter from ~2.4 to 4.3 μm. Further, SEM analysis revealed that the fiber morphology was stable after water contact at different temperatures. The second synthetic route for the preparation UCST BCPs, used poly(styrene) (PS) as macromonomer, which was subsequent chain extended with AAm and AN as copolymers, likewise *via* RAFT. After chain extension, the thermoresponsive behavior of the new BCP system was analyzed using turbidity measurements in mixtures of water : THF. The phase transition temperature presented a broad hysteresis; however, a reversible UCST behavior was obtained. The processing as film material of the BCP was achieved using NIPS. Further, the low content of PS in the BCP induced the formation of a "gel-like" film, which showed an evident thermoresponsive behavior upon cooling and heating. Whereas the film formation was successful, the processing as fiber was difficult to achieve using this system. Therefore, a blending with PS (1.0 wt%) was required to obtain a spinnable material.

The fundamental tools for the processing of UCST BCPs as film and fiber material, was achieved based on a BCP reference system (poly(St-*b*-NIPAM)) with lower critical solution temperature (LCST), which used PS as hydrophobic supporting segment. The formation of films *via* NIPS with variation of the temperature of the coagulation bath showed the self-assembly of the two blocks upon contact with water at a specific temperature. While samples

prepared at temperatures above the LCST (40 °C) showed inhomogeneous porous structures, the use of water at RT (20 °C) induced the formation of homogenous and dense porous morphology. Further, the prepared films presented a continuous porosity with porous structures in the range of 0.5 µm. The processing of the BCPs as fibers, using high humidity, showed the fabrication of nano-porous structures in the range of 13-17 nm. The high humidity conditions also increased the fiber diameter from 4.5 to 9.5 µm. Moreover, the combination of NIPS and electrospinning into one method was also effective to change the fiber morphology, in this case, the fiber surface was very rough and in the cross-section highly porous structures were obtained. Important to remark is, that the fiber morphology of LCST BCPs was stable even after several heating and cooling cycles, when BCP samples with a longer PS block ($M_n$ = 30600 Da) were used.

The work presented here contributed with important tools for the design and understanding of new UCST polymer systems. Additionally, processing strategies for this promising class of thermoresponsive polymers have been developed, which will provide the basis for further investigations and future applications.

# 6 Zusammenfassung

In der vorliegenden Arbeit wurden neue Upper Critical Solution Temperature (UCST) Polymersysteme entwickelt und grundlegende Methoden für die Verarbeitung thermoresponsiver Polymere, z.B. durch Non-Solvent Induced Phase Separation (NIPS) und Elektrospinnen, untersucht. Das Hauptziel war die Entwicklung und Charakterisierung thermoresponsiver Polymere, insbesondere des nicht-ionischen UCST-Typs und die Untersuchung wichtiger Parameter, wie der Homogenität der Polymerkonstitution und des pH-Werts, auf das UCST-Verhalten. Die Herausforderung bestand in der Herstellung wasserunlöslicher thermoresponsiver Systeme um vorrangig deren Verarbeitbarkeit zu ermöglichen. Daher lag ein weiteres Ziel in der Verarbeitung von UCST-Polymeren zu wasserbeständigen porösen Filmen und Fasern, welche deren Thermoresponsivität und Form in den verwendeten Medien beibehielten. Aufgrund der möglichen Anwendungen als synthetisches Grundgerüst und Trägermaterial mit permeablen Eigenschaften waren poröse Morphologien von besonderem Interesse.

Es besteht eine wachsende Nachfrage neue UCST-Systeme zu entwickeln und ihre Stabilität für mögliche Anwendungen zu erforschen. Deshalb war die Untersuchung der thermoresponsiven und chemischen Stabilität von UCST-Systemen ein wichtiges Kernthema dieser Arbeit. Handelsübliche und kostengünstige Monomere, wie z.B. Acrylamid (AAm), Acrylnitril (AN) und Styrol (St) wurden daher zur Herstellung von UCST-Polymeren verwendet. Um ein reversibles UCST-Verhalten solcher Systeme in Wasser zu erhalten, war das Syntheseverfahren entscheidend. Während Copolymere bestehend aus AAm und St, hergestellt durch freie radikalische Polymerisation, bei allen untersuchten Temperaturen und Konzentrationen keine Thermoresponsivität zeigten, konnte dieses für dieselben Copolymere, hergestellt durch Reversible Addition-Fragmentation Chain Transfer (RAFT) erreicht werden. Dabei wurden scharfe Phasenübergangstemperaturen im Bereich zwischen 50-62 ℃ beobachtet. Diese Ergebnisse heben den Einfluss der Kettenhomogenität für die Darstellung von UCST-Polymeren hervor, insbesondere für diejenigen Monomere deren Reaktivitätsparameter sich signifikant unterscheiden.

Im Weiteren wurde Poly(AAm-*co*-AN) als Modellsystem verwendet um Stabilitätsuntersuchungen zwecks dem chemischen und thermoresponsiven Verhalten gegenüber einer gezielten Hydrolyse zu untersuchen. Die Verwendung von sauren oder alkalisch wässrigen Medien induzierte unterschiedliche Hydrolyseraten des Polymers. Wohingegen unter neutral bis mild sauren Bedingungen die Thermoresponsivität beibehalten

werden konnte, verringerte sich oder erlosch der Phasenübergang unter alkalischen Umgebungen vollständig. Ferner wurde unter milden Hydrolysebedingungen, z.B. unter Verwendung von Pufferlösungen bei Raumtemperatur (RT), eine verminderte Hydrolyserate beobachtet. Die während der Hydrolyse gebildeten Carboxylgruppen induzierten ein pH-abhängiges thermoresponsives System. In Gegenwart von ionischen Gruppen war jedoch eine Protonierung beziehungsweise Abschirmung der Ionen erforderlich, wodurch ein schaltbares pH-thermoresponsives Verhalten erreicht werden konnte. Bisweilen war die Einführung von ionischen Gruppen für nicht-ionische UCST-Polymere als nicht wünschenswert angesehen; jedoch zeigten die Resultate dieser Arbeit das Potential auf, ein doppeltes Ansprechverhalten in wässrigen Medien zu erhalten. Eine Weiterentwicklung von UCST-Systemen konnte durch die Umwandlung von wasserlöslichen Systemen zu verarbeitbaren und wasserstabilen Polymeren erreicht werden. Um dieses Ziel zu erreichen, wurden UCST-Blockcopolymere (BCPs) auf der Basis von zwei Synthesewegen über sequenzieller Monomeraddition durch RAFT hergestellt. Die erste Route verwendete Poly(AAm-*co*-AN) als Makromonomer, um in einem zweiten Polymerisationsschritt mittels St eine Kettenverlängerung zu induzieren. In Abhängigkeit von dem St-Gehalt wurden verschiedene BCPs hergestellt, die zur Herstellung UCST-responsiver Mizellen dienten, und unter Verwendung von NIPS- bzw. dem Elektrospinnen zu Filmen oder Fasern weiterverarbeitet wurden. Die hergestellten Filme wurden dabei mittels μ-DSC-Messungen analysiert, wodurch eine breite Phasenübergangstemperatur zwischen ~45-30 °C (Kühlkurve) beobachtet wurde. Darüber hinaus bestätigten SEM-Analysen der Filmmorphologien eine hochporöse Struktur auf der Oberfläche als auch im Filmquerschnitt. Dabei war die verwendete Methode der Filmpräparation ausschlaggebend um responsive Polymerfilme zu erhalten. Das NIPS-Verfahren zum Beispiel induzierte eine Orientierung der thermoresponsiven Gruppen zur Oberfläche, was für die Erzielung einer Thermoresponsivität in BCP-Filmen entscheidend war. Ferner war die Verarbeitung von BCPs aus der Route I zu elektrogesponnen Fasern ebenfalls möglich. Da das Molekulargewicht der Polymere jedoch im Bereich von 30600 Da lag, wurden hohe Polymerkonzentrationen von 35 gew% für ein kontinuierliches Elektrospinnverfahren benötigt. Ein Quellverhalten beim Erwärmen (60 °C) durch Erhöhung des Faserdurchmessers von 2,4 auf 4,3 μm wurde für die hergestellten Fasern beobachtet. Dabei bestätigten SEM-Analysen, dass die Fasermorphologie nach Wasserkontakt bei verschiedenen Temperaturen stabil war. In der zweiten Syntheseroute zur Herstellung von UCST BCPs wurde Polystyrol (PS) als Makromonomer verwendet, um nachfolgend eine Copolymerisations-Kettenverlängerung mit AAm und AN durchzuführen, ebenfalls über RAFT. Nach der

Kettenverlängerung wurde das thermoresponsive Verhalten des neuen BCP-Systems mittels Trübungsmessungen aus Gemischen von Wasser zu THF analysiert. Die Phasenübergangstemperatur zeigte eine breite Hysterese; dennoch wurde ein reversibles UCST-Verhalten beobachtet. Die Verarbeitung dieses BCPs zu Filmen konnte ebenfalls unter Verwendung von NIPS erreicht werden. Dabei induzierte der niedrige PS Gehalt in dem BCP die Bildung eines "gelartigen" Films, wodurch ein beobachtbares thermoresponsives Verhalten beim Abkühlen und Erwärmen verfolgt werden konnte. Obwohl dieses BCP System erfolgreich zu Filmen verarbeitet werden konnte, war die Verarbeitung zu Fasermaterialien schwierig zu erreichen. Daher war ein Mischen mit PS (1,0 gew%) erforderlich, um ein spinnbare Lösung zu erhalten.

Die grundlegenden Methoden für die Verarbeitung von UCST-BCPs zu Film und Fasermaterial wurden auf Basis des Referenzsystems von BCPs (Poly(St-*b*-NIPAM)) mit Lower Critical Solution Temperature (LCST) entwickelt, welches ebenfalls PS als hydrophobes Segment verwendete. Die Filmpräparation über NIPS mit Variation der Temperatur des Koagulationsbades ermöglichte dabei die Selbstorganisation der beiden Blöcke bei Kontakt mit Wasser bei einer bestimmten Temperatur. Während Proben, die bei Temperaturen über dem LCST (40 °C) hergestellt wurden, inhomogene poröse Strukturen zeigten, führte die Verwendung von Wasser bei RT (20 °C) zur Bildung von homogenen und dicht porösen Morphologien. Dabei wurde für die hergestellten Filme eine kontinuierliche Porosität mit porösen Strukturen im Bereich von 0,5 μm beobachtet. Die Verarbeitung dieses BCPs zu Fasern, unter Verwendung hoher Feuchtigkeit, ermöglichte die Herstellung von nanoporösen Strukturen im Bereich von 13-17 nm. Die hohe Feuchtigkeit erhöhte ebenfalls den Faserdurchmesser von 4,5 auf 9,5 μm. Ferner war auch die Kombination von NIPS und Elektrospinnen in einem Verfahren wirksam um beispielsweise die Fasermorphologie zu ändern. In diesem Fall wurden eine sehr raue Faseroberfläche und im Querschnitt hochporöse Strukturen erhalten. Im besonderen Maße erwähnenswert ist, dass die Fasermorphologie von LCST-BCPs auch nach mehreren Heiz- und Kühlzyklen stabil war, wenn BCP-Proben mit einem längeren PS-Block ($Mn = 30600$ Da) verwendet wurden.

Die hier vorgestellte Arbeit zeigte wichtige Methoden für die Entwicklung und das Verständnis neuer UCST-Polymersysteme auf. Zusätzlich wurden verschiedene Verarbeitungsstrategien für diese vielversprechende Klasse von thermoresponsiven Polymere entwickelt, welche die Grundlage für weitere Untersuchungen als auch zukünftige Anwendungen bilden.

# 7 Outlook

The synthesis and characterization of responsive polymers presented in this work set a milestone for the development of new thermoresponsive materials. Further, the modification of water-soluble systems into stable film and fiber materials, with thermoresponsive properties, is expandable to other BCP systems, which could find different interesting types of applications. The use of commercially available monomers for the synthesis of UCST responsive polymers increases the possible fabrication and application of new UCST polymers, since UCST systems based, *e.g.* on NAGA, are so far of higher price, due to their uncommercial availability. However, not every polymerization method is adequate to obtain a well-defined thermoresponsive behavior. In this thesis, for instance, the importance of chain homogeneity was shown for non-ionic UCST polymers, by synthesis *via* RAFT polymerization of AAm and St. Hence, these results serve as the fundament for the preparation of new UCST copolymers, using monomers with very different polymerization reactivity. Moreover, intentional hydrolysis of UCST copolymers based on AAm and AN explore one important issue in the field of UCST systems, such as chemical stability. Further, the use of mild hydrolysis conditions enable the formation of a dual responsive polymer. This type of behavior can find interesting application as "on-off" switchable system, where the thermoresponsive behavior is activated by small variation of the pH media.

The preparation of thermoresponsive BCPs of UCST type with varied hydrophobic content increased the stability in water, which offers the exploration of new properties, since processing without post-modification is now available as film and fiber material. Further, to increase even more the stability and applicability of processed UCST BCP systems, it is important to explore new synthesis with other hydrophobic monomers. For instance, the incorporation of flexible properties (low glass transition temperatures) as well as hydrolytic resistance represents a challenging and interesting approach. The presented advances with UCST polymers demonstrate that this type of system is achieving a strong development to reach its LCST counterpart.

Moreover, controlled fabrication of porous morphologies in responsive polymers is of particular interest not only in the field scaffold materials but also for filtration membranes. Thus, LCST BCPs represent a promising material for membrane applications, since these are successfully processed *via* NIPS. This type of method enables the fabrication of highly porous structures with variable morphology.

# 8 Acknowledgments

# 9 Literature

1    J. Chen and C. Chang, *Materials*, 2014, **7**, 805–875.

2    M. A. Ward and T. K. Georgiou, *Polymers*, 2011, **3**, 1215–1242.

3    C. de las Heras Alarcón, S. Pennadam and C. Alexander, *Chem. Soc. Rev.*, 2005, **34**, 276–285.

4    E. Cabane, X. Zhang, K. Langowska, C. G. Palivan and W. Meier, *Biointerphases*, 2012, **7**, 1–27.

5    A. Gandhi, A. Paul, S. O. Sen and K. K. Sen, *Asian J. Pharm. Sci.*, 2015, **10**, 99–107.

6    J. Seuring and S. Agarwal, *Macromol. Chem. Phys.*, 2010, **211**, 2109–2117.

7    J. Seuring and S. Agarwal, *Macromolecules*, 2012, **45**, 3910–3918.

8    H. Zhang, X. Tong and Y. Zhao, *Langmuir*, 2014, **30**, 11433–11441.

9    H. Zhang, S. Guo, W. Fan and Y. Zhao, *Macromolecules*, 2016, **49**, 1424–1433.

10   B. A. Pineda-Contreras, H. Schmalz and S. Agarwal, *Polym. Chem.*, 2016, **7**, 1979–1986.

11   J. Seuring and S. Agarwal, *Macromol. Rapid Commun.*, 2012, **33**, 1898–1920.

12   F. Liu, J. Seuring and S. Agarwal, *J. Polym. Sci. Part A Polym. Chem.*, 2012, **50**, 4920–4928.

13   Y. Kim, M. Ebara and T. Aoyagi, *Sci. Technol. Adv. Mater.*, 2012, **13**, 1–9.

14   J. Li, Y. Zhou and Z. Luo, *ACS Appl. Mater. Interfaces*, 2015, **7**, 19643–19650.

15   F. Schacher, M. Ulbricht and A. H. E. Müller, *Adv. Funct. Mater.*, 2009, **19**, 1040–1045.

16   F. Schacher, T. Rudolph, F. Wieberger, M. Ulbricht and A. H. E. Müller, *ACS Appl. Mater. Interfaces*, 2009, **1**, 1492–1503.

17   A. Greiner and J. H. Wendorff, *Angew. Chemie Int. Ed.*, 2007, **46**, 5670–5703.

18   K. A. G. Katsogiannis, G. T. Vladisavljevic and S. Georgiadou, *Eur. Polym. J.*, 2015, **69**, 284–295.

19   S. S. Shah, J. Wertheim, C. T. Wang and C. G. Pitt, *J. Control. Release*, 1997, **45**, 95–101.

20      D. Schmaljohann, *Adv. Drug Deliv. Rev.*, 2006, **58**, 1655–1670.

21      C. Pietsch, A. Vollrath, R. Hoogenboom and U. S. Schubert, *Sensors*, 2010, **10**, 7979–7990.

22      I. Tan, Z. Zarafshani, J.-F. Lutz and M. Titirici, *ACS Appl. Mater. Interfaces*, 2009, **1**, 1869–1872.

23      H. Kanazawa, K. Yamamoto and Y. Matsushima, *Anal. Chem.*, 1996, **68**, 341–346.

24      F. Liu, J. Seuring and S. Agarwal, *Macromol. Chem. Phys.*, 2014, **215**, 1466–1472.

25      Y. F. Poon, Y. Cao, Y. Liu, V. Chan and M. B. Chan-Park, *ACS Appl. Mater. Interfaces*, 2012, **2**, 2012–2025.

26      C. Weber, H. Richard and U. Schubert, *Prog. Polym. Sci.*, 2012, **37**, 686–714.

27      J. Seuring and S. Agarwal, *ACS Macro Lett.*, 2013, **2**, 597–600.

28      J. Seuring, F. M. Bayer, K. Huber and S. Agarwal, *Macromolecules*, 2012, **45**, 374–384.

29      B. A. Pineda-Contreras, F. Liu and S. Agarwal, *J. Polym. Sci. Part A Polym. Chem.*, 2014, **52**, 1878–1884.

30      H. Mori and T. Endo, *Macromol. Rapid Commun.*, 2012, **33**, 1090–1107.

31      J. S. Scarpa, D. D. Mueller and I. M. Klotz, *J. Am. Chem. Soc.*, 1967, **89**, 6024–6030.

32      D. Roy, W. L. Brooks and B. S. Sumerlin, *Chem Soc Rev*, 2013, **42**, 7214–7243.

33      Y. Zhang, S. Furyk, D. E. Bergbreiter and P. S. Cremer, *J. Am. Chem. Soc.*, 2005, **127**, 14505–14510.

34      R. Liu, M. Fraylich and B. R. Saunders, *Colloid Polym. Sci.*, 2009, **287**, 627–643.

35      R. Pelton, *J. Colloid Interface Sci.*, 2010, **348**, 673–674.

36      X. Yin, A. S. Hoffman and P. S. Stayton, *Biomacromolecules*, 2006, **7**, 4–8.

37      Y. Mai and A. Eisenberg, *Chem. Soc. Rev.*, 2012, **41**, 5969–5985.

38      S. Darling, *Prog. Polym. Sci.*, 2007, **32**, 1152–1204.

39      T. H. Epps and R. K. O'Reilly, *Chem. Sci.*, 2016, **7**, 1674–1689.

40      A.-V. Ruzette and L. Leibler, *Nat. Mater.*, 2005, **4**, 19–31.

# Literature

41     F. S. Bates and G. H. Fredrickson, *Phys. Today*, 1999, **52**, 32–38.

42     D. J. Lohse and N. Hadjichristidis, *Curr. Opin. Colloid Interface Sci.*, 1997, **2**, 171–176.

43     S. E. Mastroianni and T. H. Epps, *Langmuir*, 2013, **29**, 3864–3978.

44     S. P. Gido, *Nature*, 1999, **398**, 107–108.

45     M. W. Matsen and F. S. Bates, *Macromolecules*, 1996, **29**, 1091–1098.

46     N. Kumar and J. Hahm, *Langmuir*, 2005, **21**, 6652–6655.

47     S. Park, J. Wang, B. Kim, J. Xu and T. P. Russell, *ACS Nano*, 2008, **2**, 766–772.

48     R. Ruiz, H. Kang, F. A. Detcheverry, E. Dobisz, D. S. Kercher, T. R. Albrecht, J. J. de Pablo and P. F. Nealey, *Science*, 2008, **321**, 936–940.

49     W. Joo, M. S. Park and J. K. Kim, *Langmuir*, 2006, **22**, 7960–7963.

50     K.-V. Peinemann, V. Abetz and P. F. W. Simon, *Nat. Mater.*, 2007, **6**, 992–6.

51     W. A. Phillip, B. O'Neill, M. Rodwogin, M. A. Hillmyer and E. L. Cussler, *ACS Appl. Mater. Interfaces*, 2010, **2**, 847–853.

52     J. N. L. Albert and T. H. Epps, *Mater. Today*, 2010, **13**, 24–33.

53     J. Du and R. K. O'Reilly, *Soft Matter*, 2009, **5**, 3544.

54     M. L. Adams, A. Lavasanifar and G. S. Kwon, *J. Pharm. Sci.*, 2003, **92**, 1343–1355.

55     P. Posocco, M. Fermeglia and S. Pricl, *J. Mater. Chem.*, 2010, **10**, 7742–7753.

56     C. Khemtong, C. W. Kessinger and J. Gao, *Chem. Commun.*, 2009, 3497–3510.

57     N. Nasongkla, X. Shuai, H. Ai, B. D. Weinberg, J. Pink, D. A. Boothman and J. Gao, *Angew. Chemie Int. Ed.*, 2004, **43**, 6323–6327.

58     S. Movassaghian, O. M. Merkel and V. P. Torchilin, *Wires Nanomed. Nanobi.*, 2015, 2–17.

59     C. Oerlemans, W. Bult, M. Bos, G. Storm, J. F. W. Nijsen and W. E. Hennink, *Pharm. Res.*, 2010, **27**, 2569–2589.

60     K. Kondo, A. Suzuki, M. Akita and M. Yoshizawa, *Angew. Chemie Int. Ed.*, 2013, **52**, 2308–2312.

61    G. Huang, H. Li, S. Feng, X. Li, G. Tong, J. Liu, C. Quan, Q. Jiang, C. Zhang and Z. Li, *Macromol. Chem. Phys.*, 2015, **216**, 1014–1023.

62    F. Käfer, F. Liu, U. Stahlschmidt, V. Jerome, R. Freitag, M. Karg and S. Agarwal, *Langmuir*, 2015, **31**, 8940–8946.

63    Y. Kotsuchibashi, Y. Kuboshima, K. Yamamoto and T. Aoyagi, *J. Polym. Sci. Part A Polym. Chem.*, 2008, **46**, 6142–6150.

64    J. Chiefari, Y. K. . Chong, F. Ercole, J. Krstina, J. Jeffery, T. P. T. Le, R. T. A. Mayadunne, G. F. Meijs, C. L. Moad, G. Moad, E. Rizzardo and S. H. Thang, *Macromolecules*, 1998, **31**, 5559–5562.

65    G. Moad, B. E. Rizzardo and S. H. Thang, *Aust. J. Chem.*, 2009, **62**, 1402–1472.

66    D. J. Keddie, *Chem. Soc. Rev.*, 2014, **43**, 496–505.

67    G. Moad, A. E. Rizzardo and S. H. Thang, *Aust. J. Chem.*, 2005, **58**, 379–410.

68    G. Moad, E. Rizzardo and S. H. Thang, *Polymer*, 2008, **49**, 1079–1131.

69    E. Rizzardo, M. Chen, B. Chong, G. Moad, M. Skidmore and S. H. Thang, *Macromol. Symp.*, 2007, **248**, 104–116.

70    M. R. Hill, R. N. Carmean and B. S. Sumerlin, *Macromolecules*, 2015, **48**, 5459–5469.

71    G. Moad, E. Rizzardo and S. H. Thang, *Living Radical Polymerization by the RAFT Process*, 2009, vol. 62.

72    C. Barner-Kowollik, in *Handbook of RAFT Polymerization*, ed. C. Barner-Kowollik, Wiley-VCH Verlag GmbH & Co. KGaA, Weinheim, Germany, 2008, p. 91.

73    A. B. Lowe and C. L. McCormick, *Prog. Polym. Sci.*, 2007, **32**, 283–351.

74    D. B. Thomas, A. J. Convertine, L. J. Myrick, C. W. Scales, A. E. Smith, A. B. Lowe, Y. A. Vasilieva, N. Ayres and C. L. McCormick, *Macromolecules*, 2004, **37**, 8941–8950.

75    J.-F. Lutz and A. Hoth, *Macromolecules*, 2006, **39**, 893–896.

76    H. Mori, H. Iwaya, A. Nagai and T. Endo, *Chem. Commun. (Camb).*, 2005, 4872–4874.

77    C. Tang, T. Kowalewski and K. Matyjaszewski, *Macromolecules*, 2003, **36**, 8587–8589.

78    J. Vlachopoulos and D. Strutt, *Mater. Sci. Technol.*, 2003, **19**, 1161–1169.

79    G. R. Guillen, Y. Pan, M. Li and E. M. V. Hoek, *Ind. Eng. Chem. Res.*, 2011, **50**, 3798–3817.

80    X. J. Loh, P. Peh, S. Liao, C. Sng and J. Li, *J. Control. release*, 2010, **143**, 175–82.

81    I. Letnik, R. Avrahami, J. S. Rokem, A. Greiner, E. Zussman and C. Greenblatt, *Biomacromolecules*, 2015, **16**, 3322–3328.

82    R. Suntornnond, J. An, W. Y. Yeong and C. K. Chua, *Macromol. Mater. Eng.*, 2015, **9**, 858–877.

83    J. Xue, L. Chen, H. L. Wang, Z. B. Zhang, X. L. Zhu, E. T. Kang and K. G. Neoh, *Langmuir*, 2008, **24**, 14151–14158.

84    J. I. Clodt, V. Filiz, S. Rangou, K. Buhr, C. Abetz, D. Höche, J. Hahn, A. Jung and V. Abetz, *Adv. Funct. Mater.*, 2013, **23**, 731–738.

85    F. Schacher, M. Ulbricht and A. H. E. Müller, *Adv. Funct. Mater.*, 2009, **19**, 1040–1045.

86    Q. Zhang, Y. Gu, Y. M. Li, P. A. Beaucage, T. Kao and U. Wiesner, *Chem. Mater.*, 2016, **28**, 3870–3876.

87    J. Vonch, A. Yarin and C. M. Megaridis, *J. Undergrad. Res.*, 2007, **1**, 1–6.

88    A. Formhals, *US Pat.*, 1934, 504.

89    D. H. Reneker and I. Chun, *Nanotechnology*, 1996, **7**, 216–223.

90    Z. Li and C. Wang, *One-Dimensional nanostructures Electrospinning Technique and Unique Nanofibers*, Springer Berlin Heidelberg, 2013.

91    S. Agarwal, M. Burgard, A. Greiner and J. H. Wendorff, *Electrospinning A Practical Guide to Nanofibers*, Walter De Gruyter, 2016.

92    A. C. Baptista, I. Ferreira and J. P. Borges, *J. Compos. Biodegrad. Polym.*, 2013, **1**, 56–65.

93    Y. Liu, M. H. Rafailovich, R. Malal, D. Cohn and D. Chidambaram, *PNAS*, 2009, **106**, 14201–6.

94    J. M. Gluck, P. Rahgozar, N. P. Ingle, F. Rofail, A. Petrosian, M. G. Cline, M. C. Jordan, K. P. Roos, W. R. Maclellan, R. J. Shemin and S. Heydarkhan-Hagvall, *J. Biomed. Mater. Res. B Appl. Biomater.*, 2011, **99B**, 180–190.

95    N. G. Rim, C. S. Shin and H. Shin, *Biomed. Mater.*, 2013, **8**, 1–14.

96    A. Nykänen, S.-P. Hirvonen, H. Tenhu, R. Mezzenga and J. Ruokolainen, *Polym. Int.*, 2014, **63**, 37–43.

97    D. Crespy and R. M. Rossi, *Polym. Int.*, 2007, **56**, 1461–1468.

98    L. Liu, S. Jiang, Y. Sun and S. Agarwal, *Adv. Funct. Mater.*, 2016, **26**, 1021–1027.

99    J. Wang, Y.-C. Chiu, H.-S. Sun, K. Yoshida, Y. Chen, T. Satoh, T. Kakuchi and W.-C. Chen, *Polym. Chem.*, 2015, **6**, 2327–2336.

100   N. Wang, Y. Zhao and L. Jiang, *Macromol. Rapid Commun.*, 2008, **29**, 485–489.

101   T. Tran, M. Hernandez, D. Patel, E. Burns, V. Peterman and J. Wu, *Nano Cover.*, 2015, **2**, 1–7.

102   G. V. R. Rao, M. E. Krug, S. Balamurugan, H. Xu, Q. Xu and G. P. López, *Chem. Mater.*, 2002, **14**, 5075–5080.

103   K. Troll, A. Kulkarni, W. Wang, C. Darko, A. M. Bivigou Koumba, A. Laschewsky, P. Müller-Buschbaum and C. M. Papadakis, *Colloid Polym. Sci.*, 2008, **286**, 1079–1092.

104   A. Nykänen, M. Nuopponen, A. Laukkanen, S.-P. Hirvonen, M. Rytelä, O. Turunen, H. Tenhu, R. Mezzenga, O. Ikkala and J. Ruokolainen, *Macromolecules*, 2007, **40**, 5827–5834.

105   S. Jiang, F. Liu, A. Lerch, L. Ionov and S. Agarwal, *Adv. Mater.*, 2015, **27**, 4865–4870.

106   S. Zakharchenko, N. Puretskiy, G. Stoychev, M. Stamm and L. Ionov, *Soft Matter*, 2010, **6**, 2633–2636.

107   F. Liu, S. Jiang, L. Ionov and S. Agarwal, *Polym. Chem.*, 2015, **6**, 2769–2776.

108   E. Yousif and R. Haddad, *Springerplus*, 2013, **2**, 1–32.

109   C. Brandl, A. Greiner and S. Agarwal, *Macromol. Mater. Eng.*, 2011, **296**, 858–864.

110   Z. Yuan, J. Zhao, Y. Chen, Z. Yang, W. Cui and Q. Zheng, *Mediators Inflamm.*, 2014, **2014**, 1–11.

111   L. Zhang, Z. Zeng, Y. Chen, C. Wu and J. Gao, *J. Appl. Polym. Sci.*, 1997, **66**, 2543–2549.

# Literature

112    H. Kheradmand, J. François and V. Plazanet, *Polymer*, 1988, **29**, 860–870.

113    L. V. Allen, *Secundum Artem*, **7**, 1–6.

114    A. Peled, A. Pevzner, H. Peretz Soroka and F. Patolsky, *J. Nanobiotechnology*, 2014, **12**, 7.

115    N. do Nascimento Marques, P. S. Curti, A. M. da Silva Maia and R. D. C. Balaban, *J. Appl. Polym. Sci.*, 2013, **129**, 334–345.

116    Z. Wang and R. Pelton, *Eur. Polym. J.*, 2013, **49**, 2196–2201.

117    W. Li, H. Zhao, P. R. Teasdale, R. John and S. Zhang, *React. Funct. Polym.*, 2002, **52**, 31–41.

118    N. Sagawa and T. Shikata, *Phys. Chem. Chem. Phys.*, 2014, **16**, 13262–13270.

119    L. Hou and P. Wu, *Soft Matter*, 2015, **11**, 7059–7065.

120    F. Liu, J. Seuring and S. Agarwal, *J. Polym. Sci. Part A Polym. Chem.*, 2012, **50**, 4920–4928.

121    T. Hoare and R. Pelton, *Langmuir*, 2004, **20**, 2123–2133.

122    C. O'Connor, *Q. Rev. Chem. Soc.*, 1970, **24**, 553.

123    P. Kampalanonwat and P. Supaphol, *Ind. Eng. Chem. Res.*, 2011, **50**, 11912–11921.

124    P. L. Wash, E. Maverick, J. Chiefari and D. A. Lightner, *J. Am. Chem. Soc.*, 1997, **119**, 3802–3806.

125    P. Duan, L. Dai and P. E. Savage, *J. Supercrit. Fluids*, 2010, **51**, 362–368.

126    Y. Xiong and C. G. Zhan, *J. Phys. Chem. A*, 2006, **110**, 12644–12652.

127    A. Vega-Rios and A. Licea-Claveríe, *J. Mex. Chem. Soc.*, 2011, **55**, 21–32.

128    K. H. Wong, T. P. Davis, C. Barner-Kowollik and M. H. Stenzel, *Polymer,* 2007, **48**, 4950–4965.

129    P. Vana, L. Albertin, L. Barner, T. P. Davis and C. Barner-kowollik, *J. Polym. Sci. Part A Polym. Chem.*, 2002, **40**, 4032–4037.

130    H. Chen and Y. Lo Hsieh, *J. Polym. Sci. Part A Polym. Chem.*, 2004, **42**, 6331–6339.

131    M. Chen, M. Dong, R. Havelund, V. R. Regina, R. L. Meyer, F. Besenbacher and P.

# Literature

Kingshott, *Chem. Mater.*, 2010, **22**, 4214–4221.

132 P. Muthiah, S. M. Hoppe, T. J. Boyle and W. Sigmund, *Macromol. Rapid Commun.*, 2011, **32**, 1716–1721.

133 H.-J. Lin and C.-Y. Chen, *J. Mater. Sci.*, 2016, **51**, 1620–1631.

134 Y.-C. Chiu, Y. Chen, C.-C. Kuo, S.-H. Tung, T. Kakuchi and W.-C. Chen, *ACS Appl. Mater. Interfaces*, 2012, **4**, 3387–3395.

135 L. Cheng, *Macromolecules*, 1999, **32**, 6668–6674.

136 J. Peng, Y. Su, W. Chen, Q. Shi and Z. Jiang, *Ind. Eng. Chem. Res.*, 2010, **49**, 4858–4864.

137 Y. Wang, H. Lin, Z. Xiong, Z. Wu, Y. Wang, X. Yu and F. Liu, *RSC Adv.*, 2016, **6**, 27485–27493.

138 C. A. Smolders, A. J. Reuvers, R. M. Boom and I. M. Wienk, *J. Memb. Sci.*, 1992, **73**, 259–275.

139 W. Wang, E. Metwalli, J. Perlich, C. M. Papadakis, R. Cubitt and P. Müller-Buschbaum, *Macromolecules*, 2009, **42**, 9041–9051.

140 K. Jain, R. Vedarajan, M. Watanabe, M. Ishikiriyama and N. Matsumi, *Polym. Chem.*, 2015, **6**, 6819–6825.

141 T. Ruotsalainen, J. Turku, P. Heikkilä, J. Ruokolainen, A. Nykänen, T. Laitinen, M. Torkkeli, R. Serimaa, G. Brinke, A. Harlin and O. Ikkala, *Adv. Mater.*, 2005, **17**, 1048–1052.

142 A. Kapllani, C. Tran and V. Kalra, *Soft Matter*, 2013, **9**, 11014–11020.

143 V. Kalra, P. A. Kakad, S. Mendez, T. Ivannikov, M. Kamperman and Y. L. Joo, *Macromolecules*, 2006, **39**, 5453–5457.

144 H. Fashandi and M. Karimi, *Polymer*, 2012, **53**, 5832–5849.

145 K. Nayani, H. Katepalli, C. S. Sharma, A. Sharma, S. Patil and R. Venkataraghavan, *Ind. Eng. Chem. Res.*, 2012, **51**, 1761–1766.

146 H. R. Pant, M. P. Neupane, B. Pant, G. Panthi, H.-J. Oh, M. H. Lee and H. Y. Kim, *Colloids Surfaces B Biointerfaces*, 2011, **88**, 587–592.

147   C. J. Luo, E. Stride and M. Edirisinghe, *Macromolecules*, 2012, **45**, 4669–4680.

148   R. M. Nezarati, M. B. Eifert and E. Cosgriff-hernandez, *Tissue Eng. Part C*, 2013, **19**, 810–819.

149   J. Lin, B. Ding, J. Yu and Y. Hsieh, *ACS Appl. Mater. Interfaces*, 2010, **2**, 521–528.

150   J. Zheng, H. Zhang, Z. Zhao and C. C. Han, *Polymer*, 2012, **53**, 546–554.

151   W. Chen, Y. Su, J. Peng, Y. Dong, X. Zhao and Z. Jiang, *Adv. Funct. Mater.*, 2011, 191–198.

152   K. Tanaka, A. Takahara and T. Kajiyama, *Macromolecules*, 1998, **9297**, 863–869.

153   V. Abetz and P. F. Simon, *Adv. Polym. Sci.*, 2005, 125–212.

154   M. Karunakaran, R. Shevate and K. Peinemann, *RSC Adv.*, 2016, 29064–29071.

155   C. Huang, R. Nicolay, Y. Kwak, F. Chang and K. Matyjaszewski, *Macromolecules*, 2009, 8198–8210.

156   T. S. C. Pai, C. Barner-kowollik, T. P. Davis and M. H. Stenzel, *Polymer*, 2004, **45**, 4383–4389.

157   P. G. Santangelo and C. M. Roland, *Macromolecules*, 1998, **31**, 4581–4585.

158   A. L. Agapov and A. P. Sokolov, *Macromolecules*, 2009, **42**, 2877–2878.

159   N. Yeole and D. Hundiwale, *Colloids Surfaces A Physicochem. Eng. Asp.*, 2011, **392**, 329–334.

160   N. Yeole, S. N. R. Kutcherlapati and T. Jana, *RSC Adv.*, 2014, **4**, 2382–2388.

161   S. P. Nunes, *Macromolecules*, 2016, **49**, 2905–2916.

162   S. P. Nunes, R. Sougrat, B. Hooghan, D. H. Anjum, A. R. Behzad, L. Zhao, N. Pradeep, I. Pinnau, U. Vainio and K.-V. Peinemann, *Macromolecules*, 2010, **43**, 8079–8085.

# (Eidesstattliche) Versicherung und Erklärung

Entsprechend der Promotionsordnung der Bayreuther Graduiertenschule für Mathematik und Naturwissenschaften/Bayreuth Graduate School of Mathematical and Natural Sciences (BayNAT) vom 20. März 2014

(§ 8 Abs. 2 Nr. 6 PromO)

*Hiermit erkläre ich mich damit einverstanden, dass die elektronische Fassung meiner Dissertation unter Wahrung meiner Urheberrechte und des Datenschutzes einer gesonderten Überprüfung hinsichtlich der eigenständigen Anfertigung der Dissertation unterzogen werden kann.*

(§ 8 Abs. 2 Nr. 8 PromO)

*Hiermit erkläre ich eidesstattlich, dass ich die Dissertation selbstständig verfasst und keine anderen als die von mir angegebenen Quellen und Hilfsmittel benutzt habe.*

(§ 8 Abs. 2 Nr. 9 PromO)

*Ich habe die Dissertation nicht bereits zur Erlangung eines akademischen Grades anderweitig eingereicht und habe auch nicht bereits diese oder eine gleichartige Doktorprüfung endgültig nicht bestanden.*

(§ 8 S. Abs Nr. 10 PromO)

*Hiermit erkläre ich, dass ich keine Hilfe von gewerblichen Promotionsberatern bzw. -vermittlern in Anspruch genommen habe und auch künftig nicht in Anspruch nehmen werde.*

_____

Ort, Datum, Unterschrift